468735
34 p

A CATALOG OF SOFT X-RAY SHADOWS, AND MORE CONTEMPLATION OF THE $\frac{1}{4}$ keV BACKGROUND

S. L. SNOWDEN[1,2,3], M. J. FREYBERG[2], K. D. KUNTZ[4], W. T. SANDERS[5],

ABSTRACT

This paper presents a catalog of shadows in the $\frac{1}{4}$ keV soft X-ray diffuse background (SXRB) that were identified by a comparison between *ROSAT* All-Sky Survey maps and *DIRBE*-corrected *IRAS* 100 μm maps. These "shadows" are the negative correlations between the surface brightness of the SXRB and the column density of the Galactic interstellar medium (ISM) over limited angular regions (a few degrees in extent). We have compiled an extensive but not exhaustive set of 378 shadows in the polar regions of the Galaxy ($|b| \gtrsim 20°$), and determined their foreground and background X-ray intensities (relative to the absorbing features), and the respective hardness ratios of that emission. The portion of the sky that was examined to find these shadows was restricted in general to regions where the minimum column density is $\lesssim 4 \times 10^{20}$ H cm^{-2}, i.e., relatively high Galactic latitudes, and to regions away from distinct extended features in the SXRB such as supernova remnants and superbubbles.

The results for the foreground intensities agree well with the recent results of a general analysis of the local $\frac{1}{4}$ keV emission while the background intensities show additional, but not unexpected scatter. The results also confirm the existence of a gradient in the hardness of the local $\frac{1}{4}$ keV emission along a Galactic center/anticenter axis with a temperature that varies from $10^{6.13}$ K to $10^{6.02}$ K, respectively. The average temperature of the foreground component from this analysis is $10^{6.08}$ K, compared to $10^{6.06}$ K in the previous analysis. Likewise, the average temperature for the distant component for the current and previous analyses are $10^{6.00}$ K and $10^{6.02}$ K, respectively.

Finally, the results for the $\frac{1}{4}$ keV halo emission are compared to the observed fluxes at $\frac{3}{4}$ keV, where the lack of correlation suggests that the Galactic halo's $\frac{1}{4}$ keV and $\frac{3}{4}$ keV fluxes are likely produced by separate emission regions.

---

[1]Code 662, NASA/Goddard Space Flight Center, Greenbelt, MD 20771.

[2]Max-Planck-Institut für Extraterrestrische Physik, D-85740 Garching, Germany

[3]Universities Space Research Association.

[4]Department of Astronomy, University of Maryland, Collage Park, MD 20742

[5]Department of Physics, University of Wisconsin–Madison, 1150 University Avenue, Madison, WI 53706.

Subject headings: galaxies: Milky Way — interstellar: matter — X-rays: galaxies, general

1. INTRODUCTION

A negative correlation between the column density distribution of a Galactic H I feature and the surface brightness of the $\frac{1}{4}$ keV soft X-ray diffuse background (SXRB), a "shadow," provides a mechanism for determining the location along the line of sight of X-ray emitting plasmas relative to the X-ray-absorbing H I. The fundamental result of a shadowing observation is the separation of the observed X-ray flux into foreground and background components relative to the shadowing object. An "object" in this case can be either a local column-density enhancement (i.e., cloud) or a local minimum in the Galactic H I column density. With the additional information of the distance to the shadowing object, which can be determined using interstellar absorption line measurements towards stars with a range of known distances, constraints can be placed on the locations of the emission components. If a number of shadowing observations can be combined, then it becomes possible to create a three-dimensional map of the distribution of both the X-ray emitting and absorbing material. This process becomes particularly effective when the results are compared with the extensive mappings of the distribution of neutral material in the solar neighborhood that can be found in the literature (e.g., Frisch & York 1983; Paresce 1984; Welsh et al. 1994; Sfeir et al. 1999).

Shadows in the general SXRB (i.e., away from discrete emission features such as supernova remnants) were first unambiguously detected using the *ROSAT* observatory (Snowden et al. 1991; Burrows & Mendenhall 1991). The continuing study of such shadows has provided crucial information about the soft X-ray emission from the Galactic halo and from the Local Hot Bubble (LHB), an irregularly shaped region of $\sim 10^6$ K plasma which extends $\sim 50 - 150$ pc from the Sun in all directions (Cox & Snowden 1986; Cox & Reynolds 1987; Snowden et al. 1990;1998). For example, the relationship between the $\frac{1}{4}$ keV SXRB surface brightness and the H I column density has been examined recently for a number of regions of the sky, both large and small. *ROSAT* All-Sky Survey data were used to study several regions of rather limited extent (Kerp et al. 1996; Kerp et al. 1999), a large region in Ursa Major (Snowden et al. 1994a), the M complex of high-velocity clouds (Herbstmeier et al. 1995), the Draco Nebula (Snowden et al. 1991; Moritz et al. 1998), the Eridanus enhancement (Snowden et al. 1995a), as well as the whole sky (Wang 1997; Snowden et al. 1998; Pietz et al. 1998). *ROSAT* pointed observations were used to study the Draco Nebula (Burrows & Mendenhall 1991), MBM 12 (Snowden, McCammon, & Verter 1993), several distinct clouds (Wang & Yu 1995; Kuntz, Snowden, & Verter 1997), a region of Ursa Major (Barber & Warwick 1996), and a region of Eridanus (Guo et al. 1995).

With the aim of providing a tool with which to further studies of the small-scale geometry of the local interstellar medium and to provide information on $\frac{1}{4}$ keV emission from the Galactic halo, this paper presents a catalog of 378 absorption/emission features in the $\frac{1}{4}$ keV soft X-ray background derived from the *ROSAT* All-Sky Survey (RASS). This analysis improves upon the general results reported in Snowden et al. (1998, hereafter Paper I) by selecting regions of the sky most likely to provide statistically significant results. These are regions with variations in absorption greater than one optical depth over a solid angle of typically $\lesssim 30$ deg^2 in directions of relatively low average column densities. The derived results are therefore more accurate for the sampled regions of the sky than the smoothed results of Paper I. In addition, we have slightly improved upon the analysis technique of Paper I.

The data used in this analysis are discussed in § 2, the analysis itself is described in § 3, and the results and discussion are presented in § 4. Section 5 presents the conclusions of this paper.

2. DATA

For the analysis presented here, we have used the RASS high-resolution maps of the $\frac{1}{4}$ keV and $\frac{3}{4}$ keV diffuse X-ray background presented in Snowden et al. (1997), and the *DIRBE*-corrected *IRAS* 100 μm maps of Schlegel, Finkbeiner, & Davis (1998) scaled to represent the column density of Galactic neutral hydrogen. These are the same basic data sets (with the addition of the $\frac{3}{4}$ keV data) that were used in Paper I.

2.1. X-ray Data

As described in detail in Snowden et al. (1995b;1997), the X-ray data have been cleaned of periods of anomalously high noncosmic background, have had residual noncosmic background contributions subtracted (scattered solar X-rays, Snowden & Freyberg 1993; particle background, Snowden et al. 1992, Plucinsky et al. 1993; long-term enhancements, Snowden et al. 1994b), are exposure corrected, and have had bright point sources removed. The maps cover $\sim 98\%$ of the sky with roughly 10^6 $12' \times 12'$ pixels, and consist of count rate and count-rate uncertainty pairs in six bands. In this paper we use data from the R1 and R2 bands, and the summed R12 band ($\frac{1}{4}$ keV) and R45 band ($\frac{3}{4}$ keV). The R12 band data are formed by summing the R1 and R2 band count rates (which are statistically independent) and adding their uncertainties in quadrature. The R45 band data are formed in the same manner by adding the R4 and R5 band data. Figure 1 displays the band response functions for the four bands. The R1 and R2 bands are clearly not spectrally independent, however the R45 band is reasonably cleanly separated from the R12 band. (The X-ray data used for the all-sky analysis of Paper I consisted of the R1 and R2 band data binned into $24' \times 24'$ pixels.)

The individual *ROSAT* bands are formed by pulse-height selection on individual events (detection of an X-ray photon), so each event is uniquely assigned to a single band providing statistical independence. The lack of spectral independence of the R1 and R2 bands is due to the poor intrinsic energy resolution of the proportional counters, which is $E/\Delta E \sim 1$ at $E \sim \frac{1}{4}$ keV.

The spectral separation between the R12 band and the R45 band is provided by the carbon Kα absorption edge of the proportional counter entrance window at 0.284 keV.

As will be addressed in § 3, the analysis presented here has been limited to approximately 10% of the sky, or roughly 10^5 pixels. Histograms of the statistical significance (count rate divided by the uncertainty in the count rate) of the individual pixels in the three $\frac{1}{4}$ keV maps used in this analysis are shown in Figure 2. While the significances are not in general as large as one would prefer, they are sufficient for this analysis, and the finer angular binning (than used in Paper I) allows an increased sampling of any fine structure in the column density of the absorbing interstellar medium.

2.2. Measure of Absorption Column Density

As in Paper I, we use the *DIRBE*-corrected *IRAS* 100 μm data from Schlegel et al. (1998), cast into the same projections and pixels as the X-ray data, as a measure of absorption column density. However, they are slightly different from those used in Paper I as they are the product of the final processing used for the Schlegel et al. paper. The differences are minor and do not significantly affect the results. The inherent angular resolution of the *IRAS* data ($\sim 5'$) exceeds by a factor of five the useful resolution of the X-ray data, which is limited by counting statistics rather than by the resolution of the detector (the angular resolution of RASS data, which is an average over the field of view, is $\sim 3'$). Using the *IRAS* data provides a major advantage over using the available H I surveys, which have at best $35'$ resolution with incomplete sky coverage. The disadvantage of the *IRAS* data is that they do not contain velocity information that would allow the straightforward separation of the X-ray-absorbing interstellar matter into distinct components, as can be done with the H I data. However, velocity information can be determined for distinct *IRAS* features by comparing the angular structure with the coarser resolution H I data (although that is beyond the scope of this paper). Another major advantage for the IRAS data is that they also sample molecular gas.

Since the *IRAS* data are scaled to column densities of Galactic neutral hydrogen at high Galactic latitudes, they are an appropriate measure of X-ray-absorbing interstellar matter for this analysis (see Kuntz & Snowden 1999 for a more extensive discussion of this subject). The Schlegel et al. (1998) data were scaled to the column density of interstellar hydrogen by using the Leiden-Dwingeloo 21-cm survey of Hartmann & Burton (1997). Data in the Galactic polar regions were binned into $1.6° \times 1.6°$ pixels and linear fits made to the northern and southern data separately. The range in $N_{\rm H}$ was limited to $\leq 4 \times 10^{20}$ H I cm^{-2} to avoid the contribution of molecular gas to the I_{100} intensities and therefore contamination of the results. The scatter plots and fitted relations are shown in Figure 3. The fitted lines for the north and south are given by $N_{\rm H} = 0.186 + 1.403 \times I_{100}$ and $N_{\rm H} = 0.334 + 1.305 \times I_{100}$, respectively, where $N_{\rm H}$ is in units of 10^{20} H I cm^{-2} and I_{100} is in units of MJy sr^{-1}. The turnover at higher values of I_{100} is due to the presence of molecular gas. The difference between the I_{100} to $N_{\rm H}$ scaling between the northern and southern hemispheres is not significant for our purposes. They provide similar results for low column densities where the analysis is most sensitive to systematic uncertainties (the cross-over of the curves is at $N_{\rm H} \sim 3 \times 10^{20}$ cm^{-2}). At higher column densities where the relations diverge the column densities are optically thick.

3. Analysis

3.1. Selection of Target Regions

The selection of the locations and sizes of the regions, or shadows, that were analyzed for this paper was subjective, but not arbitrary. The selection criteria were that there be an apparent absorption feature in the $\frac{1}{4}$ keV background and/or an emission feature in the $N_{\rm H}$ map, that there be a *reasonable* range in the column densities of H I in the vicinity of this feature (most of the regions have a range greater than one optical depth), and that the minimum column density of H I in the vicinity be reasonably low. These criteria select regions where the total column density is low enough for the R12 band to still be sensitive to distant emission and where the range in $N_{\rm H}$ is large enough to provide an acceptable lever arm for the fit. Since one optical depth for X-rays at $\frac{1}{4}$ keV is $\sim 1 \times 10^{20}$ H I cm^{-2}, regions with a minimum sampled column density $\lesssim 4 \times 10^{20}$ H I cm^{-2} corresponding to a minimum optical depth $\lesssim 3$ were used (note that optical depth is not a linear function of $N_{\rm H}$, see Snowden et al. 1994b). These selection criteria limited the analysis to roughly the 40% of the sky with the lowest column density. However, the criteria were occasionally relaxed in order to better sample the local component, i.e., directions of higher column density where all observed emission can reasonably be assumed to be local in origin. For these regions the background emission is not well constrained.

Regions affected by known supernova remnants and superbubbles, specifically Loop I, the Eridanus superbubble, and the Monoceros-Gemini ring, were excluded. The studies of emission and absorption variations of such features using *ROSAT* data are certainly interesting in their own right (e.g., Loop I, Egger 1993; Eridanus, Snowden et al. 1995a, Guo et al. 1995; Monogem, Plucinsky et al. 1996), but are more appropriately left for detailed investigations of the specific object. The locations of the regions selected for analysis here are shown in Figure 4, where rings showing the extent of the regions are overlayed on both $\frac{1}{4}$ keV X-ray and *IRAS* maps. The radii of the target regions were determined by the angular extents of the absorption and/or emission features. In practice, all but three of the target regions are $\leq 8°$ in diameter. Near some of the larger features, several smaller regions were also selected for analysis in order to independently sample different parts of the feature to test for variation in either the foreground or background X-ray intensities.

An effort was made to have the selected regions be distributed over the available lower column density parts of the sky, which occasionally required relaxing some of the selection criteria above. While the sky coverage is certainly not uniform, because the distribution of suitable targets is not uniform, the sky covered is reasonably representative of the whole at high latitudes.

3.2. Fitted Model

A physical picture similar to that used in Paper I was assumed here for the relative locations of the X-ray-emitting plasmas responsible for the bulk of the $\frac{1}{4}$ keV background and the cooler X-ray absorbing gas in the interstellar medium. Specifically, it consists of an unabsorbed foreground X-ray emission region (the Local Hot Bubble, see Paper I), a region of neutral, X-ray absorbing ISM that includes the shadowing cloud and all other Galactic H I along the line of sight, and a region of X-ray emitting plasma in the Galactic halo that is not intermixed in the neutral ISM and that produces most of the observed $\frac{1}{4}$ keV background of distant origin (from Paper I this component has a temperature of $\sim 10^{6.0}$ K). Paper I assumed an isotropic extragalactic background power law with an index taken from Hasinger et al. (1993) of 1.96 and a normalization fixed to be consistent with extragalactic $\frac{1}{4}$ keV shadowing results (e.g., M 101, Snowden & Pietsch 1995; NGC 55, Barber, Roberts, & Warwick 1996; several additional face-on galaxies, Cui et al. 1996).

To make our current picture more physically realistic, we added the following refinement to the distant emission of the Paper I model. The previous isotropic extragalactic background power law has been replaced with two components: 1) an isotropic power law ($10.5E^{-1.46}$ photons cm^{-2} s^{-1} sr^{-1} keV^{-1}, the fitted power law of Model A from Chen, Fabian, & Gendreau 1997), which is the extrapolation of the extragalactic background observed above ~ 1 keV and is consistent with the observed flux in the *ROSAT* $1-2$ keV band, and 2) an anisotropic $T = 10^{6.4}$ K thermal component that accounts for the observed excess of the diffuse X-ray background at $\frac{3}{4}$ keV above the extrapolation of the power law. We used the R45 band data to determine the intensity of the $10^{6.4}$ K thermal component for each shadow region individually. The sum of these two distant components, when extrapolated to the $\frac{1}{4}$ keV band, produces an intensity similar to that of the extragalactic power law assumed for Paper I. The advantage to this revision is that the model now represents the entire $0.1-2.0$ keV *ROSAT* spectrum in a self-consistent manner, at least in a general sense. The broadband intensities in the $0.5-2.0$ keV band are well fit with reasonable spectra. These spectra can then be extrapolated down to the $\frac{1}{4}$ keV band to derive reasonable estimates for their contributions to that band. As will be shown below, this more complicated model has little actual effect on the shadow results in the $\frac{1}{4}$ keV band. The assumed geometry for the LHB, absorbing gas, and cooler ($T \sim 10^{6.0}$ keV) region of halo X-ray emission is shown schematically in Figure 5a.

Mathematically, the following equation is fit separately to the R1, R2, and R12 band data:

$$I_X = I_0 + I_1 \times \exp[-\sigma(N_{\rm H}, T_{6.0}) \times N_{\rm H}] + I_{6.4} \times \exp[-\sigma(N_{\rm H}, T_{6.4}) \times N_{\rm H}] +$$
$$I_{eg} \times \exp[-\sigma(N_{\rm H}, \alpha_{1.46}) \times N_{\rm H}].$$

Note that the data in the R1, R2, and R12 bands are fit independently and that only the parameters I_0 and I_1 are allowed to vary. I_X is the observed X-ray intensity, I_0 is the fitted foreground component, I_1 is the fitted distant (halo) component, which is absorbed by the column density N_H. $\sigma(N_H, T_{6.0})$ is the theoretical band-averaged absorption cross section (based on the cross sections of Morrison & McCammon 1983), which is a function both of N_H and the temperature of the I_1 component (see Snowden et al. 1994b). The fits were first done using $T = 10^{6.02}$ K, the value from Paper I, but were refit using the value $T = 10^{6.00}$ K based on the initial results. $I_{6.4}$ is the intensity of the hot Galactic halo component that is determined from the R45 band data and is fixed separately for each region; it is absorbed by the column density N_H. $\sigma(N_H, T_{6.4})$ is the theoretical band-averaged absorption cross section for this component. I_{eg} is the fixed isotropic extragalactic power-law contribution, and $\sigma(N_H, \alpha_{1.46})$ is the theoretical band-averaged absorption cross section, which is a function both of N_H and power-law index, α. As noted above, the spectrum of the extragalactic power law is taken to be $10.5E^{-1.46}$ photons cm^{-2} s^{-1} sr^{-1} keV^{-1}, and is extrapolated to $\frac{1}{4}$ keV and evaluated on a band-by-band basis. The normalization for the hot ($10^{6.4}$ K) halo contribution was determined in the following manner. 1) The absorbed power law contribution in the R45 band was subtracted from the average R45 band intensity over each shadow region. 2) This excess, minus a small amount (10^{-5} counts s^{-1} arcmin^{-2}) assumed to arise from the LHB (with an assumed temperature of $10^{6.0}$ K and typical high-latitude normalization set by Paper I), was deabsorbed by the average column density of the region. 3) This deabsorbed value was attributed to R45 band emission from the $T = 10^{6.4}$ K component. 4) Finally, the $T = 10^{6.4}$ K spectrum was extrapolated to the R1, R2, and R12 bands to fix $I_{6.4}$.

Following Paper I, the assumed spectra of the I_1 and $I_{6.4}$ components are Raymond & Smith (1977; Raymond 1992; 1991 computer code update[6]) thermal equilibrium plasma models using cosmic abundances with $T = 10^{6.0}$ K and $T = 10^{6.4}$ K, respectively. The choice of the spectrum affects the analysis in two ways: 1) The band-averaged absorption cross sections are spectrally dependent, but only to a limited extent, and 2) the choice of the temperature for the hotter halo component affects the amount of emission and band ratios (to the few percent level) attributed to the $\frac{1}{4}$ keV band. The R12/R45 band ratio decreases by a factor of four for spectra between $10^{6.3}$ K and $10^{6.5}$ K. However, the predicted unabsorbed R12 band intensity for a typical region, even assuming a $10^{6.3}$ K spectrum, is only comparable to the intensity from the extragalactic power law. We have chosen $T = 10^{6.4}$ K following Nousek et al. (1982), but this choice is confirmed by Kuntz & Snowden (1999).

There are a number of alternatives to our simple assumed geometry. The most likely are that the cloud or absorbing feature is located within the foreground X-ray emission region (Fig. 5b) or within the X-ray emission region(s) in the halo (Fig. 5c), i.e., there is some form of intermixture of the X-ray emitting and absorbing gas. These variations, while adding some

[6]While there are more recent versions of various plasma codes, use of the 1991 vintage allows direct comparisons with previous work by these authors.

complexity to their interpretations. do not appreciably affect the results. For example, if the shadowing cloud lies within the local emission region, Figure 5b, the fitted distant component includes the emission between the cloud and the edge of the emission region (wall) as well as any more distant emission beyond the wall. In such a situation, the fitting algorithm incorrectly deabsorbs the emission between the cloud and wall by the H I of the wall and "adds" it to the total distant component. Because of this, the attributions of "foreground" and "distant" emission may need to be reevaluated once the distances to the absorbing features are known.

4. RESULTS

4.1. Shadows

The results of the fits for the R1, R2, and R12 bands are listed in Table 1. For each target region, the table lists the Galactic coordinates of the region center, the diameter of the region, the fitted values for the R1, R2, and R12 band fits and their associated χ^2_ν values for the fits, and the number of degrees of freedom. Scatter plots of the R12 band data versus the column density of H I along with the fitted curves are shown in Figure 6. Inspection of both the table and figure shows the wide range of both X-ray emission and absorption covered by the shadows. The errors quoted in the table are the 1σ values derived using the Lampton, Margon, & Bowyer (1976) criteria ($\chi^2_{min} + 2.3$ for two-parameter fits). When the 1 σ range in uncertainty includes zero, the one-sigma upper limit is listed.

Figure 7 compares the foreground and distant R12 band intensities derived in this paper with those from Paper I. The foreground (I_0) results are in reasonable agreement, showing a moderately tight correlation, while the background (I_1) results show additional scatter. This is not particularly surprising as the I_1 results are more dependent on the chosen model, and the Paper I results were significantly smoothed. Since the regions for this analysis were specifically chosen to provide good measurements, the results of this paper are more reliable.

Figure 8 shows scatter plots of the hardness ratio (R2/R1 band ratio) for the I_0 and I_1 components as a function of the R12 band I_0 and I_1 intensities, respectively. In both cases while there is significant scatter in the data, there is no suggestion of a systematic variation with intensity. Figure 9 shows histograms for the R2/R1 band ratios for the I_0 and I_1 components. The average values for the data are 1.13 and 0.98, respectively. These values imply temperatures of $10^{6.08}$ K and $10^{6.00}$ K, which are consistent with those of Paper I, where the derived values for the local and distant emission were $10^{6.06}$ K and $10^{6.02}$ K[7].

[7]The quoting of temperatures for the thermal emission must always be done with caution as they are model dependent. Different thermal emission codes will attribute different temperatures to the same broad-band ratio or fitted spectrum, and even different versions of a given code will show variations. In addition, current thermal equilibrium codes do not fit the observed data for the diffuse $\frac{1}{4}$ keV background particularly well (see Sanders et

4.2. Variation of Intensity with Direction

Figure 10 presents the variation in the fitted values for I_0 and I_1 as a function of position on the sky. The relative size of the plotted circles corresponds to the relative intensities of the emission. From the plots it can be seen that the value for I_0 varies fairly slowly over the sky with higher values generally at higher latitudes. However, this is more consistently true for the northern hemisphere than for the southern. In the south there is an asymmetry in I_0 such that the longitude range $0° < l < 180°$ has in general lower intensities than the range $180° < l < 360°$.

The I_1 results displayed in Figure 10 have a completely different character. The regions of bright emission are considerably clumpier, and in general the higher intensities are at lower latitudes. The consistently bright regions are in the direction of Draco in the north and in the directions of $l, b \sim 40°, -30°$ and the "void" in the south (the void, or "Region of Bizarre Emptiness", Cox 1997, at $l \sim 230°$ is a direction in which there is little H I near the Galactic plane out to distances of a few hundred parsecs, see, e.g., Sfeir et al. 1999 and references therein). Note that the latitudes of the displayed enhancements are relatively high ($20° < |b| < 45°$), although in all probability the enhancements would reach down closer to the Galactic plane if the analysis of this paper was able to sample them.

As expected from the correlations shown in Figure 7, the results of this Paper agree well with the position dependencies of the I_0 and I_1 values from Paper I.

4.3. Variation of Hardness Ratio with Direction

Figure 11 shows scatter plots of the average hardness ratios for the data in Figure 8 binned into 10° latitude bins. As in Figure 8, there is relatively little apparent variation in the ratios. On the other hand, when the data are binned into longitude bins they *do* show significant systematic variation (Figure 12), at least for the I_0 ratio. The I_0 ratio varies from a high of $R2/R1 \sim 1.25$ averaged over longitudes within 40° of the Galactic center to $R2/R1 \sim 1.04$ averaged over longitudes within 40° of the Galactic anticenter. The range in the I_0 ratio as a function of longitude is centered on the average value, and implies a temperature range of $10^{6.04}$ K to $10^{6.13}$ K. The magnitude of the variation is not as great as that shown in Snowden, Schmitt, & Edwards (1990), which reported a dipole gradient in the $\frac{1}{4}$ keV hardness ratio in the Wisconsin all-sky survey data (McCammon et al. 1983) with a range of $10^{5.9}$ K to $10^{6.2}$ K with the low end of the dipole axis pointing at $l, b = 168.^{\circ}7, 11.^{\circ}2$. When the data are analyzed with respect to the orientation of the Snowden, Schmitt, & Edwards (1990) dipole (Figure 13), the extrapolated range in the ratio is $1.02 - 1.24$ implying only a slightly broader temperature range of $10^{6.02}$ K

al. 1998; Sanders et al. 1999). However, the use of the temperature does provide a scale (admittedly imperfect) with which to measure various models. We have much to learn about the ionization states and abundances of the X-ray-emitting plasmas.

to $10^{6.13}$ K. The fitted line in Figure 13 is acceptable at the 30% level with $\chi^2_\nu = 1.15$ with 18 degrees of freedom. The best fit for a constant value has $\chi^2_\nu = 2.50$ with 19 degrees of freedom, which can be ruled out at the > 99.9% confidence level, demonstrating the significance of the dipole variation. The FWHM range of the local component ratio is 0.91 – 1.30 (Fig. 9a), which is dominated by the systematic variation of the fitted values across the sky.

Figure 14 displays the variation on the hardness ratio of the I_0 data versus position. The southern hemisphere data clearly show the Galactic center/anticenter gradient. The gradient is less obvious in the northern hemisphere data where the ratio appears to be more mixed with only a slight trend of hardness ratio versus position.

Because of the statistics of the results for the distant component, it is much less clear whether there is a significant variation of the hardness of the emission across the sky. The FWHM range of the I_1 ratio distribution is 0.67 – 1.22 (Fig. 9b), implying a temperature range of $10^{5.83} - 10^{6.12}$ K. Although the width of the distribution is probably enhanced due to the poorer statistics of the fits for the distant-emission parameters, it is likely that there is some true variation of the temperature in the halo. The emission appears clumpy suggesting both spatially separate emission regions and that the emission is distributed over large distances (when compared to the size of the LHB).

4.4. The LHB: I_0 and the Local H I Cavity

The premise of the Local Hot Bubble is that there is a cavity in the H I of the Galactic disk that contains the Sun and is filled with an X-ray-emitting plasma. This plasma produces half to all of the observed intensity at $\frac{1}{4}$ keV in all directions. The existence of the cavity is required by interstellar absorption-line measurements. The existence of the plasma within the cavity is absolutely required in low-latitude directions because there are nearby, optically-thick walls of H I (the edge of the cavity), yet a non-zero $\frac{1}{4}$ keV flux is observed. If the plasma is isothermal and is distributed uniformly throughout the cavity, then the fitted value for I_0, when properly scaled, should provide a measure of the distance to the boundary of the cavity. A comparison between the I_0 intensities of Paper I with the shape of the local cavity is made by Sfeir et al. (1999), who presented a mapping of the local ISM based on an extensive optical absorption-line study. The results were in reasonably good agreement over most of the sky but there are directions where the cavity extends well beyond the required path length of plasma (e.g., the RBE).

The dipole gradient in the temperature determined above produces only a $\pm 10\%$ variation in the emissivity of the plasma, with greater emissivity in directions of lower temperatures.

4.5. Galactic Halo Models

Another result of this analysis concerns the fundamental distribution of hot plasma and its temperature(s) in the halo of the Milky Way. A number of other groups have based their analyses of the diffuse X-ray background on a model where *all* of the distant Galactic emission arises from just one thermal component. This includes papers analyzing the spectrum of the diffuse X-ray background that concentrated more on the extragalactic component (e.g., Chen, Fabian, & Gendreau 1997; Miyaji et al. 1998; Parmar et al. 1999) as well as those modeling the X-ray halo of the Milky Way (e.g., Sidher et al. 1996; Wang 1997; Pietz et al. 1998). In the case of the studies focussing on the extragalactic background, the single halo component was simply used to provide a mechanism for removing the Galactic emission biasing from their determination of the extragalactic power law. However, for the studies of the Galactic X-ray halo, the fitted single halo component was used to model properties of the entire halo, usually in terms of the general Galactic potential.

If the diffuse halo X-ray emission is produced by a single-temperature component, then any variation in the ratio of the distant unabsorbed $\frac{3}{4}$ keV intensity to the distant unabsorbed $\frac{1}{4}$ keV intensity will map out variations in that temperature. For a large scale-height halo, the variation in the ratio away from the Galactic disk should be smooth over large angular scales while the intensity of the emission should also be slowly varying. For a halo which is more dominated by local variations either associated with physical processes in the Galactic disk (e.g., fountains) or in the halo (e.g., SNRs), both the hardness and intensity of the emission could vary on relatively small angular scales.

From our analysis, the halo $\frac{1}{4}$ keV intensity is the sum of the fitted value for I_1 in the R12 band plus the model contribution from the $10^{6.4}$ K component in the R12 band. The $\frac{3}{4}$ keV intensity is just the model contribution from the $10^{6.4}$ K component in the R45 band. Figure 15 shows a scatter plot of the deabsorbed $\frac{1}{4}$ keV and $\frac{3}{4}$ keV intensities from the halo. To minimize the effect of large angular scale temperature variations in the halo due to a hydrostatic distribution of the plasma, we have selected data at high Galactic latitude and away from the Galactic center (i.e., $|b| > 45°$ for $60° < l < 270°$, $|b| > 60°$ otherwise). The plot does not show evidence for a convincing correlation between the two intensities, even though both vary by over a factor of five. In addition, the plots of the $\frac{1}{4}$ keV halo intensities shown in Figures 10b,d do not show a smoothly-distributed halo intensity. This argues against a large scale-height halo model which has only one emission component but is consistent with a low scale-height variable (in both temperature and intensity) single component, which could also be considered as the superposition of multiple, spatially distinct components.

The adding of a second, lower temperature emission component to the model of the halo has several attractive aspects. Components at $\sim 10^{6.0}$ K and $\sim 10^{6.4}$ K contribute predominantly to different bands so the structures in the $\frac{1}{4}$ keV and $\frac{3}{4}$ keV bands are effectively decoupled. A high scale-height, higher-temperature halo is consistent with the smoothness of the all-sky images at

$\frac{3}{4}$ keV while the significant intensity variations on relatively short angular scales evident in the deabsorbed $\frac{1}{4}$ keV halo data can be interpreted as low scale-height phenomena associated with the Galactic disk. This contention of a two- (or more) component halo is supported by spectral analysis, the subject of another paper (Kuntz & Snowden 1999) which in part shows that while in any one direction it is possible to fit a single temperature component for the halo emission, it is not possible to do so in a consistent manner over the entire sky.

Figure 16 displays the relative strengths of the $\frac{1}{4}$ keV and $\frac{3}{4}$ keV halo emission as ellipses on the sky. In the north (Fig. 16a), the orientation of the ellipses, i.e., the band ratio of the emission, appears spatially uncorrelated except perhaps in the direction of Draco ($l, b \sim 85°, 37°$). In that region of bright $\frac{1}{4}$ keV emission, the ellipses tend to be vertical indicating that the average emission is relatively softer. In the southern hemisphere (Fig. 16b), the regions of bright $\frac{1}{4}$ keV emission show up as relatively narrow vertical ellipses as well. This implies that in these cases the $\frac{3}{4}$ keV emission does not track the $\frac{1}{4}$ keV enhancements. Thus, the halo $\frac{1}{4}$ keV enhancements are produced by a component that does not emit significantly at higher energies, which is consistent with a multi-thermal, multi-component X-ray halo.

4.6. More Support for (at Least) a Two-Component Halo

The R2/R1 I_1 band ratio that we fit here is fairly independent of the choice of the distant spectrum (extragalactic plus Galactic halo). This is demonstrated by the consistency of our present results with those of Paper I, where the assumed extragalactic background was a much softer $E^{-1.96}$ power law scaled to produce roughly the same flux as our current harder extragalactic $E^{-1.46}$ power law plus $T = 10^{6.4}$ K thermal components. The distant emission (extragalactic power law) of Paper I was softer than our fitted halo emission, while the distant emission (extragalactic power law plus $10^{6.4}$ K thermal emission) of this paper is harder than the fitted halo. There was little effect on the fitted parameters whether the assumed extra distant emission was harder or softer than the fitted emission. We repeated the analysis assuming *no* distant emission other than the $10^{6.0}$ K halo component (i.e., no extragalactic power law or $10^{6.4}$ K thermal component) and the R2/R1 I_1 ratio remained essentially unchanged. These results indicate that where the soft halo emission is bright enough to provide a reasonable measurement of the R2/R1 band ratio, it also is bright enough to completely dominate the extragalactic and hard halo emission.

Thus there is a halo component that has a R2/R1 band ratio of ~ 0.98, which implies a temperature of $\sim 10^{6.00}$ K. This temperature is *not* strongly dependent on the choice of thermal emission code (see Kuntz & Snowden 1999) as the current Raymond & Smith code (Raymond & Smith 1977, Xspec V10.00 Arnaud 1996) indicates a temperature of $\sim 10^{6.04}$ K while the current MEKAL code (Mewe, Gronenschild, & van den Oord 1985; Mewe, Lemen, & van den Oord 1986; Kaastra 1992; Liedahl, Osterheld, & Goldstein 1995, Xspec V10.00) indicates a temperature of $\sim 10^{6.00}$ K for that R2/R1 band ratio. We note again that with current thermal equilibrium emission models it is not possible to produce the observed excess at $\frac{3}{4}$ keV over the extrapolation of the extragalactic power law with the same spectrum that produces the observed R2/R1 I_1 band ratio. In addition, as shown above, the excess at $\frac{3}{4}$ keV is not correlated with the halo emission at $\frac{1}{4}$ keV. Therefore, a second harder emission component is required to produce the observed excess at $\frac{3}{4}$ keV. However, an analysis of the spatial structure of the harder component is beyond the scope of this paper.

4.7. And Perhaps a Physical Justification for the Temperatures

The bimodal temperature distribution may be providing important clues about the physical conditions of the X-ray emitting plasma, which may be interpreted in terms of diffuse-plasma radiative cooling curves[8]. Schmutzler & Tscharnuter (1993) calculated cooling curves for isochorically and isobarically cooling plasmas. The cooling rate per unit density has two minima within the soft X-ray region, at $T \sim 10^{6.0}$ K and $T \sim 10^{6.8}$ K, with the positions of those minima dependant upon the metallicity of the plasma. Curves calculated by Shelton (1999) for isobarically cooling plasmas that had been shocked to $T = 10^{8.0}$ K show similar minima, with the position of the minima also dependant upon the degree of ionization nonequilibrium, and thus upon the power source and thermal history of the plasma.

For a quasi-steady state, isochorically-cooling plasmas will remain longer at temperatures around the local minima in the cooling curve than they will at other, nearby temperatures, leading to an "accumulation" of gas at those temperatures. For the isobarically-cooling case, the density of the plasma increases as the gas cools. Thus, the volumetric luminosity goes as Λn^2, which in turn goes as ΛT^{-2}, which steepens the cooling curve and may change the local minima into no more than points of inflection.

Whether those accumulations are significant will depend upon the details of the cooling curves, which depend on metallicities, ionization states, and whether the plasma is cooling isochorically or isobarically, or more likely some state in between. Although the cooling rate per unit density is similar for both cases (Schmutzler & Tscharnuter 1993), the cooling rate per volume as noted above is very different.

The *ROSAT* PSPC is sensitive to soft X-ray emission through a wide range of plasma temperatures. That there are two dominant observed temperatures, and that those temperatures are near the minima of the (isochoric) cooling curves, suggests that the halo gas may be in some quasi-steady state of cooling. The strong differences in the volumetric cooling curve between isobaric and isochoric cases, as well as the changes in the cooling curves produced by metallicity

---

[8] Cooling curves are traditionally plotted as the cooling coefficient (Λ) versus gas temperature, where the volumetric luminosity coefficient $\Lambda_{vl} = \Lambda n^2$. Then for the isochoric case, by definition, the density remains constant, and $\Lambda \propto \Lambda_{vl}$, which is also proportional to the luminosity per atom. Thus, the traditional curve can be easily scaled to make a luminosity per atom versus temperature curve.

and thermal history, suggest that we may be able to use the temperature distribution of the X-ray emitting gas to understand the physical conditions of the galactic halo.

5. CONCLUSIONS

We have presented a catalog of shadows in the $\frac{1}{4}$ keV soft X-ray diffuse background including fitted values for the foreground and background emission relative to the shadowing features for the R1, R2, and combined R12 bands. The intensities and hardness ratios for the foreground and background components are consistent with the all-sky analysis of Snowden et al. (1998). When combined with distances to the absorbing clouds found by interstellar absorption-line measurements published elsewhere or determined by other studies, these data can aid in the mapping of the relative locations of X-ray emitting and absorbing material in the ISM.

The data presented here confirm the existence of a temperature gradient through the LHB first identified in Snowden, Schmitt, & Edwards (1990). The gradient is consistent with a dipole variation with the harder emission in the direction of the Galactic center. The magnitude of the effect identified here is not as great as that of the earlier paper.

Finally, examination of the Galactic halo emission at $\frac{1}{4}$ keV and $\frac{3}{4}$ keV strongly suggests the existence of (at least) two emission components. A hotter ($T \sim 10^{6.4}$ K) component is responsible for the bulk of the observed excess $\frac{3}{4}$ keV intensity over the extrapolation of the extragalactic power law and a cooler ($T \sim 10^{6.0}$ K) component is responsible for the majority of the halo emission observed at $\frac{1}{4}$ keV. This is a different physical model than that assumed by several other groups studying the diffuse X-ray background, who attribute the halo emission to a single component. A physical justification for a bimodal temperature distribution of halo plasma is provided by the nature of plasma cooling curves.

We wish to thank Robin Shelton for useful discussions concerning plasma cooling curves. We would also like to enthusiastically thank the referee for their comments and suggestions, which significantly improved the presentation of this paper.

Table 1. Results.

Shadow Num.	Shadow Name	Coordinates[a] l	Coordinates[a] b	Size[b]	Band R1 I_0[c]	Band R1 I_1[c]	χ^2_ν[d]	Band R2 I_0[c]	Band R2 I_1[c]	χ^2_ν[d]	Band R12 I_0[c]	Band R12 I_1[c]	χ^2_ν[d]	[illegible]
1	S0047M461	4.69	-46.09	6.00	204 ± 7	488 ± 140	1.01	236 ± 9	572 ± 83	1.05	463 ± 12	1047 ± 148	1.08	[illegible]
2	S0049M557	4.92	-55.66	4.80	329 ± 42	< 428[f]	1.16	352 ± 65	482 ± 217	1.29	714 ± 77	698 ± 328	1.31	[illegible]
3	S0070M826	7.03	-82.64	4.00	185 ± 32	< 259	1.11	234 ± 51	< 309	1.06	447 ± 60	< 449	1.11	[illegible]
4	S0078M352	7.82	-35.18	6.00	129 ± 12	1481 ± 357	0.91	117 ± 17	1613 ± 206	0.92	266 ± 21	3224 ± 370	0.97	[illegible]
5	S0131M461	13.09	-46.12	4.00	180 ± 9	1496 ± 352	1.23	190 ± 10	1957 ± 183	1.07	399 ± 14	3538 ± 343	1.10	[illegible]
6	S0138M511	13.78	-51.06	3.20	142 ± 35	1869 ± 424	1.08	119 ± 53	1814 ± 311	1.37	281 ± 64	3666 ± 509	1.42	[illegible]
7	S0140M637	13.98	-63.70	4.00	263 ± 66	524 ± 371	1.45	327 ± 105	584 ± 339	1.17	719 ± 124	774 ± 511	1.38	[illegible]
8	S0142M538	14.15	-53.82	3.20	248 ± 34	822 ± 306	1.14	343 ± 52	691 ± 240	1.13	610 ± 62	1491 ± 383	1.16	[illegible]
9	S0179M484	17.90	-48.43	4.00	210 ± 21	1146 ± 389	0.99	239 ± 29	1374 ± 245	1.05	470 ± 36	2552 ± 424	1.18	[illegible]
10	S0183M346	18.32	-34.63	3.20	104 ± 14	1959 ± 787	0.82	137 ± 19	1400 ± 403	1.16	260 ± 24	3078 ± 748	1.02	[illegible]
11	S0195M448	19.51	-44.81	4.00	176 ± 10	1567 ± 378	1.18	201 ± 12	1743 ± 203	1.25	398 ± 16	3349 ± 373	1.34	[illegible]
12	S0201M530	20.13	-53.04	4.00	160 ± 27	1549 ± 246	1.02	243 ± 43	1173 ± 199	1.21	404 ± 51	2714 ± 314	1.23	[illegible]
13	S0237M437	23.67	-43.66	3.20	184 ± 25	< 1000	1.07	228 ± 37	857 ± 387	1.16	448 ± 46	1184 ± 675	1.12	[illegible]
14	S0248M357	24.76	-35.73	4.00	143 ± 10	1244 ± 657	1.03	188 ± 14	1766 ± 357	1.18	349 ± 17	3213 ± 648	1.10	[illegible]
15	S0250M679	25.05	-67.90	6.00	215 ± 33	< 405	0.90	225 ± 47	282 ± 237	1.04	460 ± 61	790 ± 411	1.01	[illegible]
16	S0260M309	26.01	-30.93	3.20	74 ± 16	2924 ± 579	0.97	49 ± 22	3478 ± 333	1.37	132 ± 28	6849 ± 598	1.43	[illegible]
17	S0261M499	26.11	-49.87	6.00	139 ± 12	1729 ± 224	1.12	196 ± 19	1230 ± 148	1.10	354 ± 23	2783 ± 253	1.17	[illegible]
18	S0291P828	29.05	82.79	4.00	270 ± 32	380 ± 138	1.13	329 ± 49	297 ± 133	1.20	580 ± 58	757 ± 193	1.29	[illegible]
19	S0332M526	33.21	-52.65	6.00	256 ± 26	497 ± 303	1.16	286 ± 39	889 ± 221	1.12	582 ± 47	1403 ± 364	1.20	[illegible]
20	S0341M405	34.12	-40.52	6.00	114 ± 7	2612 ± 313	1.17	141 ± 9	2300 ± 174	1.28	272 ± 12	4808 ± 314	1.39	[illegible]
21	S0363P770	36.25	76.95	4.80	281 ± 34	274 ± 149	1.37	371 ± 52	163 ± 142	1.45	666 ± 61	425 ± 208	1.68	[illegible]
22	S0370M829	37.03	-82.86	4.00	139 ± 46	294 ± 269	1.08	164 ± 72	299 ± 239	1.27	329 ± 86	573 ± 364	1.25	[illegible]
23	S0373P446	37.28	44.65	3.20	168 ± 10	2981 ± 776	1.16	181 ± 12	2974 ± 352	1.24	362 ± 16	5906 ± 679	1.29	[illegible]
24	S0382M571	38.25	-57.08	4.00	229 ± 13	< 483	1.42	218 ± 39	728 ± 299	1.82	470 ± 50	1104 ± 531	2.05	[illegible]
25	S0383M214	38.26	-21.43	3.20	96 ± 9	4181 ± 1021	0.88	123 ± 12	3233 ± 469	1.11	232 ± 15	7277 ± 898	1.09	[illegible]
26	S0383M308	38.26	-30.84	3.20	117 ± 14	4032 ± 1130	1.29	205 ± 20	2673 ± 590	1.13	350 ± 25	5755 ± 1089	1.25	[illegible]
27	S0394M341	39.41	-34.10	6.00	128 ± 5	1671 ± 260	1.15	171 ± 6	2021 ± 140	1.17	318 ± 8	3811 ± 256	1.21	[illegible]
28	S0395M463	39.48	-46.33	4.00	169 ± 16	552 ± 506	1.18	199 ± 21	786 ± 271	1.16	394 ± 27	1423 ± 501	1.19	[illegible]
29	S0399M644	39.89	-64.37	4.80	157 ± 60	< 1205	0.84	< 88	1528 ± 550	0.99	239 ± 112	2181 ± 955	0.96	[illegible]
30	S0413P245	41.30	24.50	4.00	155 ± 12	1699 ± 804	1.22	214 ± 17	778 ± 390	1.37	385 ± 22	1954 ± 739	1.39	[illegible]
31	S0415M543	41.54	-54.29	4.00	92 ± 38	2447 ± 580	1.25	< 58	2771 ± 404	1.44	102 ± 70	5295 ± 677	1.71	[illegible]
32	S0421P585	42.14	58.45	4.00	214 ± 15	< 337	1.07	209 ± 20	630 ± 136	1.17	446 ± 25	915 ± 238	0.97	[illegible]
33	S0422P634	42.23	63.43	4.00	235 ± 17	428 ± 133	1.06	262 ± 25	542 ± 106	1.27	514 ± 31	981 ± 168	1.20	[illegible]
34	S0425M248	42.54	-24.79	3.20	114 ± 11	4504 ± 900	1.26	148 ± 15	3869 ± 439	1.11	275 ± 19	8210 ± 827	1.28	[illegible]
35	S0429M310	42.95	-30.99	3.20	136 ± 15	1315 ± 734	1.04	152 ± 21	2599 ± 407	1.08	298 ± 27	4673 ± 738	1.04	[illegible]
36	S0440P399	44.00	39.91	4.80	203 ± 12	< 585	1.36	226 ± 15	474 ± 175	1.28	457 ± 20	606 ± 323	1.33	[illegible]

Table 1—Continued

Shadow		Coordinates[a]		Size[b]	Band R1			Band R2			Band R12			
Num.	Name	l	b		I_0[c]	I_1[c]	χ^2_ν[d]	I_0[c]	I_1[c]	χ^2_ν[d]	I_0[c]	I_1[c]	χ^2_ν[d]	ν[e]
37	S0443M268	44.34	-26.76	3.20	109 ± 18	3085 ± 806	1.15	107 ± 27	3341 ± 462	1.46	238 ± 34	6510 ± 831	1.51	192
38	S0448P558	44.76	55.84	4.80	207 ± 24	< 377	1.01	250 ± 34	363 ± 174	1.02	490 ± 43	507 ± 290	1.06	410
39	S0450M374	45.00	-37.40	6.00	133 ± 4	1498 ± 168	1.19	169 ± 5	1215 ± 89	1.27	316 ± 7	2681 ± 165	1.34	703
40	S0456M481	45.59	-48.06	4.00	131 ± 23	1269 ± 505	1.03	186 ± 35	1489 ± 328	1.23	353 ± 43	2660 ± 568	1.23	314
41	S0458M325	45.80	-32.45	3.20	123 ± 9	1657 ± 728	0.93	133 ± 11	1665 ± 337	1.01	275 ± 15	3113 ± 649	0.94	191
42	S0461P276	46.06	27.56	4.00	175 ± 12	731 ± 702	1.15	186 ± 15	452 ± 322	1.29	373 ± 20	1127 ± 626	1.23	314
43	S0485P429	48.54	42.92	4.80	164 ± 8	601 ± 101	1.21	174 ± 10	792 ± 69	1.27	352 ± 13	1456 ± 116	1.22	409
44	S0491M253	49.13	-25.35	6.00	104 ± 6	2045 ± 852	0.94	128 ± 8	1706 ± 366	1.18	243 ± 10	3991 ± 728	1.12	695
45	S0505M709	50.54	-70.87	8.00	133 ± 14	529 ± 154	1.19	107 ± 21	664 ± 112	1.23	264 ± 26	1254 ± 186	1.29	1241
46	S0506P680	50.56	67.98	4.80	256 ± 25	522 ± 101	1.22	284 ± 39	573 ± 103	1.34	558 ± 45	1088 ± 145	1.56	409
47	S0509M404	50.91	-40.41	6.00	135 ± 14	1548 ± 246	1.19	168 ± 23	1763 ± 175	1.27	328 ± 27	3353 ± 290	1.45	705
48	S0515P386	51.54	38.62	6.00	197 ± 8	598 ± 120	1.13	189 ± 11	839 ± 77	1.21	402 ± 14	1491 ± 134	1.32	705
49	S0516M300	51.56	-30.03	4.00	133 ± 8	3536 ± 949	0.87	169 ± 10	2058 ± 407	1.18	312 ± 13	5076 ± 804	1.12	314
50	S0531M553	53.10	-55.33	8.00	186 ± 7	< 387	0.85	200 ± 18	386 ± 220	1.01	421 ± 24	602 ± 418	0.89	1158
51	S0532P549	53.23	54.87	4.00	209 ± 42	< 506	1.01	242 ± 62	384 ± 298	1.10	486 ± 76	511 ± 486	1.05	305
52	S0560P638	56.00	63.84	4.00	309 ± 30	< 260	2.58	384 ± 47	159 ± 132	3.20	692 ± 54	328 ± 192	4.83	315
53	S0567M402	56.67	-40.22	6.00	120 ± 6	1548 ± 279	1.02	133 ± 7	1775 ± 143	1.08	270 ± 9	3515 ± 267	1.15	668
54	S0573P409	57.34	40.88	3.20	219 ± 39	796 ± 303	0.97	231 ± 62	885 ± 253	1.22	454 ± 73	1748 ± 391	1.15	195
55	S0576P711	57.58	71.08	4.00	387 ± 9	< 61	1.16	448 ± 10	< 108	1.49	850 ± 14	< 81	1.44	316
56	S0578P488	57.77	48.81	6.00	188 ± 15	506 ± 87	1.25	215 ± 22	500 ± 77	1.49	419 ± 26	1019 ± 116	1.62	704
57	S0599M878	59.93	-87.80	4.80	183 ± 6	< 47	1.35	279 ± 7	< 45	1.40	484 ± 8	< 67	1.59	440
58	S0603P397	60.33	39.72	3.20	274 ± 36	541 ± 212	1.10	279 ± 50	768 ± 169	1.25	577 ± 62	1321 ± 269	1.32	195
59	S0604P359	60.43	35.93	4.00	181 ± 11	1117 ± 114	0.94	179 ± 16	1142 ± 86	1.26	367 ± 20	2258 ± 139	1.32	315
60	S0610P137	60.96	13.69	6.00	150 ± 3	2947 ± 782	1.09	186 ± 4	2457 ± 311	1.24	348 ± 5	5024 ± 620	1.21	706
61	S0611P324	61.07	32.38	3.20	183 ± 22	< 913	1.10	209 ± 31	859 ± 287	1.15	404 ± 39	1412 ± 500	1.25	195
62	S0611M340	61.11	-34.01	3.20	128 ± 11	996 ± 650	1.04	138 ± 15	1957 ± 347	1.17	283 ± 19	3369 ± 637	1.33	187
63	S0614P281	61.37	28.15	6.00	204 ± 9	1009 ± 148	1.21	254 ± 14	1133 ± 101	1.42	468 ± 17	2161 ± 169	1.49	707
64	S0618M294	61.79	-29.38	8.00	142 ± 5	1652 ± 198	1.13	184 ± 7	2065 ± 115	1.30	345 ± 8	3859 ± 204	1.37	1245
65	S0623P339	62.34	33.89	3.20	200 ± 18	512 ± 438	1.39	233 ± 25	567 ± 256	1.40	453 ± 31	980 ± 456	1.40	195
66	S0629P354	62.91	35.37	3.20	193 ± 14	988 ± 284	1.28	196 ± 19	1042 ± 174	1.23	402 ± 24	2004 ± 305	1.28	195
67	S0640P756	63.97	75.61	4.00	312 ± 35	253 ± 170	1.28	333 ± 54	355 ± 158	1.29	669 ± 64	601 ± 233	1.45	315
68	S0646P316	64.55	31.58	3.20	194 ± 24	< 797	1.44	238 ± 36	574 ± 313	1.60	438 ± 43	1020 ± 538	1.95	195
69	S0646P468	64.59	46.80	4.00	213 ± 44	688 ± 144	1.69	216 ± 71	730 ± 156	2.62	459 ± 81	1402 ± 214	2.96	315
70	S0663M410	66.30	-41.02	4.80	123 ± 8	1392 ± 337	0.81	160 ± 10	887 ± 173	0.92	304 ± 13	2119 ± 325	0.88	415
71	S0669M588	66.85	-58.84	6.00	147 ± 17	817 ± 355	1.01	177 ± 24	608 ± 215	1.25	358 ± 31	1234 ± 383	1.16	700
72	S0674P246	67.37	24.63	2.80	185 ± 13	868 ± 271	1.01	239 ± 18	970 ± 166	1.26	432 ± 22	1837 ± 288	1.48	147

Table 1—Continued

Shadow		Coordinates[a]		Size[b]	Band R1			Band R2			Band R12		
Num.	Name	l	b		I_0[c]	I_1[c]	χ^2_ν[d]	I_0[c]	I_1[c]	χ^2_ν[d]	I_0[c]	I_1[c]	χ^2_ν[d]
73	S0684P527	68.40	52.67	6.00	210 ± 12	791 ± 91	1.51	213 ± 19	809 ± 77	1.38	431 ± 22	1635 ± 116	1.82
74	S0689P459	68.87	45.93	3.20	431 ± 70	709 ± 275	1.52	446 ± 110	742 ± 277	2.01	919 ± 128	1392 ± 394	2 28
75	S0697M219	69.67	-21.90	4.00	169 ± 12	< 2545	1.29	238 ± 17	2549 ± 698	1.55	421 ± 21	4296 ± 1304	1.87
76	S0700M510	69.95	-51.04	4.00	163 ± 14	< 1319	1.01	190 ± 8	< 280	0.88	378 ± 17	< 625	1.02
77	S0715P250	71.49	24.99	2.80	188 ± 12	807 ± 277	1.19	257 ± 16	759 ± 166	1.28	452 ± 20	1513 ± 290	1.50
78	S0723P353	72.28	35.28	4.00	195 ± 11	711 ± 127	1.28	208 ± 17	843 ± 95	1.20	413 ± 21	1568 ± 154	1.39
79	S0728P393	72.75	39.28	4.00	220 ± 17	847 ± 109	1.41	278 ± 25	723 ± 93	1.63	499 ± 30	1565 ± 143	1 94
80	S0737P287	73.69	28.73	2.80	188 ± 13	686 ± 198	0.97	230 ± 19	878 ± 139	1.57	425 ± 23	1611 ± 229	1.36
81	S0740P156	74.00	15.60	3.20	169 ± 12	2685 ± 1015	1.13	225 ± 17	2548 ± 489	1.25	403 ± 21	5393 ± 921	1.09
82	S0743P807	74.31	80.75	4.00	296 ± 37	220 ± 144	1.25	385 ± 58	151 ± 144	1.57	679 ± 68	398 ± 206	1.73
83	S0744P429	74.42	42.90	3.20	334 ± 28	630 ± 156	1.47	393 ± 44	575 ± 146	2.04	722 ± 51	1255 ± 215	2.55
84	S0753M451	75.30	-45.13	4.80	136 ± 7	977 ± 573	1.01	149 ± 9	859 ± 259	1.05	305 ± 12	1707 ± 506	1.09
85	S0754P329	75.44	32.91	3.20	183 ± 17	787 ± 178	1.21	181 ± 25	971 ± 133	1.63	374 ± 30	1792 ± 215	1.75
86	S0759M501	75.93	-50.13	4.00	122 ± 9	1169 ± 508	1.09	158 ± 12	586 ± 236	1.25	309 ± 16	1351 ± 465	0.96
87	S0762P170	76.21	17.04	3.20	181 ± 17	1663 ± 785	1.08	273 ± 23	780 ± 402	1.31	464 ± 29	2058 ± 745	1.20
88	S0766P625	76.63	62.50	4.00	231 ± 23	342 ± 124	1.18	268 ± 35	475 ± 113	1.40	525 ± 42	793 ± 169	1.42
89	S0767P552	76.65	55.25	6.00	183 ± 11	1032 ± 72	1.44	175 ± 16	980 ± 60	1.57	364 ± 19	2012 ± 93	1.93
90	S0778P276	77.81	27.62	4.00	205 ± 11	709 ± 292	1.04	252 ± 15	1022 ± 175	1.41	460 ± 19	1858 ± 306	1 44
91	S0780P349	77.99	34.86	3.20	188 ± 14	576 ± 140	1.22	181 ± 21	828 ± 110	1.50	373 ± 25	1490 ± 175	1.59
92	S0783P727	78.30	72.68	4.00	349 ± 21	141 ± 85	1.19	387 ± 32	275 ± 83	1.33	751 ± 38	427 ± 120	1.50
93	S0788M583	78.76	-58.30	8.00	163 ± 11	391 ± 240	1.00	199 ± 16	364 ± 144	1.10	385 ± 20	704 ± 256	1.03
94	S0795P457	79.47	45.68	3.20	191 ± 32	1551 ± 230	1.32	219 ± 50	1264 ± 195	1.46	419 ± 59	2745 ± 300	1.64
95	S0802P420	80.23	42.04	3.20	284 ± 27	352 ± 258	1.10	273 ± 36	691 ± 177	1.44	565 ± 45	1220 ± 299	1 41
96	S0806P375	80.56	37.45	3.20	185 ± 9	841 ± 89	1.46	204 ± 11	922 ± 64	1.82	393 ± 14	1794 ± 105	2 35
97	S0815P690	81.48	68.95	4.00	332 ± 26	190 ± 85	1.40	470 ± 40	< 132	1.35	795 ± 46	247 ± 125	1.55
98	S0815P577	81.51	57.73	3.20	236 ± 21	503 ± 160	1.24	284 ± 31	455 ± 129	1.24	527 ± 38	952 ± 203	1.35
99	S0816P396	81.56	39.59	3 20	212 ± 10	911 ± 114	1.12	224 ± 13	891 ± 81	1.60	440 ± 16	1847 ± 135	1.62
100	S0829M778	82.93	-77.78	4.00	136 ± 24	446 ± 258	1.14	223 ± 35	218 ± 188	1.20	368 ± 43	675 ± 310	1.31
101	S0832M371	83.22	-37.09	6.00	117 ± 5	292 ± 225	1.15	137 ± 7	372 ± 115	1.14	270 ± 9	691 ± 217	1.21
102	S0853P257	85.35	25.69	4.00	217 ± 8	697 ± 220	1.47	260 ± 11	859 ± 125	1.91	482 ± 14	.1584 ± 224	2.30
103	S0854M663	85.38	-66.25	4.00	192 ± 7	< 292	1.16	222 ± 38	< 516	1.21	470 ± 48	< 468	1.24
104	S0854M555	85.45	-55.47	6.00	154 ± 9	699 ± 189	0.94	188 ± 11	409 ± 106	1.10	360 ± 15	993 ± 194	1.01
105	S0862P383	86.22	38.25	3.20	265 ± 27	474 ± 169	1.16	235 ± 39	844 ± 140	1.61	521 ± 48	1360 ± 218	1.88
106	S0866P286	86.58	28.58	2.80	207 ± 10	1054 ± 216	1.44	252 ± 14	1005 ± 131	1.80	461 ± 17	2012 ± 228	2.19
107	S0867P599	86.72	59.91	3.20	242 ± 17	444 ± 159	1.21	281 ± 24	475 ± 114	1.33	534 ± 30	903 ± 189	1.52
108	S0873P539	87.26	53.86	3.20	313 ± 32	424 ± 170	1.45	345 ± 48	503 ± 152	1.25	672 ± 57	927 ± 228	1.55

Table 1—Continued

Shadow Num.	Shadow Name	Coordinates[a] l	Coordinates[a] b	Size[b]	Band R1 I_0[c]	Band R1 I_1[c]	χ^2_ν[d]	Band R2 I_0[c]	Band R2 I_1[c]	χ^2_ν[d]	Band R12 I_0[c]	Band R12 I_1[c]	χ^2_ν[d]	ν[e]
109	S0877P574	87.68	57.44	3.20	308 ± 20	457 ± 149	1.08	299 ± 28	637 ± 115	1.50	622 ± 35	1111 ± 184	1.49	195
110	S0877M462	87.72	-46.21	8.00	140 ± 4	453 ± 154	1.05	169 ± 5	420 ± 77	1.13	328 ± 7	807 ± 146	1.06	1252
111	S0878P361	87.76	36.09	2.80	183 ± 20	772 ± 171	1.19	158 ± 28	1092 ± 130	1.46	352 ± 34	1934 ± 209	1.55	147
112	S0886P449	88.56	44.93	4.00	355 ± 18	490 ± 73	2.08	410 ± 28	564 ± 73	2.52	769 ± 33	1071 ± 104	3.58	315
113	S0890P269	89.02	26.95	3.20	246 ± 10	294 ± 212	1.31	322 ± 15	317 ± 132	1.60	570 ± 18	604 ± 228	1.81	195
114	S0891M414	89.13	-41.39	6.00	133 ± 4	646 ± 232	1.04	158 ± 5	475 ± 108	1.26	309 ± 7	1020 ± 209	1.13	705
115	S0894P325	89.43	32.53	2.80	172 ± 9	1379 ± 174	2.01	199 ± 12	1155 ± 110	1.42	370 ± 15	2478 ± 189	2.24	147
116	S0896P386	89.64	38.63	2.80	220 ± 11	1387 ± 84	1.70	259 ± 14	1357 ± 61	2.01	485 ± 18	2732 ± 100	2.68	147
117	S0902M614	90.20	-61.40	6.00	170 ± 15	< 306	1.07	195 ± 21	324 ± 151	1.17	387 ± 26	462 ± 261	1.12	702
118	S0906P315	90.56	31.49	2.80	200 ± 9	636 ± 160	1.83	232 ± 12	774 ± 100	1.81	437 ± 15	1421 ± 173	2.41	147
119	S0915M325	91.48	-32.53	3.60	151 ± 6	1090 ± 409	0.98	182 ± 7	660 ± 188	1.20	349 ± 10	1469 ± 363	1.07	251
120	S0923P399	92.33	39.89	2.80	213 ± 10	1573 ± 100	1.97	236 ± 15	1617 ± 77	2.49	453 ± 18	3201 ± 123	3.28	147
121	S0926P336	92.64	33.57	3.20	212 ± 14	441 ± 171	1.55	302 ± 21	260 ± 122	2.34	516 ± 25	634 ± 200	2.71	195
122	S0932P630	93.22	63.01	4.80	308 ± 21	348 ± 115	1.49	344 ± 30	377 ± 99	1.57	660 ± 36	744 ± 152	1.85	439
123	S0934P714	93.40	71.39	4.00	229 ± 25	560 ± 87	1.50	269 ± 39	536 ± 91	1.38	507 ± 45	1091 ± 127	1.94	315
124	S0936P184	93.64	18.37	6.00	180 ± 4	2725 ± 313	1.20	213 ± 6	2543 ± 146	1.85	399 ± 7	5113 ± 278	2.02	707
125	S0941P457	94.11	45.69	4.00	244 ± 24	1103 ± 103	1.78	220 ± 38	1243 ± 101	2.93	473 ± 44	2364 ± 145	3.67	315
126	S0947P375	94.66	37.54	2.80	186 ± 12	1361 ± 140	1.80	207 ± 17	1437 ± 96	2.24	396 ± 21	2820 ± 160	3.01	147
127	S0956P327	95.59	32.71	3.20	183 ± 8	810 ± 134	1.57	232 ± 11	804 ± 88	2.38	415 ± 14	1616 ± 149	2.87	195
128	S0958M331	95.84	-33.12	6.00	129 ± 4	< 801	1.01	161 ± 5	290 ± 185	1.17	305 ± 7	603 ± 362	1.16	684
129	S0959M554	95.89	-55.40	6.00	143 ± 5	105 ± 91	1.03	166 ± 7	250 ± 57	1.18	325 ± 9	405 ± 99	1.20	696
130	S0971P265	97.07	26.49	3.20	187 ± 5	< 347	1.91	270 ± 3	< 45	4.32	460 ± 4	< 138	4.85	195
131	S0980P234	98.01	23.41	6.00	165 ± 3	1986 ± 126	1.47	195 ± 4	2019 ± 66	2.59	365 ± 5	3983 ± 120	2.93	707
132	S0983P327	98.33	32.66	3.20	213 ± 7	165 ± 144	1.76	308 ± 10	141 ± 92	2.63	520 ± 12	295 ± 157	3.26	195
133	S0996P366	99.59	36.61	3.20	219 ± 11	561 ± 190	1.81	246 ± 15	658 ± 118	2.63	468 ± 19	1244 ± 205	3.32	195
134	S0999P672	99.92	67.21	4.80	295 ± 14	402 ± 63	1.16	325 ± 21	452 ± 61	1.19	634 ± 25	849 ± 88	1.42	439
135	S1000P520	100.04	52.04	8.00	353 ± 16	797 ± 60	1.77	313 ± 24	862 ± 59	1.87	678 ± 28	1662 ± 84	2.63	1255
136	S1001M607	100.15	-60.73	3.20	152 ± 12	< 269	0.98	183 ± 28	218 ± 184	1.19	355 ± 36	< 600	1.06	192
137	S1007M421	100.71	-42.09	6.00	115 ± 5	< 210	0.98	141 ± 6	270 ± 76	1.01	272 ± 8	384 ± 138	1.07	681
138	S1008P423	100.82	42.31	3.20	181 ± 20	1848 ± 274	2.53	141 ± 28	1599 ± 181	3.54	326 ± 35	3380 ± 307	4.92	195
139	S1011P274	101.08	27.44	3.20	188 ± 8	1004 ± 382	1.97	235 ± 10	446 ± 184	2.26	424 ± 13	1216 ± 348	3.02	195
140	S1018P453	101.77	45.25	4.00	267 ± 14	726 ± 119	1.50	245 ± 21	759 ± 91	2.01	507 ± 25	1561 ± 146	2.39	315
141	S1021M291	102.10	-29.06	6.00	110 ± 3	< 839	1.13	128 ± 4	665 ± 237	1.14	253 ± 6	1021 ± 475	1.18	694
142	S1041P421	104.07	42.13	3.20	211 ± 17	802 ± 197	1.56	247 ± 24	530 ± 134	1.69	456 ± 30	1285 ± 226	2.01	195
143	S1044M628	104.40	-62.80	3.20	154 ± 13	< 237	0.98	154 ± 31	401 ± 190	1.07	339 ± 40	422 ± 330	1.02	194
144	S1050P360	104.99	36.02	3.20	189 ± 12	453 ± 199	1.46	217 ± 16	345 ± 120	1.39	410 ± 20	742 ± 210	1.73	195

Table 1—Continued

Shadow Num.	Shadow Name	Coordinates[a] l	Coordinates[a] b	Size[b]	Band R1 I_0[c]	Band R1 I_1[c]	χ^2_ν[d]	Band R2 I_0[c]	Band R2 I_1[c]	χ^2_ν[d]	Band R12 I_0[c]	Band R12 I_1[c]	χ^2_ν[d]	ν[e]
145	S1061P324	106.11	32.44	3.20	148 ± 17	1299 ± 362	1.19	179 ± 23	843 ± 215	1.39	328 ± 29	1984 ± 378	1.42	195
146	S1062M432	106.20	-43.20	8.00	108 ± 4	< 152	1.00	133 ± 5	212 ± 52	1.10	257 ± 6	329 ± 93	1.09	1195
147	S1062P753	106.21	75.28	4.00	247 ± 35	578 ± 163	1.28	272 ± 54	569 ± 152	1.62	536 ± 63	1119 ± 224	1.86	315
148	S1076M374	107.62	-37.37	6.00	116 ± 5	376 ± 212	0.99	134 ± 6	358 ± 108	1.05	265 ± 8	814 ± 204	1.04	646
149	S1081P696	108.08	69.59	4.80	314 ± 14	254 ± 62	1.28	348 ± 20	320 ± 56	1.45	677 ± 25	575 ± 84	1.66	439
150	S1084M543	108.43	-54.33	4.00	114 ± 5	145 ± 93	1.04	128 ± 6	320 ± 55	1.06	253 ± 8	557 ± 98	1.11	312
151	S1090P463	109.03	46.32	3.20	366 ± 20	209 ± 131	1.32	447 ± 29	112 ± 107	1.45	816 ± 36	303 ± 167	1.76	195
152	S1093P590	109.26	59.01	4.00	390 ± 50	457 ± 139	1.44	564 ± 80	191 ± 157	1.42	942 ± 91	661 ± 210	1.64	315
153	S1093P338	109.34	33.75	3.20	208 ± 23	< 715	1.31	264 ± 32	< 440	1.23	480 ± 40	< 838	1.52	195
154	S1102M225	110.18	-22.51	8.00	127 ± 4	< 1516	0.81	140 ± 5	434 ± 311	0.94	284 ± 7	1144 ± 637	0.93	1118
155	S1120P849	112.01	84.93	4.00	275 ± 51	360 ± 220	1.15	136 ± 78	845 ± 211	1.13	463 ± 92	1184 ± 308	1.31	315
156	S1127P381	112.67	38.15	3.60	202 ± 18	338 ± 229	1.20	262 ± 26	199 ± 156	1.22	476 ± 33	442 ± 263	1.20	251
157	S1131P729	113.11	72.87	6.00	284 ± 17	257 ± 90	1.13	339 ± 25	233 ± 78	1.26	633 ± 30	489 ± 119	1.33	707
158	S1137M311	113.72	-31.06	6.00	109 ± 8	380 ± 265	0.82	116 ± 11	520 ± 141	1.01	243 ± 14	952 ± 262	0.96	626
159	S1145P499	114.54	49.94	3.20	535 ± 31	< 252	1.10	558 ± 41	< 204	1.07	1102 ± 51	< 346	1.25	195
160	S1152P362	115.23	36.20	3.20	247 ± 12	< 280	1.09	308 ± 38	< 266	1.24	573 ± 47	< 387	1.13	196
161	S1165P621	116.47	62.13	4.80	308 ± 24	357 ± 126	1.36	366 ± 36	355 ± 112	1.41	695 ± 43	678 ± 169	1.69	439
162	S1175M537	117.50	-53.66	6.00	119 ± 5	146 ± 133	0.90	135 ± 6	269 ± 81	1.03	269 ± 8	536 ± 145	1.12	646
163	S1175P541	117.51	54.13	6.00	361 ± 17	266 ± 93	1.53	372 ± 25	333 ± 80	1.51	743 ± 30	617 ± 122	1.95	707
164	S1176M681	117.62	-68.08	14.00	137 ± 3	297 ± 45	1.12	143 ± 4	469 ± 29	1.19	299 ± 5	822 ± 51	1.26	3797
165	S1179M389	117.86	-38.89	8.00	130 ± 5	< 108	0.98	146 ± 10	313 ± 79	1.18	293 ± 12	430 ± 136	1.18	1205
166	S1179P409	117.91	40.87	4.00	306 ± 14	196 ± 140	1.43	360 ± 19	212 ± 102	1.26	673 ± 24	402 ± 167	1.66	315
167	S1182M459	118.17	-45.93	4.00	130 ± 10	< 406	0.70	134 ± 12	239 ± 165	0.92	282 ± 16	344 ± 313	0.80	288
168	S1231P714	123.09	71.42	4.00	271 ± 21	671 ± 111	1.34	276 ± 29	632 ± 92	1.26	555 ± 35	1320 ± 143	1.51	315
169	S1240P515	123.98	51.53	3.20	426 ± 11	< 219	1.39	489 ± 12	< 57	1.43	928 ± 16	< 114	1.66	196
170 •	S1250P367	125.02	36.69	8.00	201 ± 4	749 ± 96	1.12	210 ± 4	685 ± 52	1.11	425 ± 6	1405 ± 96	1.21	1253
171	S1253M558	125.34	-55.78	6.00	114 ± 6	182 ± 103	0.95	138 ± 8	223 ± 65	1.19	269 ± 11	433 ± 114	1.13	677
172	S1285M259	128.48	-25.86	6.00	139 ± 10	< 623	1.08	141 ± 13	806 ± 179	1.28	306 ± 18	1195 ± 338	1.18	706
173	S1291P435	129.08	43.52	4.80	294 ± 9	614 ± 69	1.41	320 ± 11	385 ± 46	1.45	623 ± 14	933 ± 79	1.82	439
174	S1298M385	129.84	-38.53	6.00	130 ± 3	< 61	0.97	147 ± 8	176 ± 118	1.00	303 ± 9	< 222	1.03	689
175	S1302P680	130.17	68.01	4.00	348 ± 49	< 367	1.27	342 ± 76	381 ± 214	1.14	721 ± 89	527 ± 311	1.44	315
176	S1341M637	134.07	-63.75	6.00	136 ± 4	< 70	1.05	156 ± 12	136 ± 92	1.09	317 ± 16	< 280	1.08	689
177	S1348M298	134.81	-29.78	6.00	151 ± 4	< 142	1.13	127 ± 20	869 ± 234	1.08	314 ± 26	999 ± 433	1.09	702
178	S1348P407	134.83	40.69	6.00	298 ± 7	260 ± 127	1.30	312 ± 8	344 ± 74	1.19	632 ± 11	596 ± 134	1.40	704
179	S1350P292	134.97	29.22	6.00	193 ± 10	184 ± 134	1.13	184 ± 13	479 ± 89	1.13	392 ± 17	763 ± 152	1.24	707
180	S1353M597	135.27	-59.67	4.00	125 ± 8	< 208	1.01	154 ± 22	< 281	1.24	296 ± 28	< 428	1.22	313

Table 1—Continued

Shadow Num.	Shadow Name	Coordinates[a] l	Coordinates[a] b	Size[b]	Band R1 I_0[c]	Band R1 I_1[c]	Band R1 χ^2_ν[d]	Band R2 I_0[c]	Band R2 I_1[c]	Band R2 χ^2_ν[d]	Band R12 I_0[c]	Band R12 I_1[c]	Band R12 χ^2_ν[d]	ν[e]
181	S1359P512	135.85	51.22	4.00	316 ± 16	263 ± 71	1.20	304 ± 20	254 ± 57	1.45	635 ± 26	502 ± 90	1.52	315
182	S1359P548	135.94	54.80	4.00	281 ± 14	385 ± 95	1.12	285 ± 18	340 ± 70	1.20	578 ± 24	720 ± 115	1.20	315
183	S1361P745	136.05	74.54	6.00	342 ± 18	335 ± 110	1.16	357 ± 26	383 ± 91	1.44	713 ± 31	724 ± 141	1.67	707
184	S1361M467	136.15	-46.68	6.00	133 ± 6	275 ± 187	1.09	153 ± 7	188 ± 96	1.13	303 ± 10	431 ± 182	1.19	695
185	S1369P461	136.89	46.06	3.20	284 ± 35	279 ± 180	1.01	227 ± 52	503 ± 157	1.24	534 ± 62	783 ± 238	1.33	195
186	S1373P585	137.34	58.47	4.00	301 ± 22	266 ± 102	1.28	336 ± 31	276 ± 89	1.49	660 ± 38	516 ± 136	1.58	315
187	S1378M519	137.82	-51.92	6.00	134 ± 3	< 42	1.11	160 ± 3	< 22	1.21	315 ± 5	< 42	1.21	703
188	S1382M397	138.21	-39.74	6.00	154 ± 5	< 433	0.95	164 ± 7	242 ± 149	0.98	336 ± 9	340 ± 290	1.02	704
189	S1394M695	139.37	-69.47	8.00	153 ± 5	171 ± 113	1.01	168 ± 6	190 ± 60	1.19	343 ± 8	343 ± 113	1.16	123
190	S1412P350	141.20	34.99	3.20	221 ± 13	248 ± 186	1.01	238 ± 15	168 ± 107	1.26	478 ± 20	397 ± 194	1.16	195
191	S1414P485	141.41	48.54	3.20	335 ± 18	< 151	1.30	290 ± 22	263 ± 67	1.50	637 ± 29	367 ± 105	1.78	195
192	S1427P816	142.72	81.57	4.80	241 ± 32	559 ± 151	1.25	282 ± 51	562 ± 146	1.31	523 ± 60	1164 ± 212	1.52	43
193	S1436P653	143.65	65.35	8.00	254 ± 14	499 ± 93	1.33	297 ± 21	364 ± 75	1.31	571 ± 25	822 ± 119	1.55	125
194	S1444P502	144.39	50.22	4.00	291 ± 29	212 ± 95	1.25	239 ± 41	361 ± 92	1.53	553 ± 50	572 ± 134	1.70	31
195	S1456M579	145.56	-57.94	4.80	147 ± 5	< 45	1.22	185 ± 24	< 200	1.27	373 ± 9	< 84	1.18	438
196	S1463P442	146.35	44.22	4.00	346 ± 9	< 95	1.20	325 ± 10	183 ± 51	1.18	687 ± 14	225 ± 84	1.43	315
197	S1519P503	151.92	50.34	3.20	214 ± 38	500 ± 107	1.47	311 ± 57	240 ± 112	1.42	529 ± 67	715 ± 156	1.85	19
198	S1533P367	153.29	36.72	4.00	267 ± 10	< 388	0.98	254 ± 11	< 404	1.19	546 ± 15	< 525	1.11	316
199	S1556P502	155.60	50.23	3.20	308 ± 34	238 ± 107	1.12	254 ± 46	388 ± 101	1.36	580 ± 57	648 ± 148	1.31	19
200	S1559P741	155.85	74.06	4.00	296 ± 27	354 ± 165	1.19	284 ± 39	521 ± 137	1.34	613 ± 48	877 ± 215	1.33	31
201	S1571P532	157.05	53.21	3.20	292 ± 28	315 ± 121	1.36	316 ± 40	251 ± 109	1.15	609 ± 48	588 ± 163	1.43	19
202	S1596P436	159.64	43.63	4.00	317 ± 21	< 217	0.94	307 ± 27	< 217	1.10	643 ± 35	< 323	1.09	315
203	S1601P618	160.14	61.75	6.00	315 ± 23	548 ± 104	1.22	297 ± 34	594 ± 95	1.19	630 ± 40	1143 ± 141	1.38	707
204	S1603P554	160.29	55.38	3.20	307 ± 34	436 ± 167	1.33	351 ± 48	260 ± 142	1.42	660 ± 59	688 ± 218	1.67	195
205	S1621P681	162.06	68.11	3.20	346 ± 65	< 954	1.19	450 ± 21	< 394	1.17	824 ± 116	< 942	1.10	195
206	S1637M681	163.73	-68.10	4.80	156 ± 20	244 ± 184	1.17	139 ± 28	426 ± 136	1.23	312 ± 35	746 ± 224	1.28	438
207	S1664M870	166.43	-87.02	4.00	166 ± 28	214 ± 201	1.01	147 ± 39	506 ± 154	1.23	357 ± 49	694 ± 251	1.19	31
208	S1685P473	168.53	47.28	3.20	303 ± 32	197 ± 146	1.13	314 ± 45	159 ± 128	1.18	625 ± 55	364 ± 194	1.25	194
209	S1699M791	169.93	-79.12	3.20	187 ± 26	356 ± 194	1.14	159 ± 35	465 ± 144	1.55	362 ± 44	899 ± 237	1.41	195
210	S1700P578	170.03	57.80	4.80	346 ± 24	419 ± 120	1.29	406 ± 36	286 ± 108	1.29	765 ± 43	674 ± 161	1.48	439
211	S1720P706	171.95	70.62	3.20	300 ± 45	< 645	1.38	348 ± 68	< 536	1.12	694 ± 84	< 878	1.28	193
212	S1763P474	176.28	47.44	4.00	330 ± 28	348 ± 142	1.13	292 ± 41	437 ± 125	1.35	623 ± 50	850 ± 189	1.55	315
213	S1768M593	176.79	-59.29	4.00	179 ± 32	< 451	1.14	178 ± 45	< 484	1.52	356 ± 56	543 ± 441	1.70	314
214	S1770M651	176.99	-65.07	4.80	127 ± 35	375 ± 294	1.00	180 ± 51	< 373	1.18	329 ± 63	439 ± 361	1.19	435
215	S1789P647	178.86	64.69	4.00	362 ± 10	< 137	7.95	391 ± 11	< 79	16.39	767 ± 15	< 118	23.30	316
216	S1789P535	178.88	53.48	6.00	448 ± 6	< 69	1.37	506 ± 7	< 50	1.66	969 ± 9	< 53	1.85	708

Table 1—Continued

Shadow		Coordinates[a]		Size[b]	Band R1			Band R2			Band R12			
Num.	Name	l	b		I_0[c]	I_1[c]	χ^2_ν[d]	I_0[c]	I_1[c]	χ^2_ν[d]	I_0[c]	I_1[c]	χ^2_ν[d]	ν[e]
217	S1792M827	179.22	-82.69	4.00	174 ± 30	220 ± 197	1.38	62 ± 44	755 ± 163	1.40	254 ± 54	1119 ± 255	1.68	315
218	S1839P302	183.91	30.23	3.20	159 ± 28	1566 ± 976	1.18	196 ± 35	490 ± 477	1.06	393 ± 47	1210 ± 921	1.24	195
219	S1860P403	186.03	40.28	4.00	167 ± 23	541 ± 280	0.91	180 ± 35	379 ± 200	0.99	365 ± 42	857 ± 332	0.99	307
220	S1861M721	186.13	-72.13	4.80	153 ± 15	359 ± 104	1.17	177 ± 22	306 ± 84	1.42	348 ± 27	637 ± 133	1.46	439
221	S1863P325	186.26	32.49	4.00	195 ± 11	< 845	1.21	172 ± 27	492 ± 399	1.15	368 ± 36	1204 ± 787	1.35	314
222	S1868P600	186.77	59.95	4.80	427 ± 31	457 ± 165	1.41	356 ± 46	754 ± 145	1.53	810 ± 56	1244 ± 220	1.86	439
223	S1888P737	188.83	73.65	4.80	193 ± 42	1001 ± 321	1.00	173 ± 61	850 ± 248	1.17	387 ± 76	1817 ± 400	1.11	439
224	S1911P696	191.09	69.61	4.00	297 ± 34	260 ± 254	1.20	299 ± 49	306 ± 198	1.34	638 ± 60	520 ± 318	1.25	315
225	S1917P565	191.72	56.54	4.00	342 ± 32	605 ± 158	1.44	376 ± 46	447 ± 139	1.48	731 ± 56	1024 ± 211	1.83	315
226	S1923M679	192.33	-67.85	4.00	228 ± 11	< 189	1.56	247 ± 25	< 266	1.33	495 ± 32	< 474	1.62	316
227	S1947P657	194.67	65.73	4.00	368 ± 34	< 312	1.15	361 ± 48	281 ± 199	1.29	763 ± 59	324 ± 323	1.49	315
228	S1969M646	196.85	-64.61	3.20	322 ± 13	< 199	1.35	289 ± 43	< 471	1.11	653 ± 56	< 592	1.39	195
229	S1983P357	198.26	35.67	4.00	184 ± 28	< 666	0.90	193 ± 39	< 696	0.97	392 ± 50	< 1180	1.06	302
230	S1984P321	198.37	32.14	3.20	190 ± 20	< 728	1.20	224 ± 25	238 ± 213	1.10	453 ± 33	< 761	1.10	195
231	S1985P565	198.54	56.51	4.80	363 ± 24	341 ± 224	1.11	441 ± 34	< 280	1.25	814 ± 42	420 ± 265	1.43	439
232	S2016P421	201.55	42.06	8.00	156 ± 8	947 ± 96	1.08	136 ± 11	890 ± 65	1.30	311 ± 14	1816 ± 110	1.28	1247
233	S2020P849	202.01	84.93	4.80	265 ± 29	563 ± 192	1.25	305 ± 43	474 ± 160	1.45	591 ± 52	977 ± 248	1.58	439
234	S2030M805	203.04	-80.54	3.20	179 ± 33	216 ± 160	1.17	104 ± 47	527 ± 138	1.34	322 ± 58	742 ± 213	1.31	195
235	S2043P662	204.28	66.24	4.00	378 ± 35	410 ± 285	1.07	378 ± 48	441 ± 208	1.11	769 ± 60	915 ± 342	1.19	315
236	S2045M738	204.50	-73.79	3.20	233 ± 47	< 286	1.17	187 ± 70	310 ± 218	1.45	448 ± 85	351 ± 332	1.72	195
237	S2061M627	206.09	-62.69	4.80	349 ± 9	< 147	1.43	359 ± 9	< 75	1.28	731 ± 11	< 111	1.69	440
238	S2062M520	206.22	-51.96	3.20	234 ± 16	1454 ± 531	1.16	179 ± 16	627 ± 223	1.25	435 ± 23	1929 ± 462	1.32	194
239	S2070P734	207.03	73.44	4.00	249 ± 62	< 906	1.17	201 ± 91	670 ± 380	1.36	502 ± 111	1002 ± 610	1.46	315
240	S2081P503	208.08	50.34	8.00	266 ± 11	< 144	1.19	306 ± 16	131 ± 84	1.25	593 ± 20	151 ± 141	1.38	1255
241	S2098P617	209.77	61.72	6.00	371 ± 15	445 ± 138	1.18	440 ± 21	220 ± 100	1.27	830 ± 26	583 ± 162	1.43	707
242	S2107P443	210.65	44.28	4.80	187 ± 14	412 ± 197	1.08	211 ± 20	443 ± 130	1.12	410 ± 25	896 ± 222	1.16	439
243	S2128M511	212.82	-51.06	3.20	219 ± 17	704 ± 286	1.12	191 ± 20	503 ± 160	1.39	420 ± 27	1298 ± 295	1.37	194
244	S2151P263	215.08	26.33	3.20	239 ± 19	< 651	1.17	228 ± 24	701 ± 199	1.08	479 ± 31	1369 ± 354	1.11	194
245	S2156P371	215.59	37.11	6.00	201 ± 11	181 ± 142	1.21	209 ± 15	427 ± 97	1.14	437 ± 19	617 ± 164	1.31	707
246	S2184M789	218.42	-78.88	4.00	218 ± 48	< 324	1.18	243 ± 70	< 290	1.49	493 ± 85	< 412	1.54	315
247	S2194M696	219.41	-69.57	4.00	411 ± 9	< 74	1.34	440 ± 10	< 178	1.02	870 ± 14	< 98	1.24	316
248	S2195M494	219.49	-49.37	3.20	231 ± 18	614 ± 139	1.13	221 ± 24	571 ± 106	1.14	471 ± 30	1173 ± 172	1.28	195
249	S2198P745	219.76	74.47	3.20	311 ± 35	< 635	0.86	349 ± 48	< 426	0.93	664 ± 60	497 ± 386	1.00	195
250	S2199P441	219.92	44.06	6.00	184 ± 10	352 ± 135	1.15	233 ± 14	265 ± 92	1.28	435 ± 18	585 ± 156	1.26	707
251	S2219P369	221.94	36.88	6.00	205 ± 9	< 277	1.19	264 ± 12	< 143	1.26	491 ± 15	< 271	1.27	706
252	S2222P609	222.18	60.95	4.00	295 ± 28	1121 ± 341	0.97	320 ± 37	840 ± 218	1.24	625 ± 47	2003 ± 379	1.02	315

Table 1—Continued

Shadow Num.	Shadow Name	Coordinates[a] l	Coordinates[a] b	Size[b]	Band R1 I_0[c]	Band R1 I_1[c]	Band R1 χ^2_ν[d]	Band R2 I_0[c]	Band R2 I_1[c]	Band R2 χ^2_ν[d]	Band R12 I_0[c]	Band R12 I_1[c]	Band R12 χ^2_ν[d]	
253	S2223M405	222.30	-40.48	8.00	157 ± 9	1292 ± 152	1.23	158 ± 12	1047 ± 98	1.24	335 ± 15	2286 ± 170	1.43	1
254	S2229P543	222.92	54.33	4.80	168 ± 14	1046 ± 219	1.05	186 ± 19	631 ± 134	1.27	364 ± 24	1605 ± 237	1.25	4
255	S2246P257	224.58	25.70	3.20	235 ± 18	< 485	1.18	208 ± 32	496 ± 270	1.25	475 ± 44	737 ± 497	1.18	1
256	S2259M349	225.92	-34.86	6.00	148 ± 12	1416 ± 156	1.22	114 ± 17	1179 ± 105	1.50	278 ± 21	2532 ± 179	1.59	7
257	S2266M473	226.55	-47.28	4.00	200 ± 13	828 ± 83	1.15	211 ± 18	722 ± 67	1.56	424 ± 22	1535 ± 106	1.68	3
258	S2267M661	226.70	-66.06	4.00	356 ± 25	387 ± 159	1.08	266 ± 28	569 ± 100	1.48	655 ± 39	947 ± 178	1.50	3
259	S2271M209	227.10	-20.93	2.40	224 ± 9	< 297	1.03	271 ± 12	< 288	1.18	503 ± 14	< 293	1.46	1
260	S2279M285	227.90	-28.46	3.20	184 ± 20	1343 ± 318	1.30	191 ± 25	1022 ± 184	1.37	402 ± 34	2184 ± 335	1.46	1
261	S2287P516	228.66	51.59	4.80	200 ± 16	287 ± 284	1.09	223 ± 22	278 ± 174	1.13	441 ± 28	535 ± 307	1.18	4
262	S2289M180	228.86	-17.99	3.20	172 ± 13	2750 ± 769	1.06	210 ± 16	1173 ± 363	0.90	388 ± 21	3216 ± 692	1.16	1
263	S2295M456	229.50	-45.63	4.80	183 ± 9	794 ± 80	1.12	201 ± 12	709 ± 60	1.47	398 ± 15	1488 ± 98	1.47	4
264	S2303M284	230.26	-28.43	3.20	180 ± 24	1279 ± 303	1.20	202 ± 30	853 ± 183	1.32	400 ± 40	1978 ± 326	1.33	1
265	S2305M219	230.50	-21.93	2.40	138 ± 59	1942 ± 1028	0.91	144 ± 85	1391 ± 655	1.21	317 ± 105	2887 ± 1128	1.02	1
266	S2306P622	230.59	62.16	4.80	302 ± 30	354 ± 213	1.31	401 ± 44	< 268	1.21	715 ± 53	429 ± 270	1.43	4
267	S2307M403	230.73	-40.27	4.00	215 ± 37	791 ± 392	1.06	177 ± 50	1019 ± 261	1.04	472 ± 65	1617 ± 457	1.13	2
268	S2321M310	232.05	-31.00	4.00	217 ± 21	1026 ± 172	1.19	163 ± 28	1074 ± 125	1.15	398 ± 36	2109 ± 206	1.32	3
269	S2326M246	232.60	-24.60	2.40	234 ± 42	< 1092	1.12	234 ± 59	668 ± 362	1.55	491 ± 74	1153 ± 619	1.63	1
270	S2345P562	234.54	56.24	4.80	187 ± 27	479 ± 286	1.12	144 ± 40	851 ± 209	1.32	369 ± 50	1342 ± 346	1.40	4
271	S2352P460	235.24	45.95	10.00	224 ± 6	138 ± 65	1.06	267 ± 9	264 ± 46	1.29	514 ± 11	405 ± 77	1.28	1
272	S2356P377	235.65	37.69	6.00	222 ± 6	626 ± 129	1.17	281 ± 7	416 ± 73	1.23	520 ± 9	929 ± 132	1.35	7
273	S2364P750	236.42	74.95	4.00	327 ± 20	436 ± 249	1.33	356 ± 28	396 ± 163	1.65	691 ± 35	883 ± 280	1.90	3
274	S2366M353	236.57	-35.29	3.20	331 ± 35	1280 ± 251	1.15	350 ± 48	701 ± 187	1.32	677 ± 59	1903 ± 305	1.34	1
275	S2367M413	236.75	-41.32	3.20	219 ± 44	843 ± 288	1.23	157 ± 62	1251 ± 230	1.25	465 ± 78	1978 ± 370	1.28	1
276	S2371P188	237.10	18.81	3.20	171 ± 22	725 ± 680	1.22	180 ± 30	1200 ± 375	1.15	373 ± 39	2124 ± 684	1.29	1
277	S2372P255	237.17	25.49	4.00	212 ± 13	436 ± 271	1.31	284 ± 18	378 ± 170	1.08	522 ± 23	682 ± 297	1.33	3
278	S2373M564	237.32	-56.37	4.80	301 ± 28	188 ± 151	1.20	301 ± 39	235 ± 127	1.29	612 ± 49	559 ± 199	1.27	4
279	S2378M377	237.79	-37.74	4.00	474 ± 37	446 ± 194	0.95	460 ± 52	406 ± 161	1.23	948 ± 64	863 ± 250	1.20	3
280	S2378M455	237.81	-45.53	4.80	211 ± 11	524 ± 60	1.04	272 ± 16	393 ± 54	1.28	497 ± 19	884 ± 81	1.24	4
281	S2392P686	239.22	68.58	4.80	261 ± 17	1083 ± 203	1.32	246 ± 23	1008 ± 133	1.15	525 ± 29	2067 ± 228	1.28	4
282	S2396M168	239.55	-16.77	6.00	218 ± 6	1329 ± 357	1.10	206 ± 7	1874 ± 166	1.22	444 ± 9	3255 ± 319	1.14	7
283	S2399M734	239.87	-73.41	4.80	163 ± 30	718 ± 155	1.12	225 ± 44	343 ± 136	1.29	398 ± 53	994 ± 206	1.27	4
284	S2408P344	240.76	34.39	4.00	194 ± 11	612 ± 230	1.23	206 ± 16	988 ± 145	1.06	414 ± 20	1756 ± 251	1.35	3
285	S2421M288	242.15	-28.80	3.20	174 ± 20	1694 ± 426	1.29	161 ± 27	1188 ± 246	1.37	352 ± 34	2654 ± 442	1.35	1
286	S2425M653	242.49	-65.34	4.00	293 ± 17	1332 ± 163	1.66	242 ± 20	999 ± 104	2.10	541 ± 27	2296 ± 181	2.59	3
287	S2432M399	243.17	-39.90	4.00	197 ± 46	1004 ± 337	1.37	283 ± 69	592 ± 271	1.16	475 ± 85	1798 ± 437	1.27	3
288	S2437M448	243.73	-44.79	4.00	248 ± 17	205 ± 134	1.61	338 ± 8	< 69	1.66	611 ± 31	< 252	2.12	3

Table 1—Continued

Shadow Num.	Shadow Name	Coordinates[a] l	Coordinates[a] b	Size[b]	Band R1 I_0[c]	Band R1 I_1[c]	Band R1 χ^2_ν[d]	Band R2 I_0[c]	Band R2 I_1[c]	Band R2 χ^2_ν[d]	Band R12 I_0[c]	Band R12 I_1[c]	Band R12 χ^2_ν[d]	ν
289	S2442P450	244.19	44.98	4.00	199 ± 17	< 849	1.17	246 ± 23	322 ± 308	1.24	478 ± 30	< 991	1.17	31
290	S2445P347	244.55	34.65	4.00	180 ± 9	299 ± 239	1.01	182 ± 11	816 ± 131	1.11	385 ± 15	1205 ± 240	1.04	31
291	S2457P732	245.73	73.16	3.20	300 ± 21	1167 ± 410	1.08	290 ± 25	1096 ± 223	1.23	614 ± 34	2167 ± 412	1.07	19
292	S2468M280	246.84	-28.04	6.00	206 ± 8	703 ± 203	1.28	233 ± 10	242 ± 111	1.56	447 ± 13	797 ± 204	1.68	70
293	S2472P475	247.20	47.49	4.00	216 ± 14	< 965	1.11	263 ± 19	485 ± 301	1.09	493 ± 24	1030 ± 558	1.14	31
294	S2483M436	248.27	-43.64	4.80	192 ± 23	548 ± 143	1.29	184 ± 35	540 ± 122	1.46	402 ± 42	1028 ± 187	1.75	43
295	S2486M322	248.61	-32.21	3.20	137 ± 22	1780 ± 350	1.59	137 ± 31	1166 ± 223	1.51	273 ± 39	2840 ± 385	2.09	19
296	S2489P764	248.90	76.36	3.20	333 ± 25	727 ± 278	1.26	328 ± 35	846 ± 194	1.16	681 ± 44	1591 ± 324	1.22	19
297	S2495P347	249.54	34.73	4.00	176 ± 17	< 1273	1.09	188 ± 21	761 ± 461	0.94	381 ± 28	1358 ± 891	1.01	31
298	S2509P588	250.86	58.81	12.00	251 ± 4	303 ± 60	1.38	267 ± 5	432 ± 39	1.39	540 ± 7	759 ± 68	1.60	28
299	S2540M809	253.97	-80.94	4.00	234 ± 33	< 317	1.18	274 ± 48	< 295	1.16	517 ± 59	< 504	1.51	31
300	S2544P423	254.42	42.33	4.00	160 ± 16	1343 ± 421	1.30	208 ± 23	1009 ± 254	1.48	401 ± 28	2145 ± 453	1.40	31
301	S2551M300	255.11	-30.01	6.00	152 ± 6	1325 ± 199	1.30	152 ± 8	980 ± 106	1.47	308 ± 11	2239 ± 195	1.78	70
302	S2554P729	255.39	72.89	4.00	313 ± 18	1121 ± 291	1.03	242 ± 21	1560 ± 161	1.26	579 ± 28	2750 ± 297	1.21	31
303	S2555M621	255.51	-62.15	4.00	257 ± 33	737 ± 194	1.43	334 ± 50	506 ± 167	1.32	605 ± 60	1179 ± 255	1.53	31
304	S2559P681	255.90	68.11	4.00	371 ± 19	578 ± 293	1.29	366 ± 24	706 ± 174	1.57	753 ± 31	1318 ± 310	1.78	31
305	S2560M560	256.01	-56.01	4.80	394 ± 29	262 ± 149	1.17	365 ± 40	386 ± 123	1.45	787 ± 50	630 ± 193	1.47	43
306	S2573P344	257.34	34.43	6.00	198 ± 4	< 337	1.05	224 ± 10	748 ± 322	1.07	448 ± 14	756 ± 630	1.10	70
307	S2587M464	258.74	-46.44	4.80	102 ± 30	685 ± 130	1.10	144 ± 47	463 ± 125	1.27	266 ± 56	1130 ± 184	1.30	43
308	S2599P486	259.91	48.58	6.00	230 ± 9	688 ± 160	1.17	265 ± 12	763 ± 102	1.13	519 ± 15	1404 ± 177	1.18	70
309	S2614P261	261.42	26.05	4.00	155 ± 18	2428 ± 764	1.00	133 ± 23	2304 ± 390	1.10	313 ± 30	4562 ± 732	1.19	31
310	S2624M289	262.36	-28.95	8.00	176 ± 3	314 ± 148	1.19	187 ± 4	498 ± 70	1.40	370 ± 5	885 ± 134	1.44	12
311	S2632P841	263.23	84.06	4.00	179 ± 19	1249 ± 147	1.45	181 ± 28	1048 ± 115	1.24	369 ± 34	2277 ± 184	1.53	31
312	S2639P429	263.85	42.92	6.00	223 ± 11	668 ± 224	1.07	252 ± 16	869 ± 138	1.22	493 ± 20	1626 ± 242	1.23	70
313	S2643P666	264.31	66.62	4.00	328 ± 21	265 ± 120	1.21	378 ± 31	280 ± 103	1.12	718 ± 37	557 ± 158	1.27	31
314	S2645P806	264.47	80.65	4.00	207 ± 23	1457 ± 276	1.13	203 ± 33	1169 ± 191	1.13	420 ± 41	2556 ± 320	1.29	31
315	S2646M675	264.62	-67.46	4.00	354 ± 8	< 146	1.25	453 ± 9	< 76	1.31	818 ± 12	< 92	1.45	31
316	S2648P234	264.77	23.44	4.00	244 ± 17	1320 ± 1099	1.15	317 ± 23	1374 ± 546	1.51	587 ± 30	2459 ± 1022	1.61	31
317	S2658M582	265.80	-58.21	4.80	405 ± 25	< 361	1.18	481 ± 7	< 130	1.32	902 ± 44	< 331	1.48	43
318	S2659P547	265.88	54.65	6.00	281 ± 8	179 ± 101	1.14	320 ± 10	294 ± 67	1.19	624 ± 14	465 ± 114	1.18	70
319	S2688P435	268.85	43.54	4.00	233 ± 7	< 411	1.01	255 ± 23	456 ± 380	1.08	521 ± 30	< 979	1.14	31
320	S2692M522	269.23	-52.22	4.00	243 ± 18	981 ± 107	1.26	193 ± 24	711 ± 82	1.46	449 ± 31	1613 ± 132	1.46	31
321	S2694M311	269.44	-31.08	6.00	193 ± 5	223 ± 142	1.38	183 ± 7	568 ± 77	1.41	385 ± 8	836 ± 141	1.69	70
322	S2696M443	269.61	-44.30	3.20	194 ± 20	319 ± 146	1.24	288 ± 30	< 194	1.30	479 ± 36	365 ± 187	1.44	19
323	S2697P237	269.68	23.67	6.00	236 ± 13	3761 ± 773	1.30	307 ± 18	2771 ± 393	1.54	566 ± 23	6081 ± 728	1.62	70
324	S2711P401	271.11	40.11	3.20	172 ± 18	2111 ± 687	1.17	210 ± 23	1207 ± 346	1.00	407 ± 30	2887 ± 652	0.87	19

Table 1—Continued

Shadow Num.	Shadow Name	Coordinates[a] l	Coordinates[a] b	Size[b]	Band R1 I_0[c]	Band R1 I_1[c]	Band R1 χ^2_ν[d]	Band R2 I_0[c]	Band R2 I_1[c]	Band R2 χ^2_ν[d]	Band R12 I_0[c]	Band R12 I_1[c]	Band R12 χ^2_ν[d]
325	S2726M564	272.59	-56.39	4.00	482 ± 7	< 66	1.04	530 ± 9	< 59	1.14	1022 ± 10	< 63	1.20
326	S2733M457	273.32	-45.74	3.20	269 ± 7	< 98	1.20	291 ± 18	< 175	1.64	576 ± 16	< 172	1.83
327	S2755M764	275.50	-76.41	4.80	279 ± 8	< 100	1.32	327 ± 72	< 279	1.29	640 ± 12	< 271	1.53
328	S2755P531	275.54	53.10	6.00	240 ± 10	316 ± 141	1.11	258 ± 13	304 ± 87	1.11	517 ± 17	617 ± 154	1.17
329	S2759M475	275.94	-47.51	3.20	303 ± 18	1349 ± 255	0.88	292 ± 22	1002 ± 153	1.08	605 ± 29	2270 ± 273	1.08
330	S2774M721	277.40	-72.08	6.00	331 ± 9	< 153	1.07	327 ± 46	287 ± 141	1.17	670 ± 53	364 ± 209	1.33
331	S2788M588	278.76	-58.75	4.00	362 ± 10	< 150	1.09	413 ± 57	< 516	1.07	832 ± 17	< 386	1.22
332	S2788M453	278.84	-45.25	3.20	232 ± 16	1841 ± 391	1.08	221 ± 19	1392 ± 215	1.23	480 ± 26	3044 ± 396	1.18
333	S2792M549	279.16	-54.91	4.00	354 ± 41	987 ± 539	1.30	382 ± 53	468 ± 332	1.15	776 ± 69	1184 ± 586	1.29
334	S2816M422	281.55	-42.18	4.80	188 ± 6	1448 ± 234	1.21	184 ± 7	1132 ± 115	1.21	382 ± 10	2466 ± 218	1.40
335	S2825M653	282.50	-65.33	3.20	200 ± 48	832 ± 351	1.05	256 ± 72	586 ± 283	1.14	474 ± 87	1381 ± 446	1.08
336	S2829M446	282.94	-44.60	3.20	214 ± 14	1970 ± 268	1.47	207 ± 16	1159 ± 140	1.26	432 ± 21	2836 ± 263	1.61
337	S2840M628	283.98	-62.85	3.20	242 ± 46	< 623	1.09	353 ± 69	< 397	1.19	623 ± 84	< 770	1.23
338	S2852M532	285.23	-53.20	4.00	322 ± 39	< 705	1.41	410 ± 15	< 181	1.09	798 ± 30	< 517	1.25
339	S2855M394	285.53	-39.36	3.20	160 ± 9	3220 ± 361	1.28	166 ± 10	1502 ± 173	1.19	332 ± 14	4167 ± 332	1.54
340	S2879P832	287.90	83.17	4.00	141 ± 17	1463 ± 183	1.21	55 ± 24	1619 ± 129	1.19	214 ± 30	3112 ± 215	1.35
341	S2897M591	289.74	-59.14	4.80	232 ± 15	< 418	1.17	288 ± 86	< 630	1.12	564 ± 104	< 989	1.13
342	S2904M450	290.42	-45.00	4.00	344 ± 19	529 ± 269	1.07	343 ± 24	420 ± 163	1.12	721 ± 31	773 ± 289	1.18
343	S2924M390	292.39	-39.00	4.00	287 ± 10	< 748	1.20	279 ± 11	386 ± 223	1.25	579 ± 16	662 ± 445	1.40
344	S2996M565	299.59	-56.52	4.80	332 ± 10	< 107	1.28	412 ± 60	< 381	1.24	773 ± 72	< 583	1.35
345	S3018M527	301.82	-52.75	4.80	330 ± 66	< 617	1.18	476 ± 13	< 128	1.12	866 ± 17	< 277	1.26
346	S3026M628	302.57	-62.81	4.80	191 ± 49	387 ± 294	1.19	278 ± 79	304 ± 267	1.14	508 ± 94	633 ± 406	1.25
347	S3041M389	304.11	-38.93	4.00	253 ± 33	2915 ± 1765	1.02	228 ± 40	1948 ± 799	1.11	537 ± 55	4121 ± 1592	1.12
348	S3069M605	306.91	-60.54	4.80	225 ± 39	408 ± 194	1.23	128 ± 64	884 ± 192	1.22	393 ± 75	1421 ± 281	1.36
349	S3075P846	307.50	84.58	4.00	199 ± 16	758 ± 189	1.24	170 ± 20	909 ± 119	1.26	394 ± 26	1631 ± 208	1.46
350	S3102M375	310.25	-37.49	6.00	269 ± 10	3676 ± 1006	1.19	295 ± 12	1203 ± 422	1.20	605 ± 16	4526 ± 870	1.42
351	S3138M476	313.83	-47.59	6.00	292 ± 4	< 50	1.22	354 ± 23	< 169	1.34	668 ± 8	< 73	1.49
352	S3148M538	314.77	-53.76	4.00	326 ± 43	< 534	1.14	451 ± 18	< 216	1.21	783 ± 79	< 640	1.28
353	S3206M204	320.61	-20.39	6.00	184 ± 32	< 2797	0.58	224 ± 43	< 1838	0.79	427 ± 57	3631 ± 1982	0.79
354	S3207M569	320.71	-56.85	4.00	370 ± 13	< 98	1.40	533 ± 125	< 429	1.27	965 ± 21	< 393	1.36
355	S3222M718	322.18	-71.82	6.00	214 ± 44	< 171	1.11	300 ± 10	< 66	1.27	574 ± 13	< 78	1.12
356	S3227M773	322.68	-77.27	4.80	193 ± 26	< 193	1.09	234 ± 40	167 ± 121	1.13	456 ± 47	236 ± 181	1.10
357	S3229M410	322.86	-40.98	6.00	245 ± 40	< 1060	0.98	293 ± 59	564 ± 366	1.20	530 ± 73	1510 ± 621	1.11
358	S3242M533	324.24	-53.27	4.00	182 ± 42	997 ± 289	1.04	264 ± 66	636 ± 248	1.13	460 ± 78	1534 ± 380	1.21
359	S3251M265	325.10	-26.54	6.00	204 ± 24	1436 ± 1358	0.63	250 ± 31	1125 ± 670	0.86	500 ± 41	2604 ± 1292	0.83
360	S3256M637	325.64	-63.73	6.00	293 ± 49	< 218	1.21	239 ± 78	430 ± 213	1.15	598 ± 92	511 ± 313	1.20

Table 1—Continued

Shadow		Coordinates[a]		Size[b]	Band R1			Band R2			Band R12		
Num.	Name	l	b		I_0[c]	I_1[c]	χ^2_ν[d]	I_0[c]	I_1[c]	χ^2_ν[d]	I_0[c]	I_1[c]	χ^2_ν[d]
361	S3259M479	325.89	-47.87	6.00	242 ± 21	395 ± 208	1.19	324 ± 32	258 ± 158	1.26	574 ± 39	671 ± 256	1.29
362	S3286M294	328.55	-29.37	6.00	219 ± 20	< 1436	0.60	247 ± 24	< 1052	0.71	514 ± 33	< 2106	0.71
363	S3331M529	333.08	-52.91	4.80	235 ± 40	731 ± 248	1.65	283 ± 64	661 ± 221	1.54	557 ± 75	1285 ± 335	2.07
364	S3337M404	333.70	-40.39	6.00	211 ± 7	< 274	1.01	154 ± 32	1120 ± 258	1.13	408 ± 40	1346 ± 451	1.23
365	S3388M370	338.83	-36.98	6.00	174 ± 17	2069 ± 791	1.00	192 ± 22	880 ± 383	0.99	395 ± 28	2408 ± 737	1.06
366	S3393P835	339.34	83.48	4.00	244 ± 13	641 ± 98	1.14	231 ± 18	732 ± 75	1.64	499 ± 22	1340 ± 121	1.60
367	S3402M436	340.20	-43.57	4.00	201 ± 15	712 ± 299	1.09	223 ± 21	853 ± 187	1.18	450 ± 27	1591 ± 327	1.05
368	S3416M503	341.57	-50.32	4.00	276 ± 39	352 ± 288	0.99	391 ± 60	303 ± 238	1.32	681 ± 71	661 ± 371	1.30
369	S3455M463	345.48	-46.28	4.00	278 ± 39	356 ± 293	1.23	462 ± 63	< 351	1.22	751 ± 73	421 ± 385	1.32
370	S3476M506	347.58	-50.63	3.20	213 ± 35	392 ± 285	1.13	304 ± 54	341 ± 232	1.21	542 ± 65	693 ± 365	1.28
371	S3478M618	347.80	-61.79	4.00	220 ± 71	340 ± 285	1.12	164 ± 122	705 ± 309	1.24	404 ± 138	1174 ± 429	1.20
372	S3494M494	349.42	-49.38	3.20	235 ± 41	< 699	0.94	238 ± 65	684 ± 290	1.32	476 ± 77	1225 ± 456	1.35
373	S3526M544	352.61	-54.44	4.00	307 ± 9	< 71	1.22	452 ± 16	< 174	1.32	777 ± 14	< 138	1.51
374	S3538M684	353.84	-68.45	8.00	206 ± 34	216 ± 193	1.02	286 ± 55	< 300	1.25	523 ± 66	475 ± 273	1.16
375	S3541M613	354.15	-61.25	4.00	213 ± 49	456 ± 222	1.26	197 ± 82	674 ± 227	1.47	483 ± 95	1045 ± 327	1.45
376	S3559M578	355.85	-57.79	4.00	258 ± 69	< 603	1.23	228 ± 117	643 ± 345	1.41	546 ± 134	876 ± 497	1.36
377	S3564M288	356.35	-28.79	3.20	166 ± 36	2637 ± 2447	0.99	261 ± 49	< 2002	1.15	429 ± 64	3368 ± 2253	1.14
378	S3574M334	357.36	-33.36	3.20	233 ± 14	< 688	1.35	324 ± 16	< 436	1.25	578 ± 21	< 707	1.75

[a]Center of analyzed region, not necessarily the center of a shadow.

[b]Diameter of the circular analyzed region in degrees.

[c]Units of 10^{-6} counts s^{-1} $arcmin^{-2}$.

[d]Reduced χ^2 value.

[e]Degrees of freedom for the fits.

[f]1σ upper limit.

REFERENCES

Arnaud, K.A., 1996, in Astronomical Data Analysis Software and Systems V, eds. G. Jacoby, J. Barnes, ASP Conf. Series, 10, 17

Barber, C. R., Roberts, T. P., & Warwick, R. S. 1996, MNRAS, 282, 157

Barber, C. R., & Warwick, R. S. 1996, in Proceedings of the IAU Colloquium No. 152 Astrophysics in the Extreme Ultraviolet, eds. S. Bowyer, R. F. Malina (Dordrecht:Kluwer Academic Publications), 295

Burrows, D. N., & Mendenhall, J. A. 1991, Nature, 351, 629

Chen, L.-W., Fabian, A. C., & Gendreau, K. C. 1997, MNRAS, 285, 449

Cox, D. P. 1997, IAU Colloquium #166, The Local Bubble and Beyond, eds. D. Breitschwerdt, M. J. Freyberg, & J. Trümper (Springer Verlag:Berlin), 121

Cox, D. P., & Reynolds, R. J. 1987, ARA&A, 25, 303

Cox, D. P, & Snowden, S. L. 1986, Adv. Space Res., 6, 97

Cui, W., McCammon, D., Sanders, W. T., Snowden, S. L., & Womble, D. S. 1996, ApJ, 468, 102

Egger, R. 1993, Ph.D. Thesis, Technischen Universität München, Max Planck Institute for Extraterrestrial Physics Report #249

Frisch, P. C., & York, D. G. 1983, ApJL, 271, L59

Gehrels, N., & Williams, E. D. 1993, ApJL, 418, L25

Guo, Z., Burrows, D. N., Sanders, W. T., Snowden, S. L., & Penprase, B. E. 1995, ApJ, 453, 256

Hartmann, D. & Burton, W. B. 1997, Atlas of Galactic Neutral Hydrogen, (Cambridge:Cambridge University Press)

Hasinger, G., Burg, R., Giacconi, R., Hartner, G., Schmidt, M., Trümper, J., & Zamorani, G. 1993, A&A, 275, 1

Herbstmeier, U., Mebold, U., Snowden, S. L., Hartmann, D., Burton, W. B., Moritz, P., Kalberla, P. M. W., & Egger, R. 1985, A&A, 298, 606

Kaastra, J. S. 1992, An X-Ray Spectral Code for Optically Thin Plasmas (Internal SRON-Leiden Report V2.0)

Kerp, J., Burton, W. B., Egger, R., Freyberg, M. J., Hartmann, D., Kalberla, P. M. W., Mebold, U., & Pietz, J. 1999, A&A, 342, 213

Kerp, J., Mack, K.-H., Egger, R., Pietz, J., Zimmer, F., Mebold, U., & Burton, W. B. 1996, A&A, 312, 67

Kuntz, K. D., & Snowden, S. L. 1999, ApJ, in preparation

Kuntz, K. D., Snowden, S. L., & Verter, F. 1997, ApJ, 484, 245

Lampton, M., Margon, B., & Bowyer, S. ApJ, 208, 177

Liedahl, D. A., Osterheld, A. L., & Goldstein, W. H. 1995, ApJ, 438, L115

McCammon, D., Burrows, D. N., Sanders, W. T., & Kraushaar, W. L. 1983, ApJ, 269, 107

Mewe, R., Gronenschild, E. H. B. M, & van den Oord, G. H. J. 1985, A&AS, 62, 197

Mewe, R., Lemen, J. R., & van den Oord, G. H. J. 1986, A&AS, 65, 511

Miyaji, T., Ishisaki, Y., Ogasaka, Y., Ueda, Y., Freyberg, M. J., Hasinger, G., & Tanaka, Y. 1998, A&A, 334, L13

Moritz, P., Wennmacher, A., Herbstmeier, U., Mebold, U., Egger, R., & Snowden, S. L. 1998, A&A, 336, 682

Morrison, R., & McCammon, D. 1983, ApJ, 270, 119

Nousek, J. A., Fried, P. M., Sanders, W. T., & Kraushaar, W. L. 1982, ApJ, 258, 83

Paresce, F. 1984, AJ, 89, 1022

Parmar, A. N., Guainazzi, M., Oosterbroek, T., Orr, A., Favata, F., Lumb, D., & Malizia, A. 1999, A&A, 345, 611

Pietz, J., Kerp, J., Kalberla, P. M. W., Burton, W. B., Hartmann, D., & Mebold, U. & 1998, A&A, 332, 55

Plucinsky, P. P., Snowden, S. L., Aschenbach, B., Egger, R., Edgar, R. J., & McCammon, D. 1996, ApJ, 463, 224

Plucinsky, P. P., Snowden, S. L., Briel, U. G, Hasinger, G., & Pfeffermann, E. 1993, ApJ, 418, 519

Raymond, J. C. 1991, private communication, computer code update

Raymond, J. C. 1992, ApJ, 384, 502

Raymond, J. C., & Smith, B. W. 1977, ApJS, 35, 419

Sanders, W. T., Edgar, R. J., Liedahl, D. A., & Morgenthaler, J. P. 1998, in Proceedings of the IAU Colloquium No. 166 The Local Bubble and Beyond, eds. D. Breitschwerdt, M.J. Freyberg, J. Trümper, Lecture Notes in Physics 506, 83

Sanders, et al. 1999, ApJ, in preparation

Schlegel, D. J., Finkbeiner, D. P., & Davis, M. 1998, ApJ, 500, 525

Schmutzler, T. & Tscharnuter, W. M. 1993, A&A, 273, 318

Sfeir, D., Lallement, R., Crifo, F., & Welsh, B. Y. 1999, A&A, in press

Shelton, R. 1998, private communication

Sidher, S. D., Sumner, T. J., Quenby, J. J, & Gambhir, M. 1996, A&A, 305, 308

Snowden, S. L., Aschenbach, B., Pfeffermann, E., Burrows, D. N., & Sanders, W. T. 1995a, 439, 399

Snowden, S. L., Cox, D. P., McCammon, D., & Sanders, W. T. 1990, ApJ, 354, 211, SCMS

Snowden, S. L., Egger, R., Finkbeiner, D. P., Freyberg, M. J., & Plucinsky, P. P. 1998, ApJ, 493, 715, Paper I

Snowden, S. L., & Freyberg, M. J. 1993, ApJ, 404, 403

Snowden, S. L., Freyberg, M. J., Schmitt, J. H. M. M., Voges, W., Trümper, J., Edgar, R. J., McCammon, D., Plucinsky, P. P., & Sanders, W. T. 1995b, ApJ, 454, 643

Snowden, S. L., Freyberg, M. J., Schmitt, J. H. M. M., Voges, W., Trümper, J., McCammon, D., Plucinsky, P. P., & Sanders, W. T. 1997, ApJ, 485, 125

Snowden, S. L., Hasinger, G., Jahoda, K., Lockman, F. J., McCammon, D., & Sanders, W. T. 1994a, 430, 601

Snowden, S. L., McCammon, D., Burrows, D. N., & Mendenhall, J. A. 1994b, ApJ, 424, 714

Snowden, S. L., McCammon, D., & Verter, F. 1993, ApJL, 409, L21

Snowden, S. L., Mebold, U., Hirth, W., Herbstmeier, U., & Schmitt, J. H. M. M. 1991, Science, 252, 1529

Snowden, S. L., & Pietsch, W. 1995, ApJ, 452, 627

Snowden, S. L., Plucinsky, P. P., Briel, U., Hasinger, G., & Pfeffermann, E. 1992, ApJ, 393, 81

Snowden, S. L., Schmitt, J. H. M. M., & Edwards, B. E. 1990, ApJ, 364, 118

Wang, Q. D. 1997, IAU Colloquium #166, The Local Bubble and Beyond, eds. D. Breitschwerdt, M. J. Freyberg, & J. Trümper (Springer Verlag:Berlin), 503

Wang, Q. D., & Yu, K. C. 1995, AJ, 109, 698

Welsh, B. Y., Craig, N., Vedder, P. W., & Vallerga, J. V. 1994, ApJ, 437, 638

This preprint was prepared with the AAS LaTeX macros v4.0.

Fig. 1.— On-axis band response curves for the *ROSAT* R1 (dashed), R2 (dotted), R12 (solid), and R45 (solid) bands. The sharp break at 0.284 keV is due to the carbon Kα absorption edge of the PSPC plastic entrance window. Other jumps in the curves are caused by the oxygen absorption edge at 0.532 keV from the window and the argon absorption edge at 0.245 keV and xenon absorption edge at 0.928 keV from the proportional counter gas. Note the very small overlap between the R45 band and the lower energy bands.

Fig. 2.— Histograms of the statistical significances (count rate divided by the uncertainty in the count rate, I/σ_I) for the $12' \times 12'$ pixels for the R1 (dashed), R2 (dotted), and R12 (solid) bands.

Fig. 3.— Scatter plots comparing the binned Schlegel et al. (1998) *IRAS* 100 μm data versus the binned Hartmann & Burton (1997) $N_{\rm H}$ data in the a) northern and b) southern Galactic hemispheres (see text for details). The lines show the best-fit linear relation for H I column densities $\leq 4.0 \times 10^{20}$ H I cm^{-2}. The turnover at higher values of I_{100} is due to the presence of molecular gas.

Fig. 4.— Locations and extents of the regions selected for this analysis. Panels a) and d) show copies of the *IRAS* 100 μm data with the Galactic coordinate grid overlayed. The data are shown using the same zenith equal area (ZEA) projection as used in Snowden et al. (1997). Panel b) shows the northern regions overlayed on the R12 band X-ray data. The color range is $200 - 1500 \times 10^{-6}$ R12 band counts s^{-1} arcmin^{-2}. Panel c) shows the northern regions overlayed on the scaled *IRAS* 100 μm data in the same projection. The color range is $0.2 - 15.0 \times 10^{20}$ H cm^{-2} in a square-root scaling. Panels e) and f) are the same as panels b) and c) except that they show the southern regions.

Fig. 5.— Schematic diagrams of ISM shadowing geometries. a) The assumed geometry for the model fits. b) Shadowing cloud located within the foreground emission region. c) Shadowing cloud located within the distant (halo) emission region.

Fig. 6.— Scatter plots of the R12 band fits. The curves show the model fit to the data. The units of the horizontal axis are 10^{20} H I cm^{-2}. The units for the vertical axis are 10^{-6} R12 band counts s^{-1} arcmin^{-2}.

Fig. 7.— a) Scatter plot comparing values for the foreground emission derived in this paper with those derived in Paper I. The units for both axes are 10^{-6} R12 band counts s^{-1} arcmin^{-2}. b) Same as a) except that the values for the distant emission are compared.

Fig. 8.— a) Scatter plot of the fitted value for the foreground R12 band intensity versus the R2/R1 band ratio for the foreground component. b) Scatter plot of the fitted value for the distant R12 band intensity versus the R2/R1 band ratio for the distant component. In both cases only values for those shadows where the ratio divided by the uncertainty in the ratio is > 3.0 are plotted.

Fig. 9.— a) Histogram of the R2/R1 band ratio for the foreground component. b) Same as a)

except for the distant component. In both cases only values for those shadows where the ratio divided by the uncertainty in the ratio is > 3.0 are plotted.

Fig. 10.— Plots showing the relative R12 band intensities of the foreground (I_0, Figs. a and c) and background (I_1, Figs. b and d) emission for the northern (Figs. a and b) and southern (Figs. c and d) Galactic hemispheres. The size of the circles indicates the size of the fitted values, with the reference circle for the I_0 results indicating an intensity of 300×10^{-6} counts s^{-1} $arcmin^{-2}$ and the reference circle for the I_1 results indicating an intensity of 1000×10^{-6} counts s^{-1} $arcmin^{-2}$. The latitude spacing of the coordinate grid is $15°$ with a minimum latitude of $|b| = 15°$. The longitude spacing is $30°$.

Fig. 11.— a) Scatter plot of the average R2/R1 band ratio for the foreground component in $10°$ latitude bins. b) Scatter plot of the average R2/R1 band ratio for the distant component in $10°$ latitude bins. In both cases only values for those shadows where the ratio divided by the uncertainty in the ratio is > 3.0 were included in the plotted average.

Fig. 12.— a) Scatter plot of the average R2/R1 band ratio for the foreground component in $20°$ longitude bins. b) Scatter plot of the average R2/R1 band ratio for the distant component in $20°$ longitude bins. In both cases only values for those shadows where the ratio divided by the uncertainty in the ratio is > 3.0 were included in the plotted average.

Fig. 13.— Scatter plot of the average R2/R1 band ratio for the foreground component binned by the cosine along the Snowden, Schmitt, & Edwards (1990) dipole. The line shows the best-fit linear relation between the cosine and the hardness ratio.

Fig. 14.— Plots showing the hardness ratios of the of the foreground (I_0) emission for the northern (Fig. a) and southern (Fig. b) Galactic hemispheres. The size of the circles indicates the hardness of the emission, with harder emission shown with larger radii. The coordinate grid is the same as in Fig. 10.

Fig. 15.— Scatter plot of the halo $\frac{3}{4}$ keV intensity versus the halo $\frac{1}{4}$ keV intensity as determined by this analysis. The units for both axes are 10^{-6} counts s^{-1} $arcmin^{-2}$.

Fig. 16.— Plots of the relative halo emission in the $\frac{1}{4}$ keV and $\frac{3}{4}$ keV bands in the northern (a) and southern (b) hemispheres. The data are plotted as ellipses where the vertical axis is proportional to the relative emission at $\frac{1}{4}$ keV and the horizontal axis is proportional to the relative emission at $\frac{3}{4}$ keV. The data are the same as in Fig. 15 except for increased sky coverage. The coordinate grid is the same as in Fig. 10.

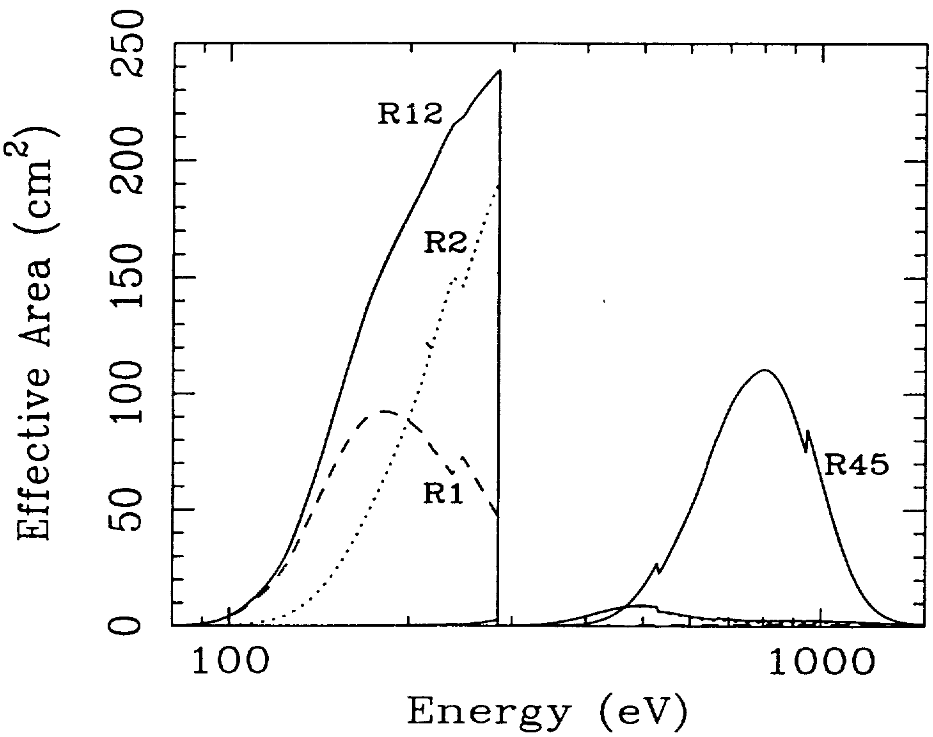
Effective Area (cm²)
Energy (eV)
0
50
100
150
200
250
100
1000
R12
R2
R1
R45

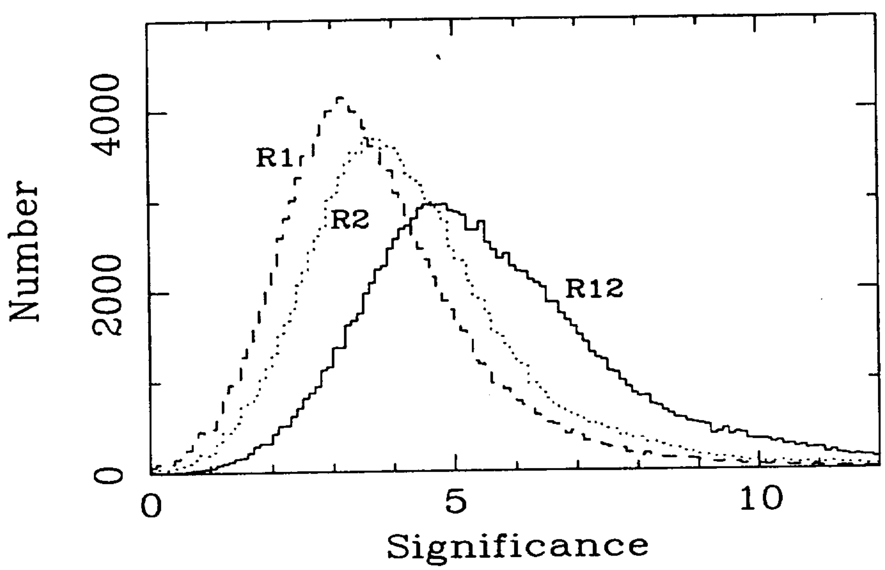
Number
0
2000
4000
0
5
10
Significance
R1
R2
R12

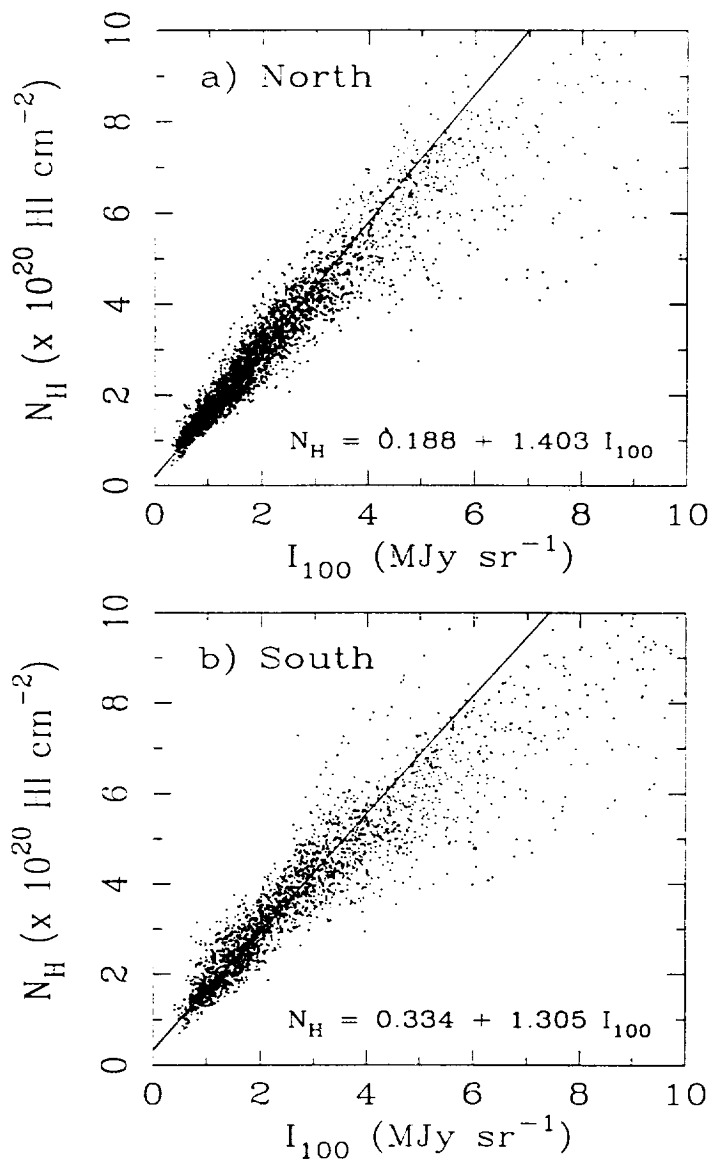
a) North
$N_H = 0.188 + 1.403\ I_{100}$
N_H (x 10^{20} HI cm^{-2})
I_{100} (MJy sr^{-1})
b) South
$N_H = 0.334 + 1.305\ I_{100}$
N_H (x 10^{20} HI cm^{-2})
I_{100} (MJy sr^{-1})

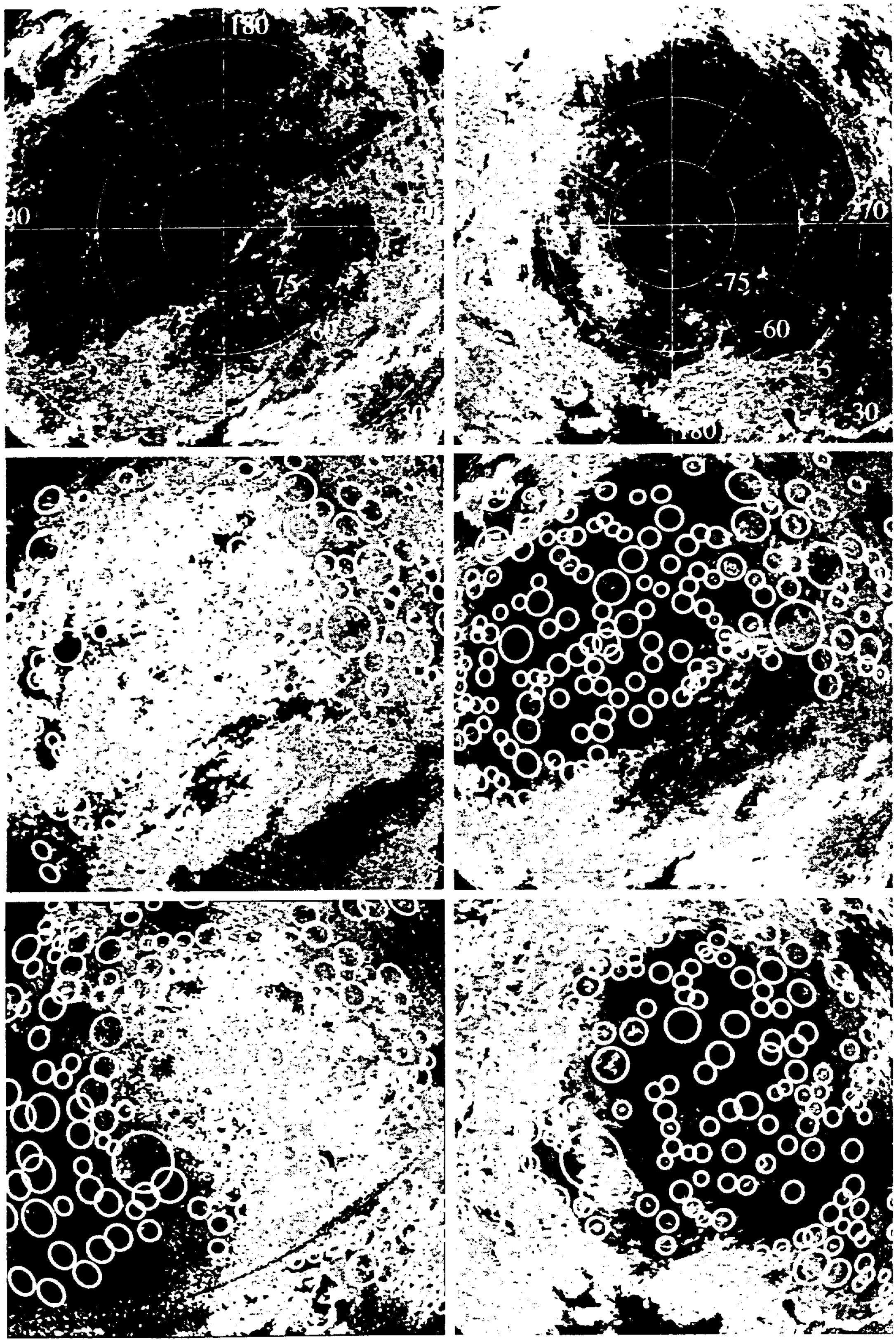

180
90
75
270
-75
-60
180

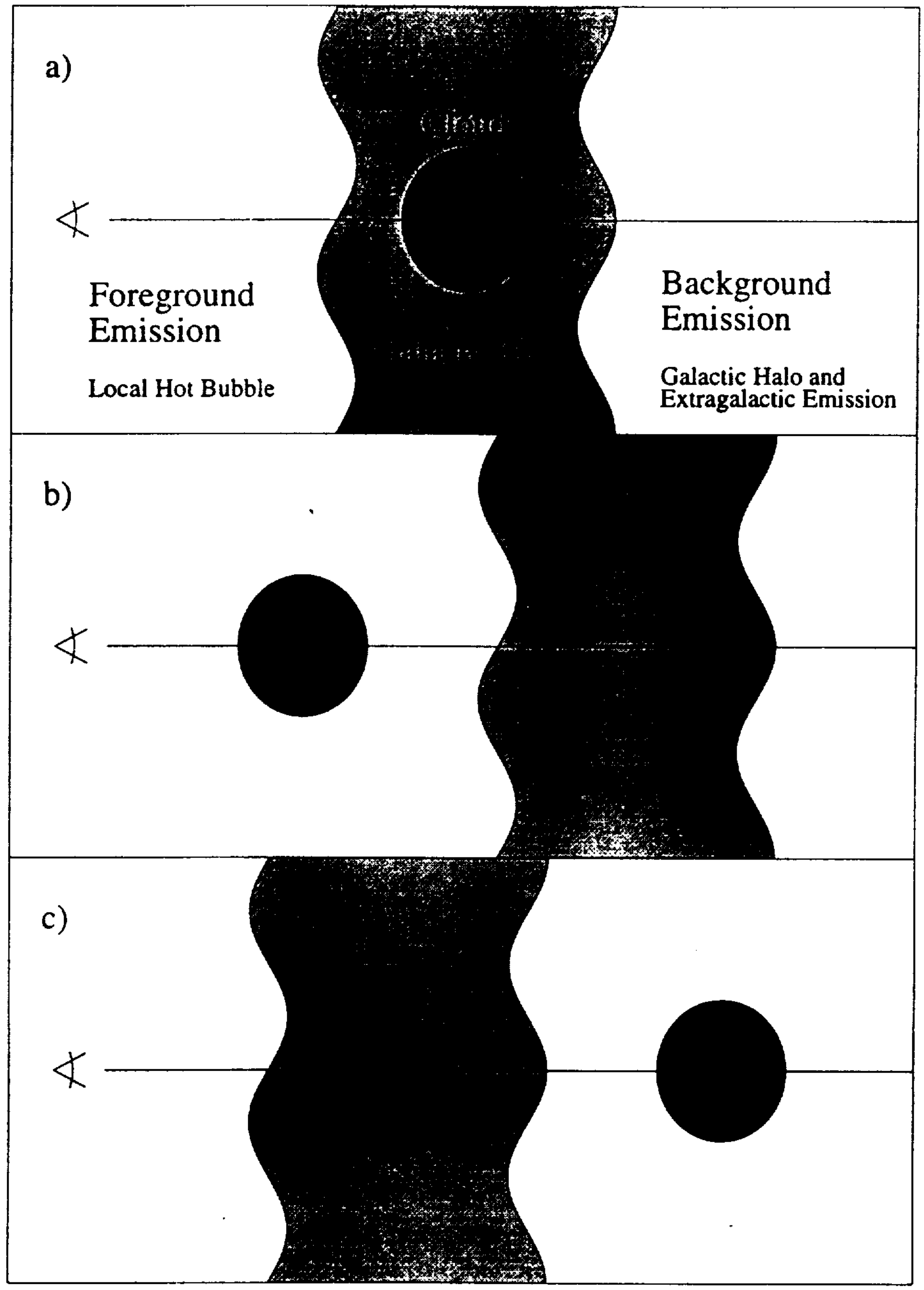
a)
Foreground Emission
Local Hot Bubble
Background Emission
Galactic Halo and Extragalactic Emission
b)
c)

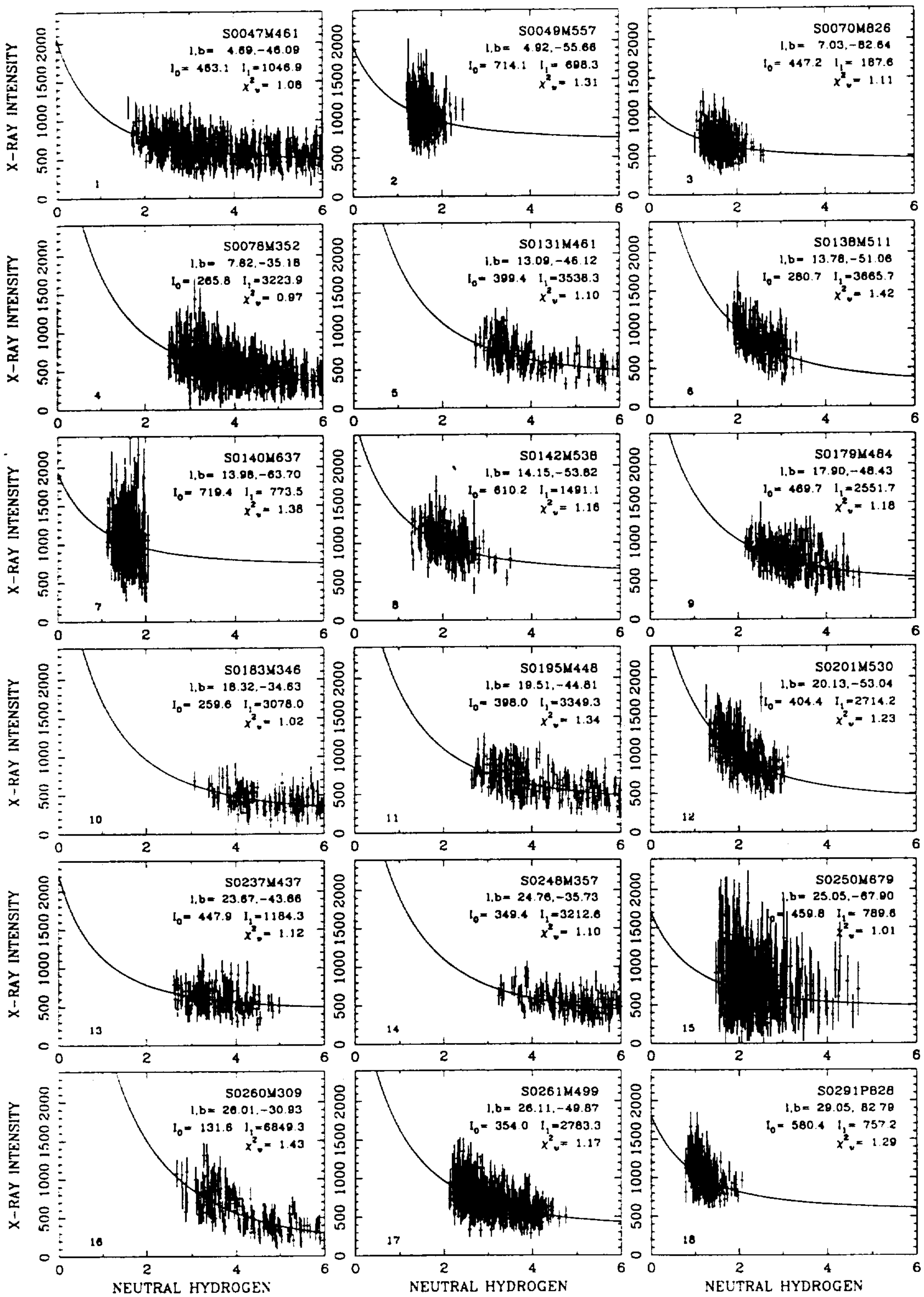
X-RAY INTENSITY
NEUTRAL HYDROGEN
S0047M461
l,b= 4.69,-46.09
I0= 463.1 I1=1046.9
χ²ν= 1.06
S0049M557
l,b= 4.92,-55.66
I0= 714.1 I1= 698.3
χ²ν= 1.31
S0070M826
l,b= 7.03,-82.64
I0= 447.2 I1= 187.6
χ²ν= 1.11
S0078M352
l,b= 7.82,-35.18
I0= 265.8 I1=3223.9
χ²ν= 0.97
S0131M461
l,b= 13.09,-46.12
I0= 399.4 I1=3538.3
χ²ν= 1.10
S0138M511
l,b= 13.78,-51.06
I0= 280.7 I1=3665.7
χ²ν= 1.42
S0140M637
l,b= 13.98,-63.70
I0= 719.4 I1= 773.5
χ²ν= 1.38
S0142M538
l,b= 14.15,-53.82
I0= 610.2 I1=1491.1
χ²ν= 1.16
S0179M484
l,b= 17.90,-48.43
I0= 469.7 I1=2551.7
χ²ν= 1.18
S0183M346
l,b= 18.32,-34.63
I0= 259.6 I1=3078.0
χ²ν= 1.02
S0195M448
l,b= 19.51,-44.81
I0= 398.0 I1=3349.3
χ²ν= 1.34
S0201M530
l,b= 20.13,-53.04
I0= 404.4 I1=2714.2
χ²ν= 1.23
S0237M437
l,b= 23.67,-43.66
I0= 447.9 I1=1184.3
χ²ν= 1.12
S0248M357
l,b= 24.76,-35.73
I0= 349.4 I1=3212.6
χ²ν= 1.10
S0250M679
l,b= 25.05,-67.90
I0= 459.8 I1= 789.6
χ²ν= 1.01
S0260M309
l,b= 26.01,-30.93
I0= 131.6 I1=6849.3
χ²ν= 1.43
S0261M499
l,b= 26.11,-49.87
I0= 354.0 I1=2763.3
χ²ν= 1.17
S0291P828
l,b= 29.05, 82.79
I0= 580.4 I1= 757.2
χ²ν= 1.29

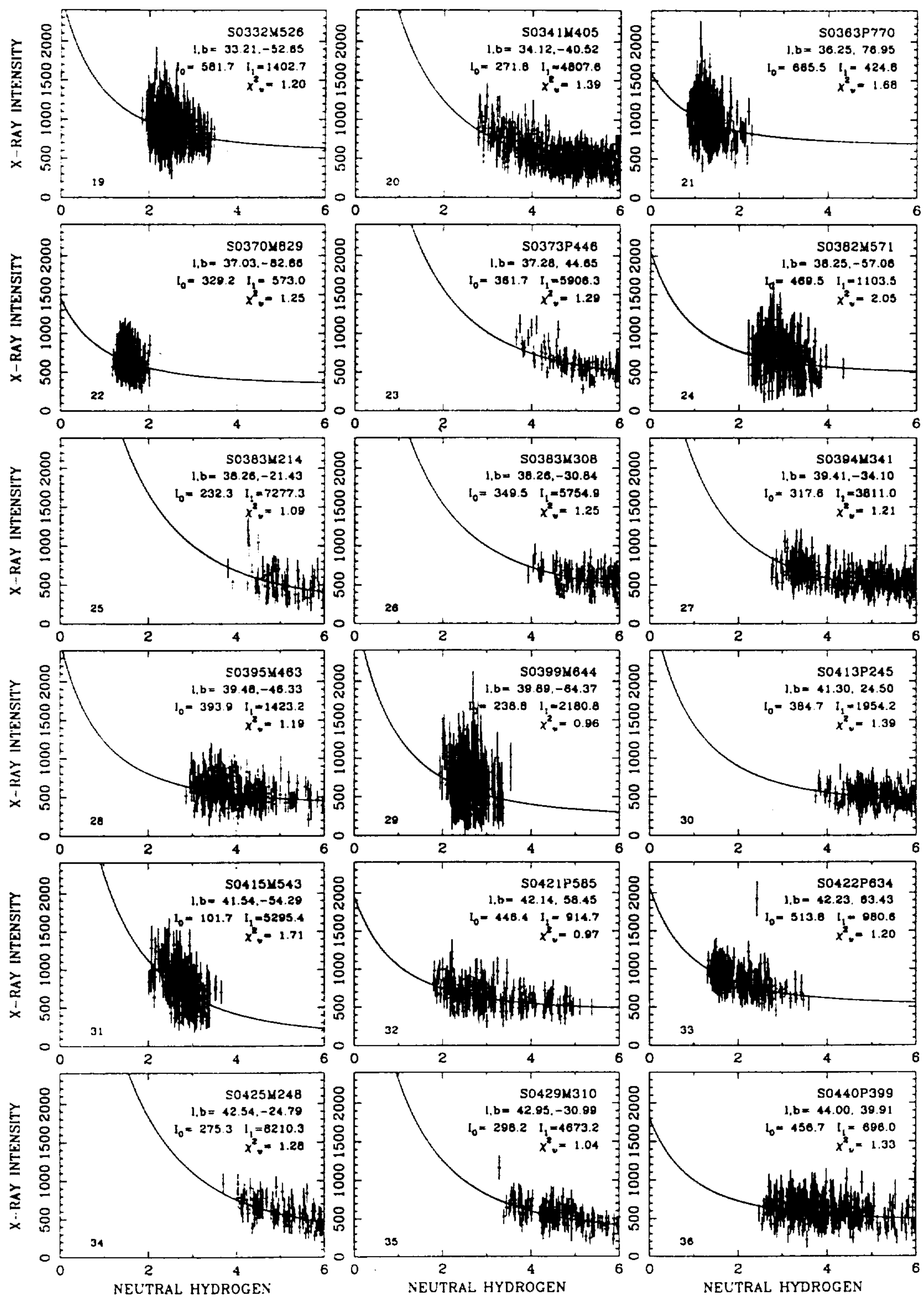
X-RAY INTENSITY
NEUTRAL HYDROGEN
S0332M526
l,b= 33.21,-52.65
I_0= 581.7 I_1=1402.7
χ^2_ν= 1.20
19
S0341M405
l,b= 34.12,-40.52
I_0= 271.8 I_1=4807.6
χ^2_ν= 1.39
20
S0363P770
l,b= 36.25, 76.95
I_0= 665.5 I_1= 424.6
χ^2_ν= 1.68
21
S0370M629
l,b= 37.03,-62.66
I_0= 329.2 I_1= 573.0
χ^2_ν= 1.25
22
S0373P446
l,b= 37.28, 44.65
I_0= 361.7 I_1=5906.3
χ^2_ν= 1.29
23
S0382M571
l,b= 38.25,-57.06
I_0= 469.5 I_1=1103.5
χ^2_ν= 2.05
24
S0383M214
l,b= 38.26,-21.43
I_0= 232.3 I_1=7277.3
χ^2_ν= 1.09
25
S0383M308
l,b= 38.26,-30.84
I_0= 349.5 I_1=5754.9
χ^2_ν= 1.25
26
S0394M341
l,b= 39.41,-34.10
I_0= 317.6 I_1=3811.0
χ^2_ν= 1.21
27
S0395M463
l,b= 39.48,-46.33
I_0= 393.9 I_1=1423.2
χ^2_ν= 1.19
28
S0399M644
l,b= 39.89,-64.37
I_0= 238.8 I_1=2180.8
χ^2_ν= 0.96
29
S0413P245
l,b= 41.30, 24.50
I_0= 384.7 I_1=1954.2
χ^2_ν= 1.39
30
S0415M543
l,b= 41.54,-54.29
I_0= 101.7 I_1=5295.4
χ^2_ν= 1.71
31
S0421P585
l,b= 42.14, 58.45
I_0= 446.4 I_1= 914.7
χ^2_ν= 0.97
32
S0422P634
l,b= 42.23, 63.43
I_0= 513.8 I_1= 980.6
χ^2_ν= 1.20
33
S0425M248
l,b= 42.54,-24.79
I_0= 275.3 I_1=8210.3
χ^2_ν= 1.28
34
S0429M310
l,b= 42.95,-30.99
I_0= 298.2 I_1=4673.2
χ^2_ν= 1.04
35
S0440P399
l,b= 44.00, 39.91
I_0= 456.7 I_1= 696.0
χ^2_ν= 1.33
36

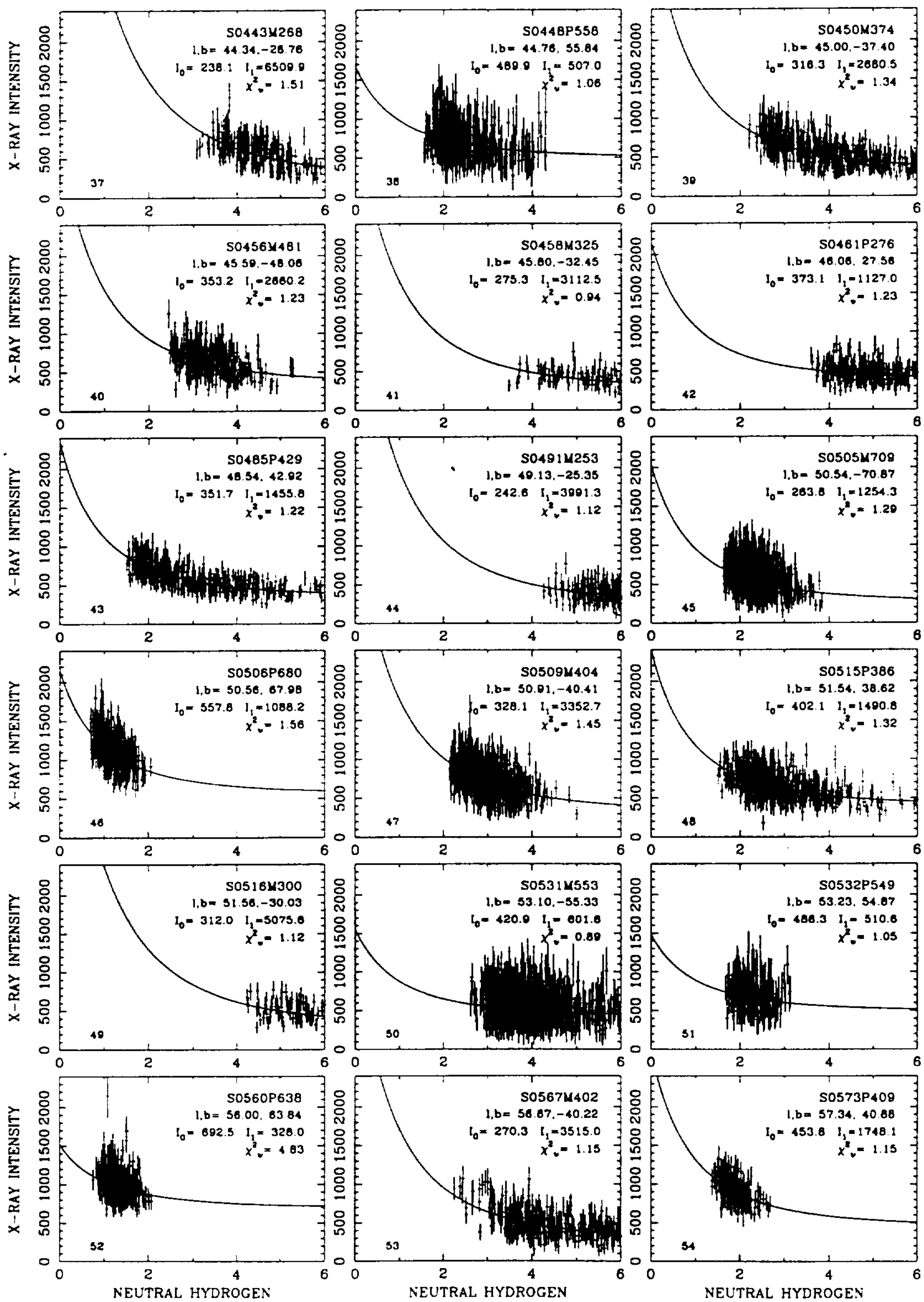
X-RAY INTENSITY
NEUTRAL HYDROGEN
S0443M268
l,b= 44.34,-28.76
I0= 238.1 I1=6509.9
χ2ν= 1.51
37
S0448P558
l,b= 44.76, 55.84
I0= 489.9 I1= 507.0
χ2ν= 1.06
38
S0450M374
l,b= 45.00,-37.40
I0= 316.3 I1=2680.5
χ2ν= 1.34
39
S0456M481
l,b= 45.59,-48.08
I0= 353.2 I1=2660.2
χ2ν= 1.23
40
S0458M325
l,b= 45.80,-32.45
I0= 275.3 I1=3112.5
χ2ν= 0.94
41
S0461P276
l,b= 46.06, 27.58
I0= 373.1 I1=1127.0
χ2ν= 1.23
42
S0485P429
l,b= 48.54, 42.92
I0= 351.7 I1=1455.8
χ2ν= 1.22
43
S0491M253
l,b= 49.13,-25.35
I0= 242.6 I1=3991.3
χ2ν= 1.12
44
S0505M709
l,b= 50.54,-70.87
I0= 263.8 I1=1254.3
χ2ν= 1.29
45
S0506P680
l,b= 50.56, 67.98
I0= 557.8 I1=1088.2
χ2ν= 1.56
46
S0509M404
l,b= 50.91,-40.41
I0= 328.1 I1=3352.7
χ2ν= 1.45
47
S0515P386
l,b= 51.54, 38.62
I0= 402.1 I1=1490.8
χ2ν= 1.32
48
S0516M300
l,b= 51.56,-30.03
I0= 312.0 I1=5075.6
χ2ν= 1.12
49
S0531M553
l,b= 53.10,-55.33
I0= 420.9 I1= 601.6
χ2ν= 0.89
50
S0532P549
l,b= 53.23, 54.87
I0= 486.3 I1= 510.6
χ2ν= 1.05
51
S0560P638
l,b= 56.00, 63.84
I0= 692.5 I1= 328.0
χ2ν= 4.63
52
S0567M402
l,b= 56.67,-40.22
I0= 270.3 I1=3515.0
χ2ν= 1.15
53
S0573P409
l,b= 57.34, 40.88
I0= 453.6 I1=1748.1
χ2ν= 1.15
54

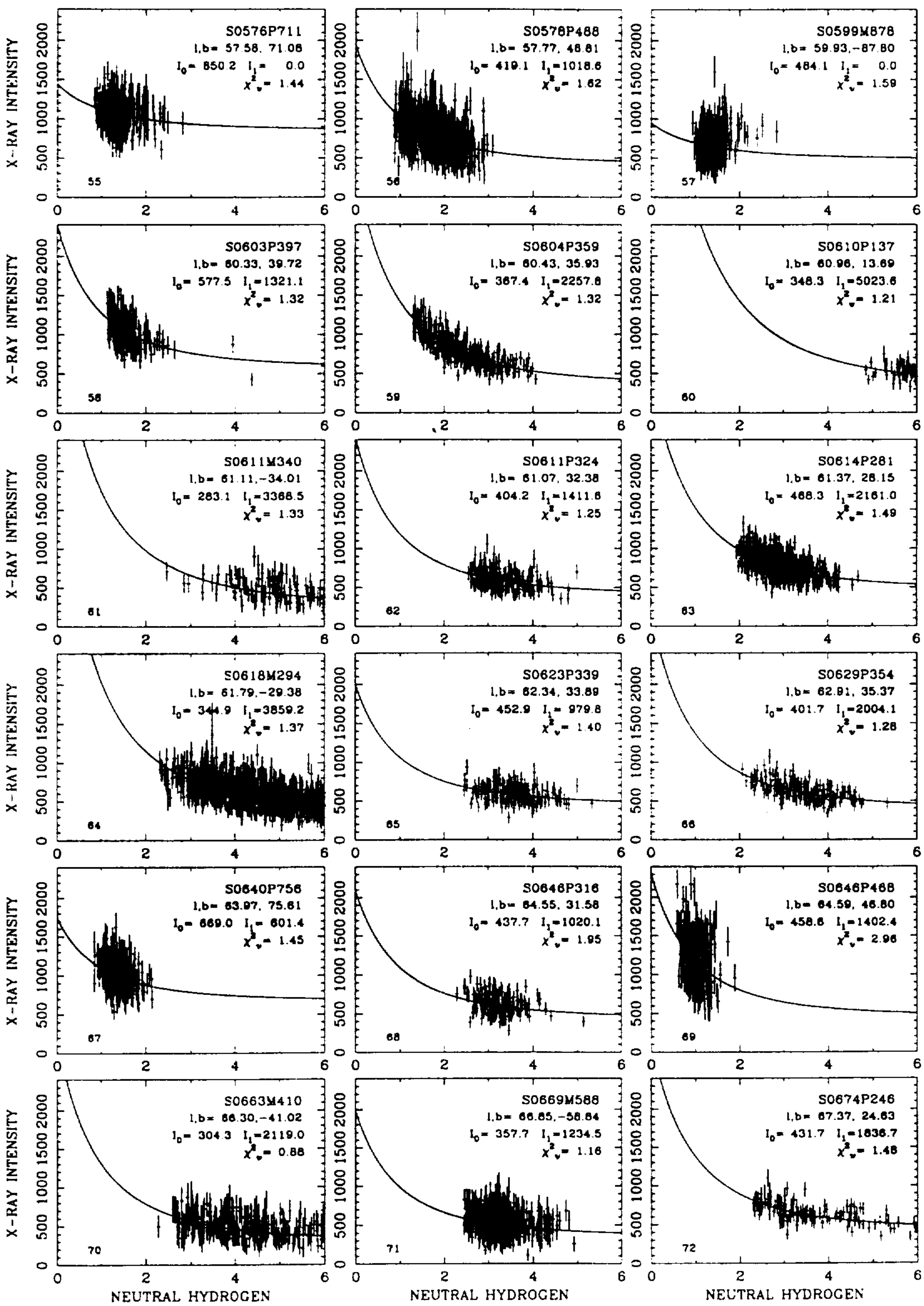

X-RAY INTENSITY
NEUTRAL HYDROGEN
S0576P711
l,b= 57.58, 71.08
I0= 850.2 I1= 0.0
χ²ν= 1.44
55
S0578P488
l,b= 57.77, 48.81
I0= 419.1 I1=1018.6
χ²ν= 1.62
56
S0599M878
l,b= 59.93,-87.80
I0= 484.1 I1= 0.0
χ²ν= 1.59
57
S0603P397
l,b= 60.33, 39.72
I0= 577.5 I1=1321.1
χ²ν= 1.32
58
S0604P359
l,b= 60.43, 35.93
I0= 367.4 I1=2257.8
χ²ν= 1.32
59
S0610P137
l,b= 60.96, 13.69
I0= 348.3 I1=5023.6
χ²ν= 1.21
60
S0611M340
l,b= 61.11,-34.01
I0= 283.1 I1=3368.5
χ²ν= 1.33
61
S0611P324
l,b= 61.07, 32.38
I0= 404.2 I1=1411.6
χ²ν= 1.25
62
S0614P281
l,b= 61.37, 28.15
I0= 468.3 I1=2161.0
χ²ν= 1.49
63
S0618M294
l,b= 61.79,-29.38
I0= 344.9 I1=3859.2
χ²ν= 1.37
64
S0623P339
l,b= 62.34, 33.89
I0= 452.9 I1= 979.8
χ²ν= 1.40
65
S0629P354
l,b= 62.91, 35.37
I0= 401.7 I1=2004.1
χ²ν= 1.28
66
S0640P756
l,b= 63.97, 75.61
I0= 669.0 I1= 601.4
χ²ν= 1.45
67
S0646P316
l,b= 64.55, 31.58
I0= 437.7 I1=1020.1
χ²ν= 1.95
68
S0646P468
l,b= 64.59, 46.80
I0= 458.6 I1=1402.4
χ²ν= 2.96
69
S0663M410
l,b= 66.30,-41.02
I0= 304.3 I1=2119.0
χ²ν= 0.88
70
S0669M588
l,b= 66.65,-58.64
I0= 357.7 I1=1234.5
χ²ν= 1.16
71
S0674P246
l,b= 67.37, 24.63
I0= 431.7 I1=1836.7
χ²ν= 1.48
72

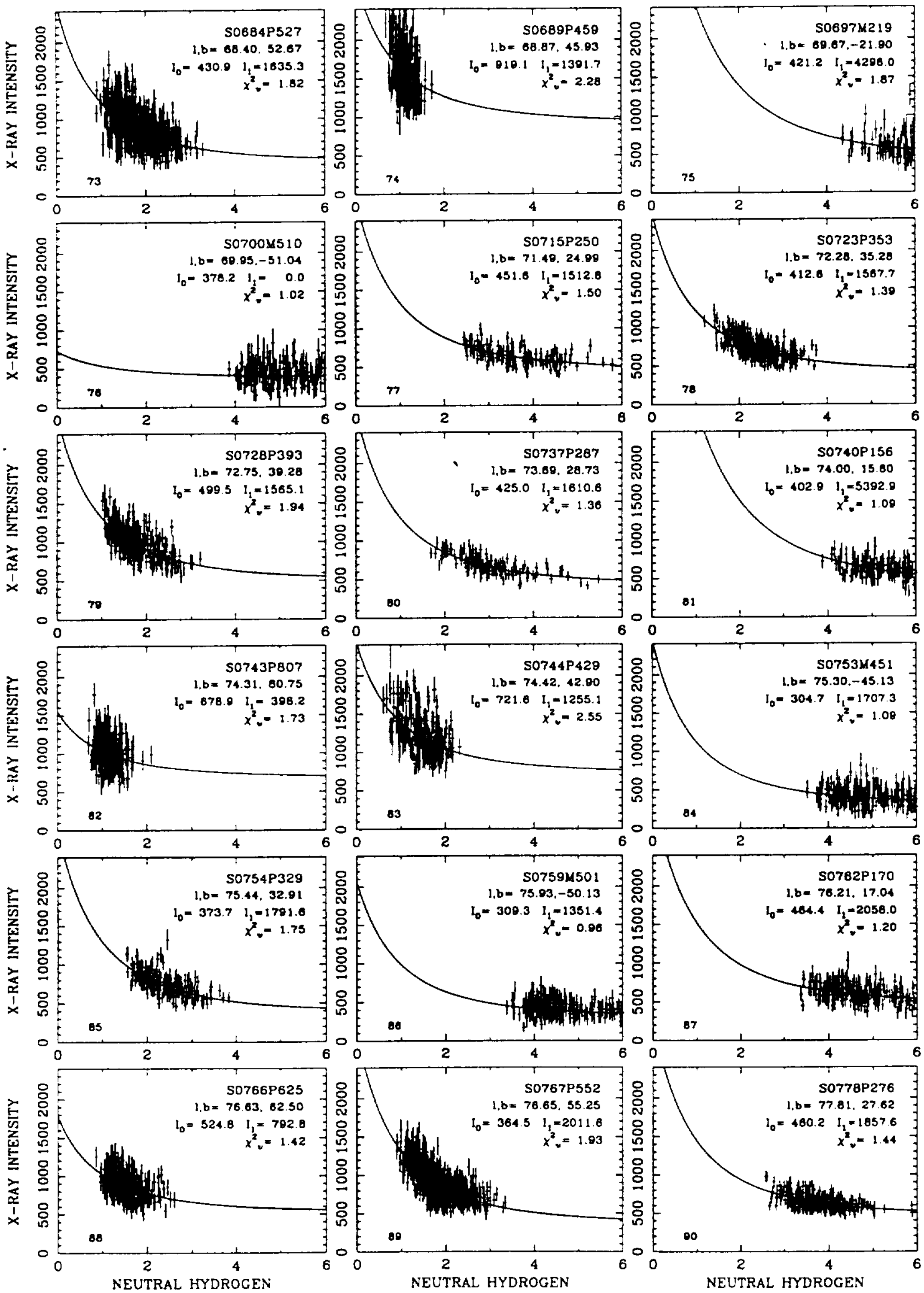
X-RAY INTENSITY
NEUTRAL HYDROGEN
73 S0684P527 l,b= 68.40, 52.67 I_0= 430.9 I_1=1635.3 χ^2_ν= 1.82
74 S0689P459 l,b= 68.87, 45.93 I_0= 919.1 I_1=1391.7 χ^2_ν= 2.28
75 S0697M219 l,b= 69.67,-21.90 I_0= 421.2 I_1=4296.0 χ^2_ν= 1.67
76 S0700M510 l,b= 69.95,-51.04 I_0= 378.2 I_1= 0.0 χ^2_ν= 1.02
77 S0715P250 l,b= 71.49, 24.99 I_0= 451.6 I_1=1512.8 χ^2_ν= 1.50
78 S0723P353 l,b= 72.28, 35.28 I_0= 412.6 I_1=1567.7 χ^2_ν= 1.39
79 S0728P393 l,b= 72.75, 39.28 I_0= 499.5 I_1=1565.1 χ^2_ν= 1.94
80 S0737P287 l,b= 73.69, 28.73 I_0= 425.0 I_1=1610.6 χ^2_ν= 1.36
81 S0740P156 l,b= 74.00, 15.60 I_0= 402.9 I_1=5392.9 χ^2_ν= 1.09
82 S0743P807 l,b= 74.31, 80.75 I_0= 678.9 I_1= 398.2 χ^2_ν= 1.73
83 S0744P429 l,b= 74.42, 42.90 I_0= 721.6 I_1=1255.1 χ^2_ν= 2.55
84 S0753M451 l,b= 75.30,-45.13 I_0= 304.7 I_1=1707.3 χ^2_ν= 1.09
85 S0754P329 l,b= 75.44, 32.91 I_0= 373.7 I_1=1791.6 χ^2_ν= 1.75
86 S0759M501 l,b= 75.93,-50.13 I_0= 309.3 I_1=1351.4 χ^2_ν= 0.96
87 S0762P170 l,b= 76.21, 17.04 I_0= 464.4 I_1=2058.0 χ^2_ν= 1.20
88 S0766P625 l,b= 76.63, 62.50 I_0= 524.6 I_1= 792.8 χ^2_ν= 1.42
89 S0767P552 l,b= 76.65, 55.25 I_0= 364.5 I_1=2011.6 χ^2_ν= 1.93
90 S0778P276 l,b= 77.81, 27.62 I_0= 460.2 I_1=1857.6 χ^2_ν= 1.44

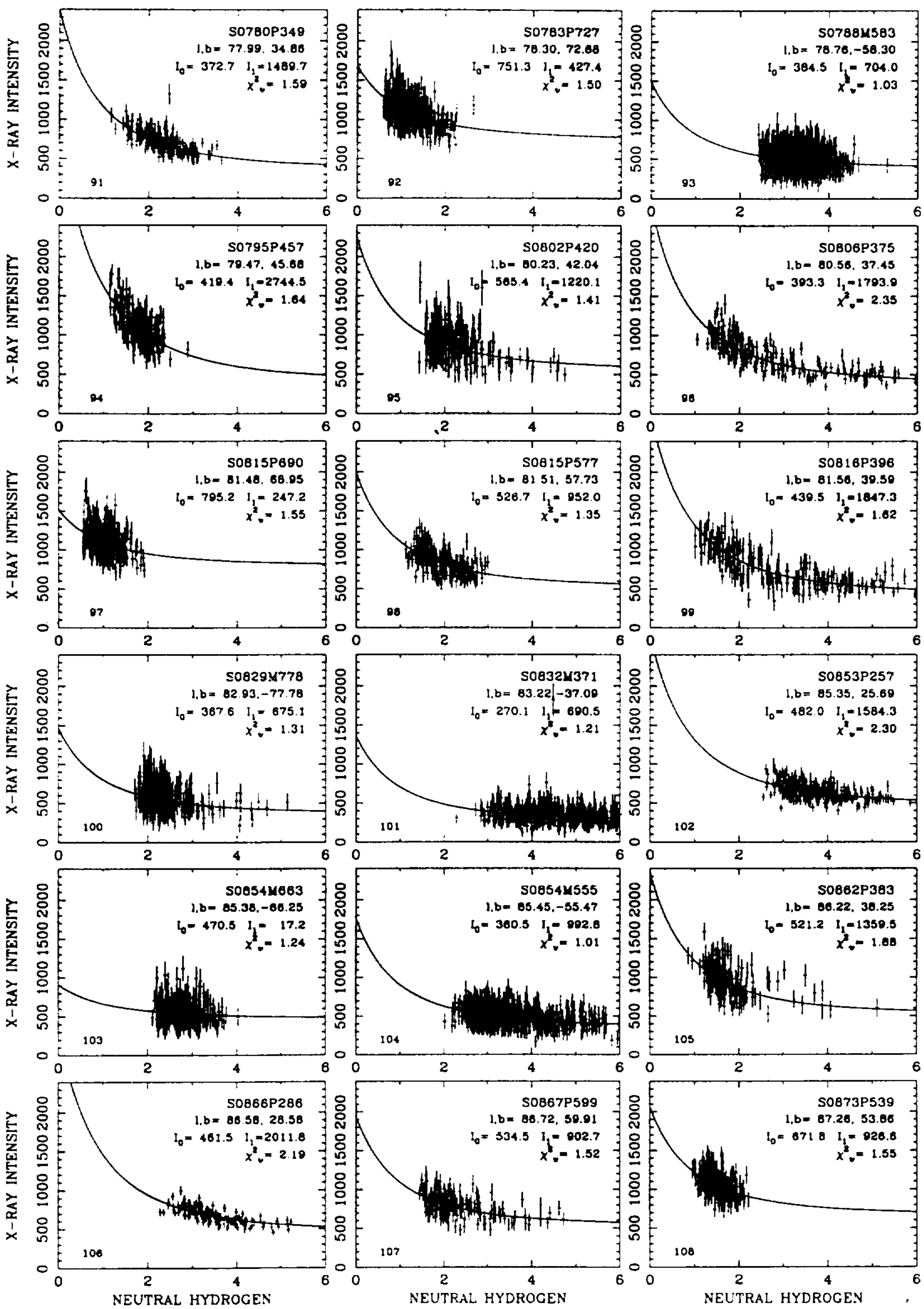
X-RAY INTENSITY
NEUTRAL HYDROGEN
S0780P349 l,b= 77.99, 34.86 I_0= 372.7 I_1=1489.7 χ^2_ν= 1.59 91
S0783P727 l,b= 78.30, 72.68 I_0= 751.3 I_1= 427.4 χ^2_ν= 1.50 92
S0788M583 l,b= 78.76,−58.30 I_0= 384.5 I_1= 704.0 χ^2_ν= 1.03 93
S0795P457 l,b= 79.47, 45.68 I_0= 419.4 I_1=2744.5 χ^2_ν= 1.64 94
S0802P420 l,b= 80.23, 42.04 I_0= 565.4 I_1=1220.1 χ^2_ν= 1.41 95
S0806P375 l,b= 80.56, 37.45 I_0= 393.3 I_1=1793.9 χ^2_ν= 2.35 96
S0815P690 l,b= 81.48, 68.95 I_0= 795.2 I_1= 247.2 χ^2_ν= 1.55 97
S0815P577 l,b= 81.51, 57.73 I_0= 526.7 I_1= 952.0 χ^2_ν= 1.35 98
S0816P396 l,b= 81.56, 39.59 I_0= 439.5 I_1=1847.3 χ^2_ν= 1.62 99
S0829M778 l,b= 82.93,−77.78 I_0= 367.6 I_1= 675.1 χ^2_ν= 1.31 100
S0832M371 l,b= 83.22,−37.09 I_0= 270.1 I_1= 690.5 χ^2_ν= 1.21 101
S0853P257 l,b= 85.35, 25.69 I_0= 482.0 I_1=1584.3 χ^2_ν= 2.30 102
S0854M663 l,b= 85.38,−66.25 I_0= 470.5 I_1= 17.2 χ^2_ν= 1.24 103
S0854M555 l,b= 85.45,−55.47 I_0= 360.5 I_1= 992.8 χ^2_ν= 1.01 104
S0862P383 l,b= 86.22, 38.25 I_0= 521.2 I_1=1359.5 χ^2_ν= 1.88 105
S0866P286 l,b= 86.58, 28.58 I_0= 461.5 I_1=2011.8 χ^2_ν= 2.19 106
S0867P599 l,b= 86.72, 59.91 I_0= 534.5 I_1= 902.7 χ^2_ν= 1.52 107
S0873P539 l,b= 87.26, 53.86 I_0= 671.8 I_1= 926.8 χ^2_ν= 1.55 108

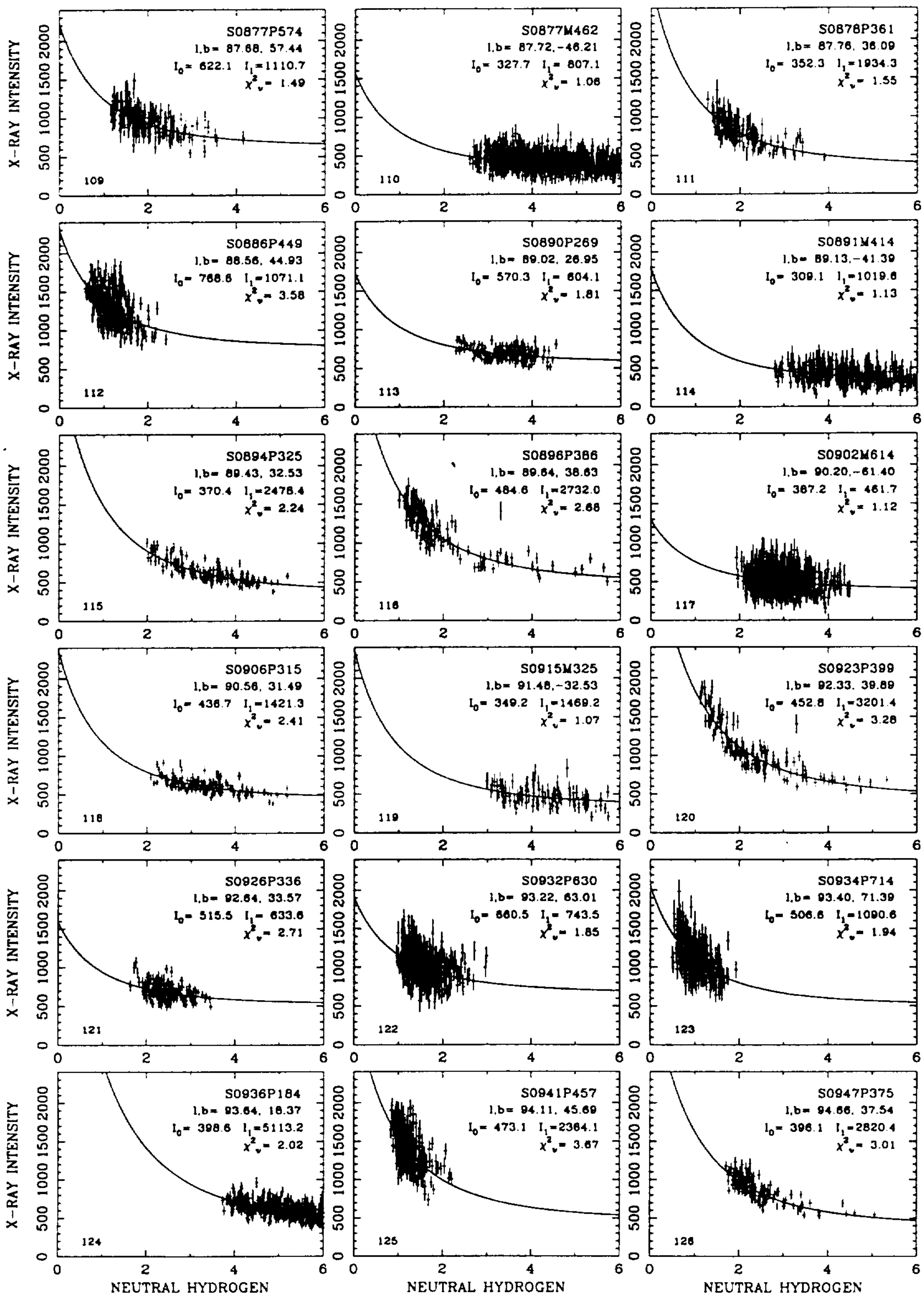
X-RAY INTENSITY
NEUTRAL HYDROGEN
S0877P574
l,b= 87.68, 57.44
I0= 622.1 I1=1110.7
χ²ν= 1.49
109
S0877M462
l,b= 87.72,-46.21
I0= 327.7 I1= 807.1
χ²ν= 1.06
110
S0878P361
l,b= 87.76, 36.09
I0= 352.3 I1=1934.3
χ²ν= 1.55
111
S0886P449
l,b= 88.56, 44.93
I0= 768.6 I1=1071.1
χ²ν= 3.58
112
S0890P269
l,b= 89.02, 26.95
I0= 570.3 I1= 604.1
χ²ν= 1.81
113
S0891M414
l,b= 89.13,-41.39
I0= 309.1 I1=1019.6
χ²ν= 1.13
114
S0894P325
l,b= 89.43, 32.53
I0= 370.4 I1=2478.4
χ²ν= 2.24
115
S0896P386
l,b= 89.64, 38.63
I0= 484.6 I1=2732.0
χ²ν= 2.68
116
S0902M614
l,b= 90.20,-61.40
I0= 387.2 I1= 461.7
χ²ν= 1.12
117
S0906P315
l,b= 90.56, 31.49
I0= 436.7 I1=1421.3
χ²ν= 2.41
118
S0915M325
l,b= 91.48,-32.53
I0= 349.2 I1=1469.2
χ²ν= 1.07
119
S0923P399
l,b= 92.33, 39.89
I0= 452.8 I1=3201.4
χ²ν= 3.28
120
S0926P336
l,b= 92.64, 33.57
I0= 515.5 I1= 633.6
χ²ν= 2.71
121
S0932P630
l,b= 93.22, 63.01
I0= 660.5 I1= 743.5
χ²ν= 1.85
122
S0934P714
l,b= 93.40, 71.39
I0= 506.6 I1=1090.6
χ²ν= 1.94
123
S0936P184
l,b= 93.64, 18.37
I0= 398.6 I1=5113.2
χ²ν= 2.02
124
S0941P457
l,b= 94.11, 45.69
I0= 473.1 I1=2364.1
χ²ν= 3.67
125
S0947P375
l,b= 94.66, 37.54
I0= 396.1 I1=2820.4
χ²ν= 3.01
126

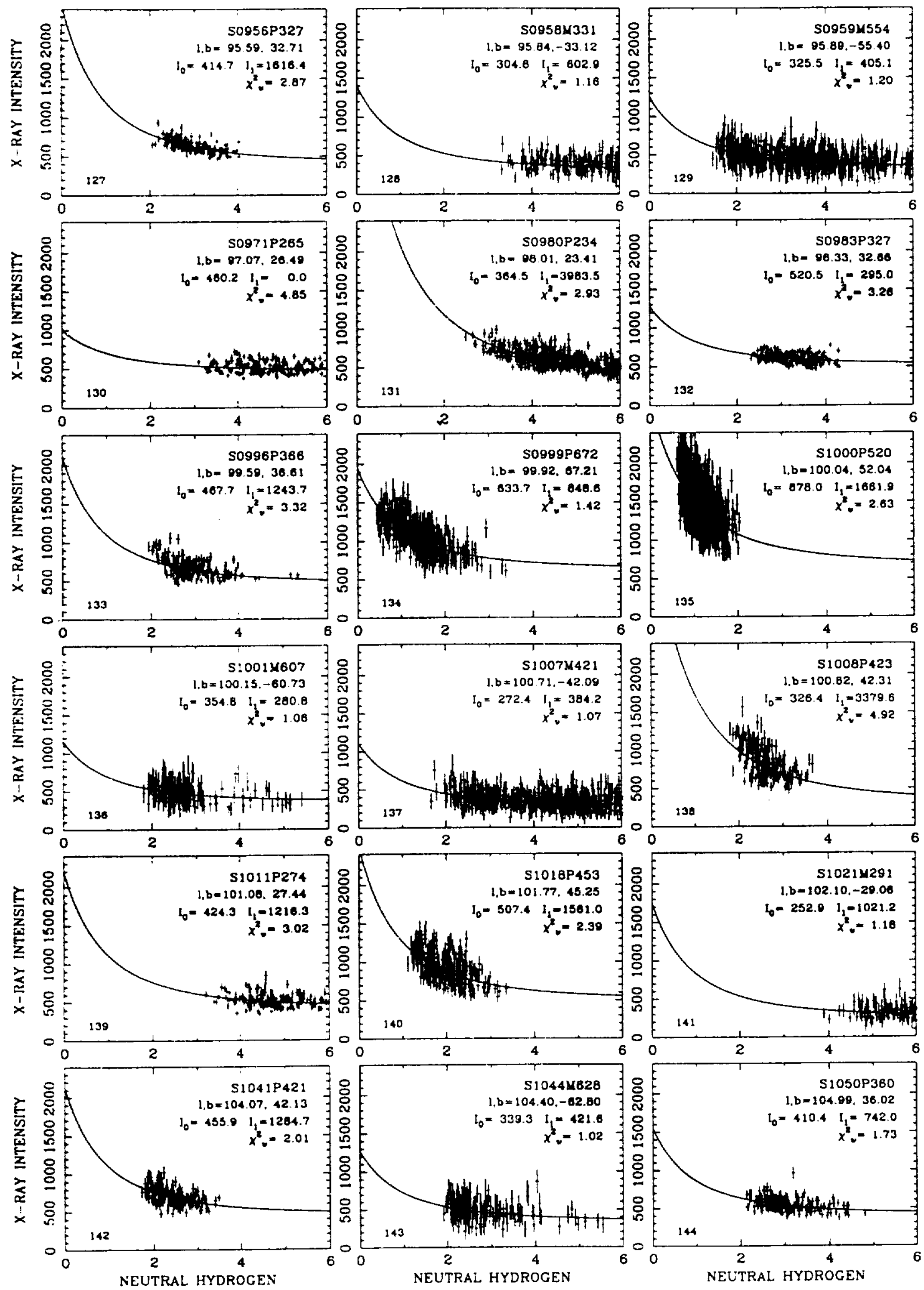
S0956P327
l,b= 95.59, 32.71
I_0= 414.7 I_1=1616.4
χ^2_ν= 2.87
127
S0958M331
l,b= 95.84,-33.12
I_0= 304.6 I_1= 602.9
χ^2_ν= 1.16
128
S0959M554
l,b= 95.89,-55.40
I_0= 325.5 I_1= 405.1
χ^2_ν= 1.20
129
S0971P265
l,b= 97.07, 26.49
I_0= 460.2 I_1= 0.0
χ^2_ν= 4.85
130
S0980P234
l,b= 98.01, 23.41
I_0= 364.5 I_1=3983.5
χ^2_ν= 2.93
131
S0983P327
l,b= 98.33, 32.66
I_0= 520.5 I_1= 295.0
χ^2_ν= 3.26
132
S0996P366
l,b= 99.59, 36.61
I_0= 467.7 I_1=1243.7
χ^2_ν= 3.32
133
S0999P672
l,b= 99.92, 67.21
I_0= 633.7 I_1= 848.6
χ^2_ν= 1.42
134
S1000P520
l,b=100.04, 52.04
I_0= 678.0 I_1=1661.9
χ^2_ν= 2.63
135
S1001M607
l,b=100.15,-60.73
I_0= 354.8 I_1= 280.8
χ^2_ν= 1.06
136
S1007M421
l,b=100.71,-42.09
I_0= 272.4 I_1= 384.2
χ^2_ν= 1.07
137
S1008P423
l,b=100.82, 42.31
I_0= 326.4 I_1=3379.6
χ^2_ν= 4.92
138
S1011P274
l,b=101.06, 27.44
I_0= 424.3 I_1=1216.3
χ^2_ν= 3.02
139
S1018P453
l,b=101.77, 45.25
I_0= 507.4 I_1=1561.0
χ^2_ν= 2.39
140
S1021M291
l,b=102.10,-29.06
I_0= 252.9 I_1=1021.2
χ^2_ν= 1.16
141
S1041P421
l,b=104.07, 42.13
I_0= 455.9 I_1=1264.7
χ^2_ν= 2.01
142
S1044M628
l,b=104.40,-62.80
I_0= 339.3 I_1= 421.6
χ^2_ν= 1.02
143
S1050P360
l,b=104.99, 36.02
I_0= 410.4 I_1= 742.0
χ^2_ν= 1.73
144
X-RAY INTENSITY
NEUTRAL HYDROGEN

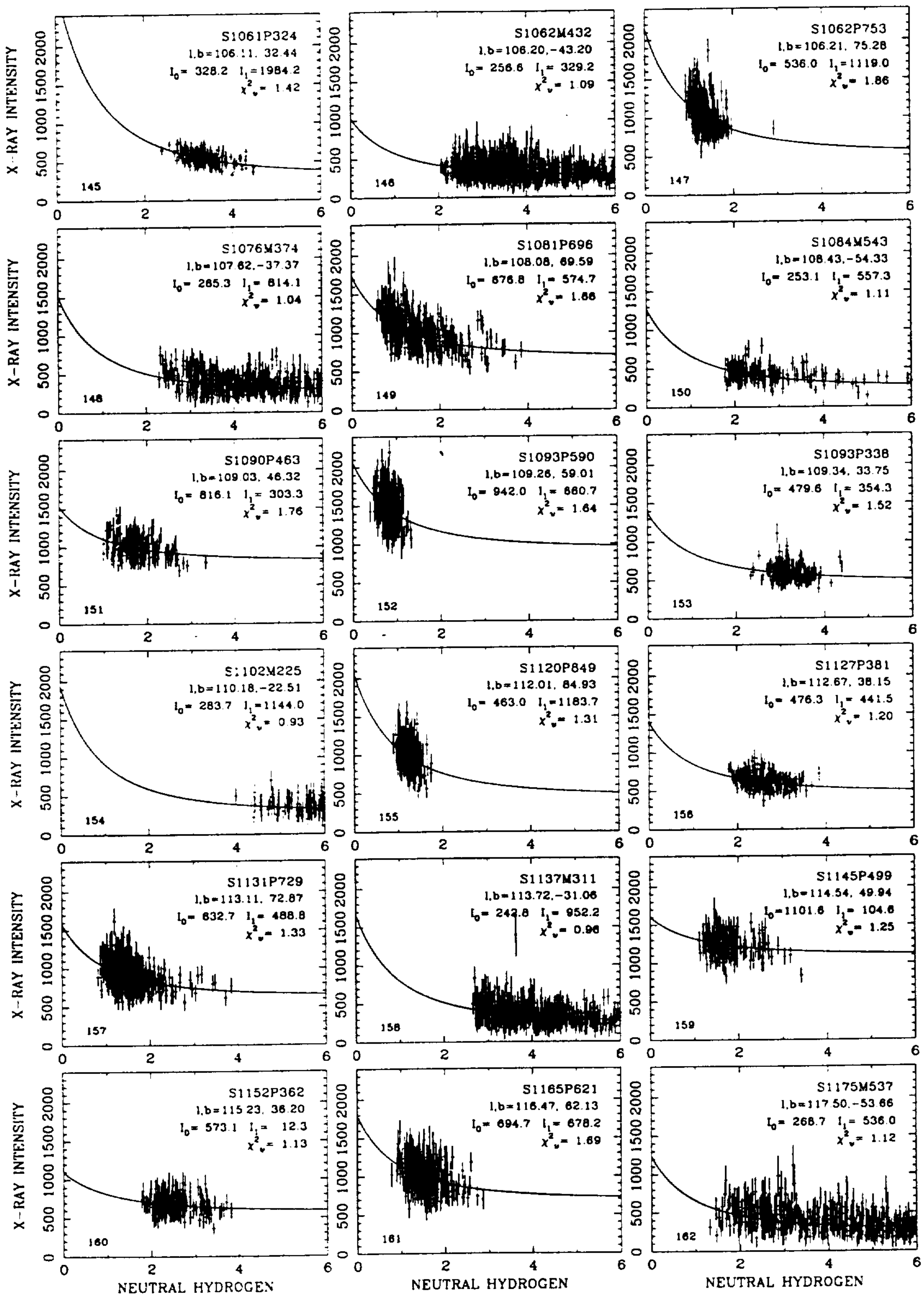
S1061P324
l,b=106.11, 32.44
I_0= 328.2 I_1=1984.2
χ^2_ν= 1.42
145
S1062M432
l,b=106.20,-43.20
I_0= 256.6 I_1= 329.2
χ^2_ν= 1.09
146
S1062P753
l,b=106.21, 75.28
I_0= 536.0 I_1=1119.0
χ^2_ν= 1.86
147
S1076M374
l,b=107.62,-37.37
I_0= 265.3 I_1= 814.1
χ^2_ν= 1.04
148
S1081P696
l,b=108.08, 69.59
I_0= 676.8 I_1= 574.7
χ^2_ν= 1.66
149
S1084M543
l,b=108.43,-54.33
I_0= 253.1 I_1= 557.3
χ^2_ν= 1.11
150
S1090P463
l,b=109.03, 46.32
I_0= 816.1 I_1= 303.3
χ^2_ν= 1.76
151
S1093P590
l,b=109.26, 59.01
I_0= 942.0 I_1= 660.7
χ^2_ν= 1.64
152
S1093P338
l,b=109.34, 33.75
I_0= 479.6 I_1= 354.3
χ^2_ν= 1.52
153
S1102M225
l,b=110.18,-22.51
I_0= 283.7 I_1=1144.0
χ^2_ν= 0.93
154
S1120P849
l,b=112.01, 84.93
I_0= 463.0 I_1=1183.7
χ^2_ν= 1.31
155
S1127P381
l,b=112.67, 38.15
I_0= 476.3 I_1= 441.5
χ^2_ν= 1.20
156
S1131P729
l,b=113.11, 72.87
I_0= 632.7 I_1= 488.8
χ^2_ν= 1.33
157
S1137M311
l,b=113.72,-31.06
I_0= 242.8 I_1= 952.2
χ^2_ν= 0.96
158
S1145P499
l,b=114.54, 49.94
I_0=1101.6 I_1= 104.6
χ^2_ν= 1.25
159
S1152P362
l,b=115.23, 36.20
I_0= 573.1 I_1= 12.3
χ^2_ν= 1.13
160
S1165P621
l,b=116.47, 62.13
I_0= 694.7 I_1= 678.2
χ^2_ν= 1.69
161
S1175M537
l,b=117.50,-53.66
I_0= 268.7 I_1= 536.0
χ^2_ν= 1.12
162
X-RAY INTENSITY
0 500 1000 1500 2000
NEUTRAL HYDROGEN
0 2 4 6

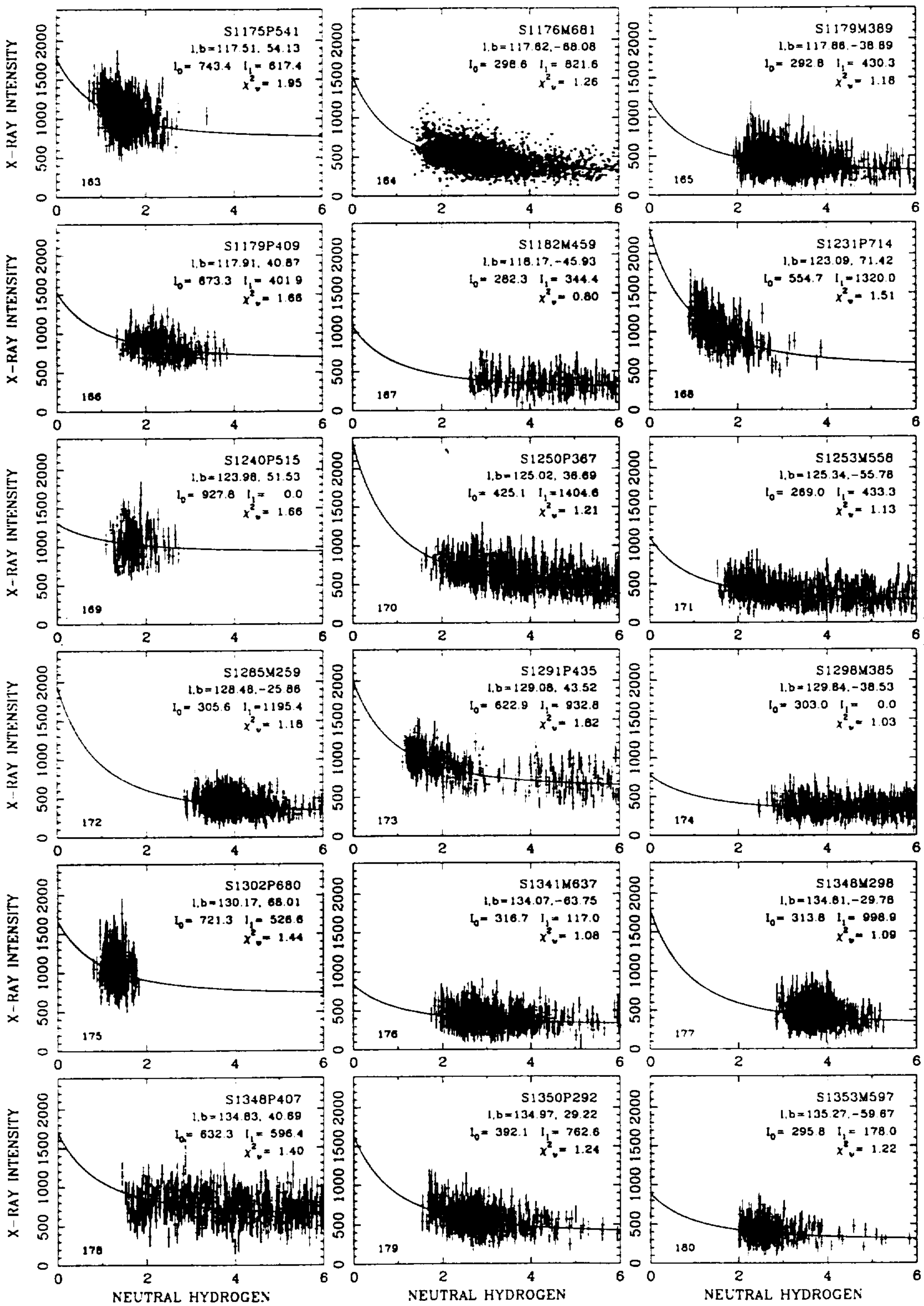
X-RAY INTENSITY
NEUTRAL HYDROGEN
S1175P541
l,b=117.51, 54.13
I_0= 743.4 I_1= 617.4
χ^2_ν= 1.95
163
S1176M681
l,b=117.82,-68.08
I_0= 298.6 I_1= 821.6
χ^2_ν= 1.26
164
S1179M389
l,b=117.88,-38.89
I_0= 292.8 I_1= 430.3
χ^2_ν= 1.18
165
S1179P409
l,b=117.91, 40.87
I_0= 673.3 I_1= 401.9
χ^2_ν= 1.66
166
S1182M459
l,b=118.17,-45.93
I_0= 282.3 I_1= 344.4
χ^2_ν= 0.80
167
S1231P714
l,b=123.09, 71.42
I_0= 554.7 I_1=1320.0
χ^2_ν= 1.51
168
S1240P515
l,b=123.98, 51.53
I_0= 927.8 I_1= 0.0
χ^2_ν= 1.66
169
S1250P367
l,b=125.02, 36.69
I_0= 425.1 I_1=1404.6
χ^2_ν= 1.21
170
S1253M558
l,b=125.34,-55.78
I_0= 269.0 I_1= 433.3
χ^2_ν= 1.13
171
S1285M259
l,b=128.48,-25.86
I_0= 305.6 I_1=1195.4
χ^2_ν= 1.18
172
S1291P435
l,b=129.08, 43.52
I_0= 622.9 I_1= 932.8
χ^2_ν= 1.82
173
S1298M385
l,b=129.84,-38.53
I_0= 303.0 I_1= 0.0
χ^2_ν= 1.03
174
S1302P680
l,b=130.17, 68.01
I_0= 721.3 I_1= 526.6
χ^2_ν= 1.44
175
S1341M637
l,b=134.07,-63.75
I_0= 316.7 I_1= 117.0
χ^2_ν= 1.08
176
S1348M298
l,b=134.81,-29.78
I_0= 313.8 I_1= 998.9
χ^2_ν= 1.09
177
S1348P407
l,b=134.83, 40.89
I_0= 632.3 I_1= 596.4
χ^2_ν= 1.40
178
S1350P292
l,b=134.97, 29.22
I_0= 392.1 I_1= 762.6
χ^2_ν= 1.24
179
S1353M597
l,b=135.27,-59.67
I_0= 295.8 I_1= 178.0
χ^2_ν= 1.22
180

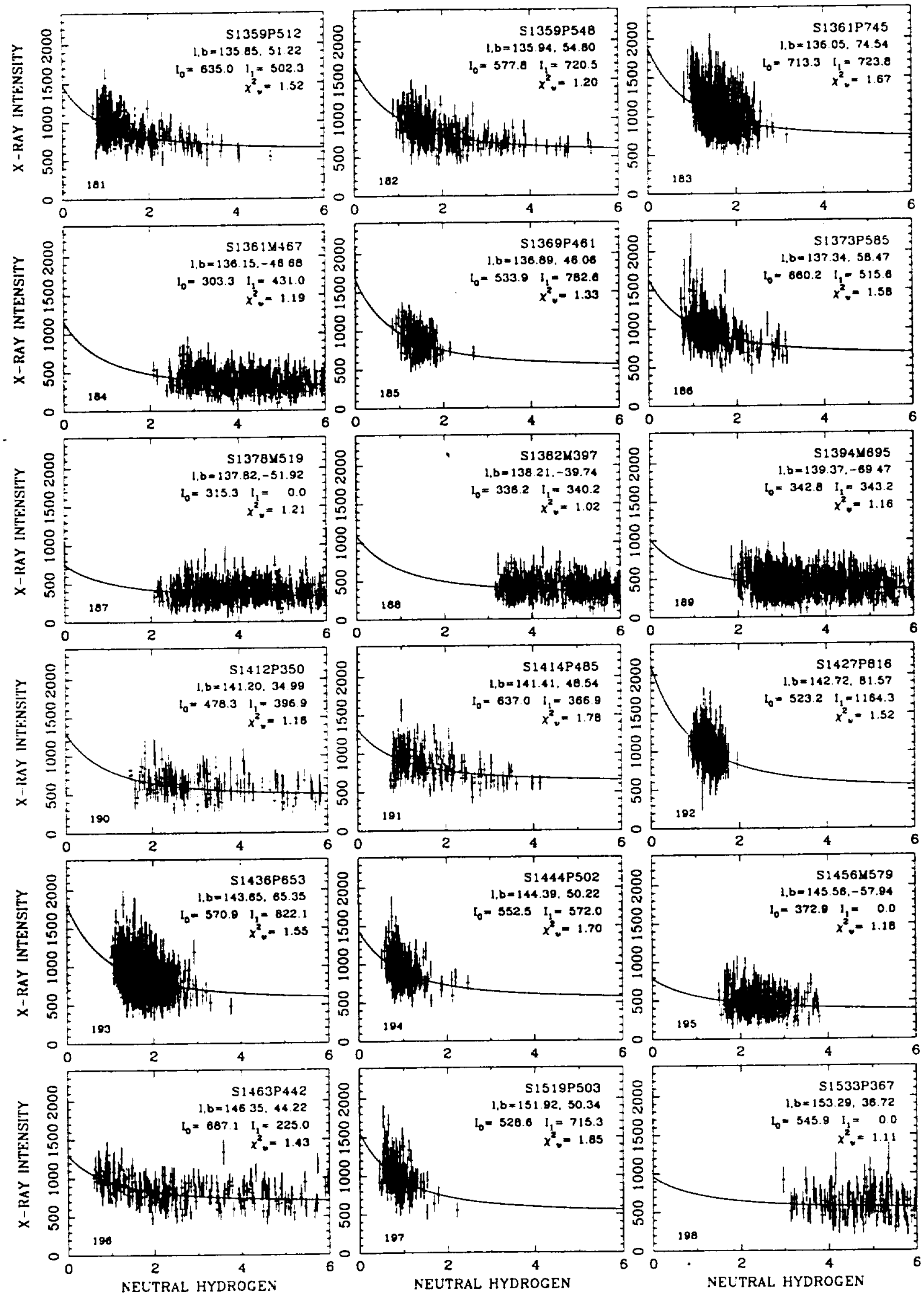
X-RAY INTENSITY
NEUTRAL HYDROGEN
S1359P512
l,b=135.85, 51.22
I_0= 635.0 I_1= 502.3
χ^2_ν= 1.52
181
S1359P548
l,b=135.94, 54.80
I_0= 577.8 I_1= 720.5
χ^2_ν= 1.20
182
S1361P745
l,b=136.05, 74.54
I_0= 713.3 I_1= 723.8
χ^2_ν= 1.67
183
S1361M467
l,b=136.15,-46.68
I_0= 303.3 I_1= 431.0
χ^2_ν= 1.19
184
S1369P461
l,b=136.89, 46.06
I_0= 533.9 I_1= 782.6
χ^2_ν= 1.33
185
S1373P585
l,b=137.34, 58.47
I_0= 660.2 I_1= 515.6
χ^2_ν= 1.58
186
S1378M519
l,b=137.82,-51.92
I_0= 315.3 I_1= 0.0
χ^2_ν= 1.21
187
S1382M397
l,b=138.21,-39.74
I_0= 336.2 I_1= 340.2
χ^2_ν= 1.02
188
S1394M695
l,b=139.37,-69.47
I_0= 342.8 I_1= 343.2
χ^2_ν= 1.16
189
S1412P350
l,b=141.20, 34.99
I_0= 478.3 I_1= 396.9
χ^2_ν= 1.16
190
S1414P485
l,b=141.41, 48.54
I_0= 637.0 I_1= 366.9
χ^2_ν= 1.78
191
S1427P816
l,b=142.72, 81.57
I_0= 523.2 I_1=1164.3
χ^2_ν= 1.52
192
S1436P653
l,b=143.65, 65.35
I_0= 570.9 I_1= 822.1
χ^2_ν= 1.55
193
S1444P502
l,b=144.39, 50.22
I_0= 552.5 I_1= 572.0
χ^2_ν= 1.70
194
S1456M579
l,b=145.58,-57.94
I_0= 372.9 I_1= 0.0
χ^2_ν= 1.18
195
S1463P442
l,b=146.35, 44.22
I_0= 687.1 I_1= 225.0
χ^2_ν= 1.43
196
S1519P503
l,b=151.92, 50.34
I_0= 528.6 I_1= 715.3
χ^2_ν= 1.85
197
S1533P367
l,b=153.29, 36.72
I_0= 545.9 I_1= 0.0
χ^2_ν= 1.11
198

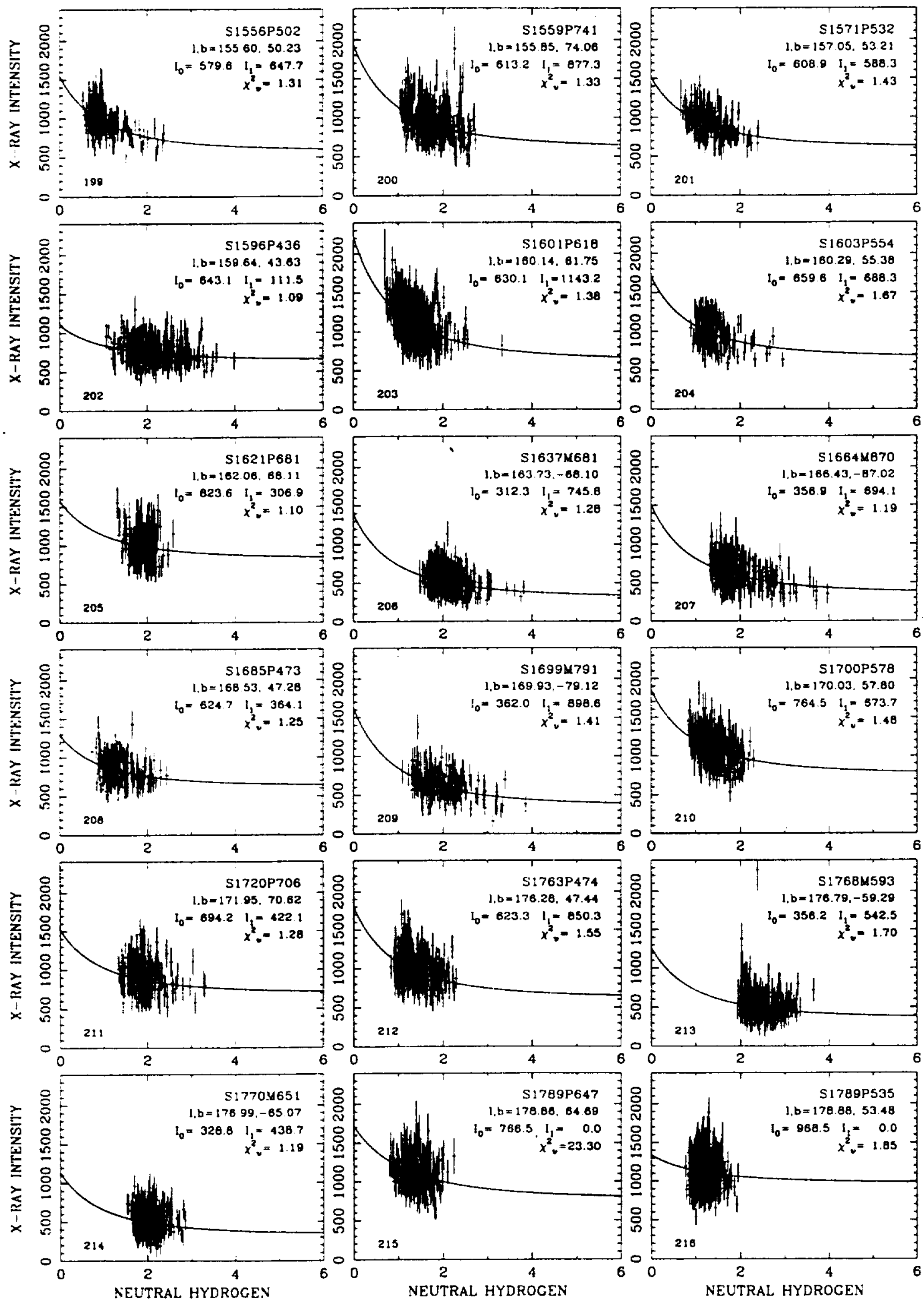
S1556P502
l,b=155.60, 50.23
I0= 579.8 I1= 647.7
χ²ν= 1.31
199
S1559P741
l,b=155.85, 74.06
I0= 613.2 I1= 877.3
χ²ν= 1.33
200
S1571P532
l,b=157.05, 53.21
I0= 608.9 I1= 588.3
χ²ν= 1.43
201
S1596P436
l,b=159.64, 43.63
I0= 643.1 I1= 111.5
χ²ν= 1.09
202
S1601P618
l,b=160.14, 61.75
I0= 630.1 I1=1143.2
χ²ν= 1.38
203
S1603P554
l,b=160.29, 55.38
I0= 659.6 I1= 688.3
χ²ν= 1.67
204
S1621P681
l,b=162.06, 68.11
I0= 823.6 I1= 306.9
χ²ν= 1.10
205
S1637M681
l,b=163.73,-68.10
I0= 312.3 I1= 745.8
χ²ν= 1.28
206
S1664M870
l,b=166.43,-87.02
I0= 356.9 I1= 694.1
χ²ν= 1.19
207
S1685P473
l,b=168.53, 47.28
I0= 624.7 I1= 364.1
χ²ν= 1.25
208
S1699M791
l,b=169.93,-79.12
I0= 362.0 I1= 898.6
χ²ν= 1.41
209
S1700P578
l,b=170.03, 57.80
I0= 764.5 I1= 573.7
χ²ν= 1.48
210
S1720P706
l,b=171.95, 70.62
I0= 694.2 I1= 422.1
χ²ν= 1.28
211
S1763P474
l,b=176.28, 47.44
I0= 623.3 I1= 850.3
χ²ν= 1.55
212
S1768M593
l,b=176.79,-59.29
I0= 356.2 I1= 542.5
χ²ν= 1.70
213
S1770M651
l,b=176.99,-65.07
I0= 328.8 I1= 438.7
χ²ν= 1.19
214
S1789P647
l,b=178.86, 64.69
I0= 766.5 I1= 0.0
χ²ν=23.30
215
S1789P535
l,b=178.88, 53.48
I0= 968.5 I1= 0.0
χ²ν= 1.85
216
X-RAY INTENSITY
NEUTRAL HYDROGEN

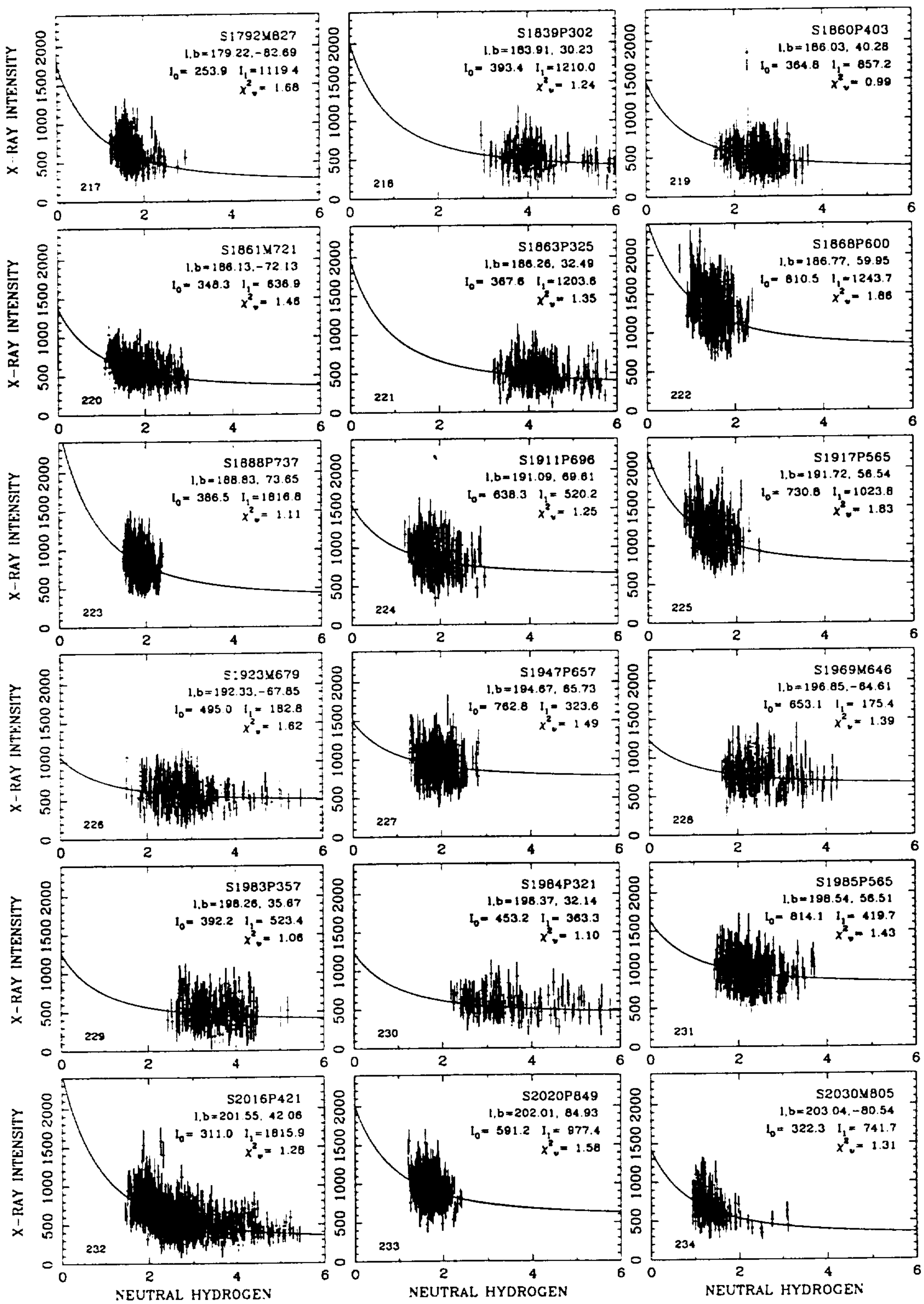
S1792M827
l,b=179.22,-82.69
I_0= 253.9 I_1=1119.4
χ^2_ν= 1.68
217
S1839P302
l,b=183.91, 30.23
I_0= 393.4 I_1=1210.0
χ^2_ν= 1.24
218
S1860P403
l,b=186.03, 40.28
I_0= 364.8 I_1= 857.2
χ^2_ν= 0.99
219
S1861M721
l,b=186.13,-72.13
I_0= 348.3 I_1= 636.9
χ^2_ν= 1.46
220
S1863P325
l,b=186.26, 32.49
I_0= 367.6 I_1=1203.6
χ^2_ν= 1.35
221
S1868P600
l,b=186.77, 59.95
I_0= 810.5 I_1=1243.7
χ^2_ν= 1.86
222
S1888P737
l,b=188.83, 73.65
I_0= 386.5 I_1=1816.8
χ^2_ν= 1.11
223
S1911P696
l,b=191.09, 69.61
I_0= 638.3 I_1= 520.2
χ^2_ν= 1.25
224
S1917P565
l,b=191.72, 56.54
I_0= 730.8 I_1=1023.8
χ^2_ν= 1.83
225
S1923M679
l,b=192.33,-67.85
I_0= 495.0 I_1= 182.8
χ^2_ν= 1.62
226
S1947P657
l,b=194.67, 65.73
I_0= 762.8 I_1= 323.6
χ^2_ν= 1.49
227
S1969M646
l,b=196.85,-64.61
I_0= 653.1 I_1= 175.4
χ^2_ν= 1.39
228
S1983P357
l,b=198.26, 35.67
I_0= 392.2 I_1= 523.4
χ^2_ν= 1.06
229
S1984P321
l,b=198.37, 32.14
I_0= 453.2 I_1= 363.3
χ^2_ν= 1.10
230
S1985P565
l,b=198.54, 56.51
I_0= 814.1 I_1= 419.7
χ^2_ν= 1.43
231
S2016P421
l,b=201.55, 42.06
I_0= 311.0 I_1=1815.9
χ^2_ν= 1.28
232
S2020P849
l,b=202.01, 84.93
I_0= 591.2 I_1= 977.4
χ^2_ν= 1.58
233
S2030M805
l,b=203.04,-80.54
I_0= 322.3 I_1= 741.7
χ^2_ν= 1.31
234
X-RAY INTENSITY
NEUTRAL HYDROGEN
0 500 1000 1500 2000
0 2 4 6

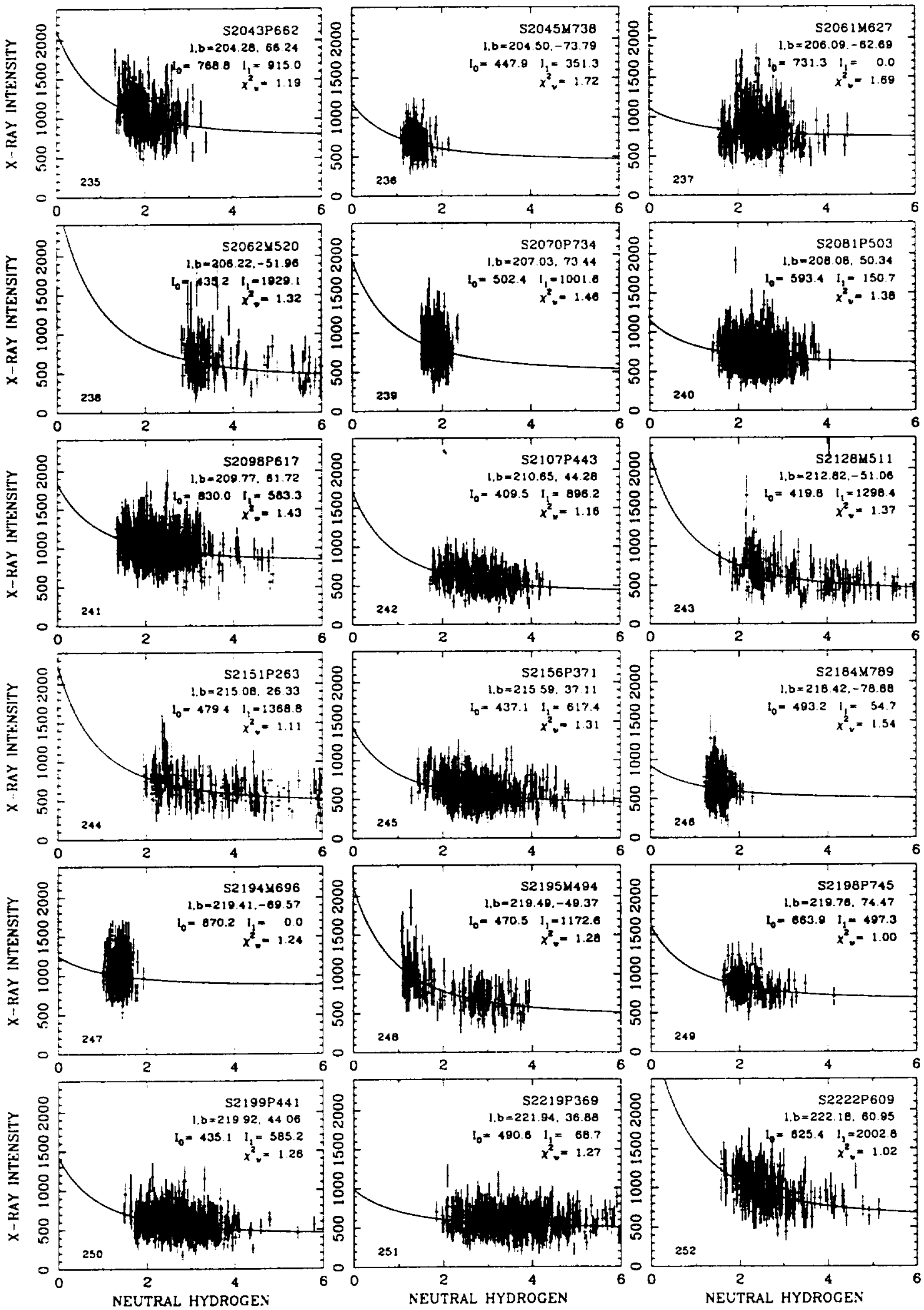
S2043P662
l,b=204.28, 66.24
I_0= 768.8 I_1= 915.0
χ^2_ν= 1.19
235
S2045M738
l,b=204.50,-73.79
I_0= 447.9 I_1= 351.3
χ^2_ν= 1.72
236
S2061M627
l,b=206.09,-62.69
I_0= 731.3 I_1= 0.0
χ^2_ν= 1.69
237
S2062M520
l,b=206.22,-51.96
I_0= 435.2 I_1=1929.1
χ^2_ν= 1.32
238
S2070P734
l,b=207.03, 73.44
I_0= 502.4 I_1=1001.6
χ^2_ν= 1.46
239
S2081P503
l,b=208.08, 50.34
I_0= 593.4 I_1= 150.7
χ^2_ν= 1.38
240
S2098P617
l,b=209.77, 61.72
I_0= 830.0 I_1= 583.3
χ^2_ν= 1.43
241
S2107P443
l,b=210.65, 44.28
I_0= 409.5 I_1= 896.2
χ^2_ν= 1.16
242
S2128M511
l,b=212.82,-51.06
I_0= 419.8 I_1=1298.4
χ^2_ν= 1.37
243
S2151P263
l,b=215.08, 26.33
I_0= 479.4 I_1=1368.8
χ^2_ν= 1.11
244
S2156P371
l,b=215.59, 37.11
I_0= 437.1 I_1= 617.4
χ^2_ν= 1.31
245
S2184M789
l,b=218.42,-78.88
I_0= 493.2 I_1= 54.7
χ^2_ν= 1.54
246
S2194M696
l,b=219.41,-69.57
I_0= 870.2 I_1= 0.0
χ^2_ν= 1.24
247
S2195M494
l,b=219.49,-49.37
I_0= 470.5 I_1=1172.6
χ^2_ν= 1.28
248
S2198P745
l,b=219.76, 74.47
I_0= 663.9 I_1= 497.3
χ^2_ν= 1.00
249
S2199P441
l,b=219.92, 44.06
I_0= 435.1 I_1= 585.2
χ^2_ν= 1.26
250
S2219P369
l,b=221.94, 36.88
I_0= 490.6 I_1= 68.7
χ^2_ν= 1.27
251
S2222P609
l,b=222.18, 60.95
I_0= 625.4 I_1=2002.8
χ^2_ν= 1.02
252
X-RAY INTENSITY
0 500 1000 1500 2000
0 2 4 6
NEUTRAL HYDROGEN

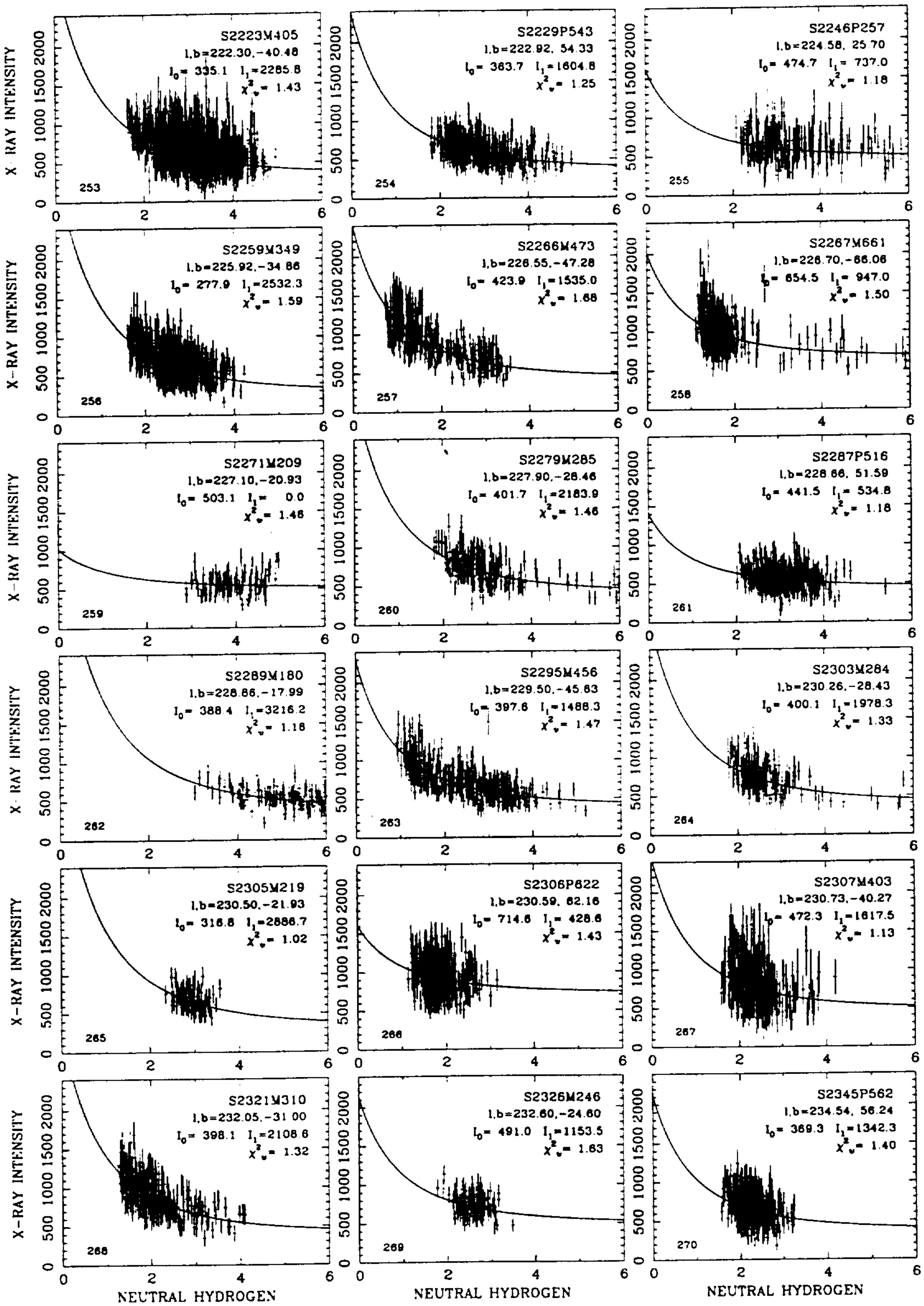
X-RAY INTENSITY
NEUTRAL HYDROGEN
S2223M405
l,b=222.30,-40.48
I_0= 335.1 I_1=2285.8
χ^2_ν= 1.43
253
S2229P543
l,b=222.92, 54.33
I_0= 363.7 I_1=1604.8
χ^2_ν= 1.25
254
S2246P257
l,b=224.58, 25.70
I_0= 474.7 I_1= 737.0
χ^2_ν= 1.18
255
S2259M349
l,b=225.92,-34.86
I_0= 277.9 I_1=2532.3
χ^2_ν= 1.59
256
S2266M473
l,b=226.55,-47.28
I_0= 423.9 I_1=1535.0
χ^2_ν= 1.68
257
S2267M661
l,b=226.70,-66.06
I_0= 654.5 I_1= 947.0
χ^2_ν= 1.50
258
S2271M209
l,b=227.10,-20.93
I_0= 503.1 I_1= 0.0
χ^2_ν= 1.46
259
S2279M285
l,b=227.90,-28.46
I_0= 401.7 I_1=2183.9
χ^2_ν= 1.46
260
S2287P516
l,b=228.66, 51.59
I_0= 441.5 I_1= 534.8
χ^2_ν= 1.18
261
S2289M180
l,b=228.66,-17.99
I_0= 388.4 I_1=3216.2
χ^2_ν= 1.16
262
S2295M456
l,b=229.50,-45.63
I_0= 397.6 I_1=1488.3
χ^2_ν= 1.47
263
S2303M284
l,b=230.26,-28.43
I_0= 400.1 I_1=1978.3
χ^2_ν= 1.33
264
S2305M219
l,b=230.50,-21.93
I_0= 316.8 I_1=2886.7
χ^2_ν= 1.02
265
S2306P622
l,b=230.59, 62.16
I_0= 714.6 I_1= 428.6
χ^2_ν= 1.43
266
S2307M403
l,b=230.73,-40.27
I_0= 472.3 I_1=1617.5
χ^2_ν= 1.13
267
S2321M310
l,b=232.05,-31.00
I_0= 398.1 I_1=2108.6
χ^2_ν= 1.32
268
S2326M246
l,b=232.60,-24.60
I_0= 491.0 I_1=1153.5
χ^2_ν= 1.63
269
S2345P562
l,b=234.54, 56.24
I_0= 369.3 I_1=1342.3
χ^2_ν= 1.40
270

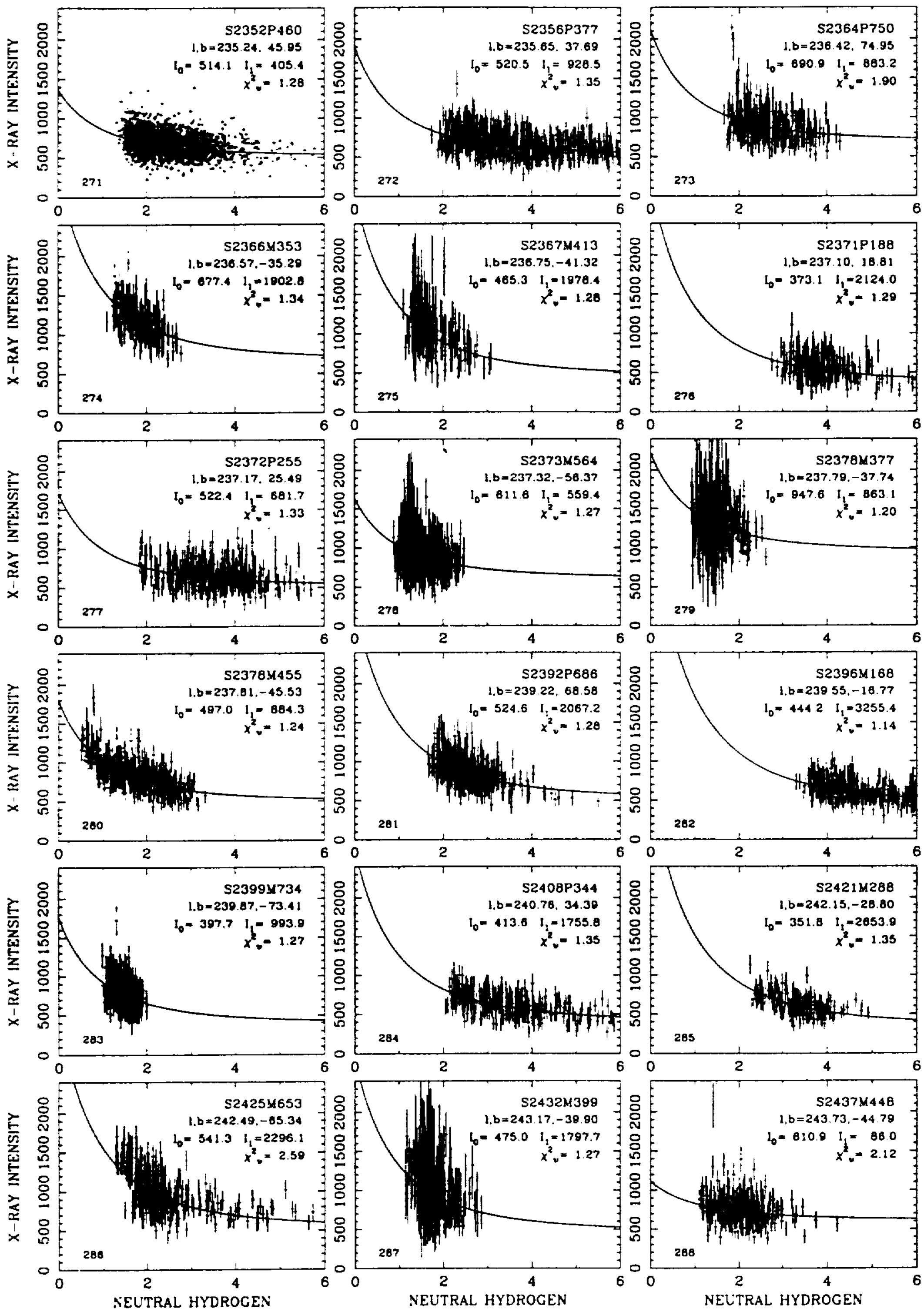
S2352P460
l,b=235.24, 45.95
I0= 514.1 I1= 405.4
χ²ν= 1.28
271
S2356P377
l,b=235.65, 37.69
I0= 520.5 I1= 928.5
χ²ν= 1.35
272
S2364P750
l,b=236.42, 74.95
I0= 690.9 I1= 883.2
χ²ν= 1.90
273
S2366M353
l,b=236.57,-35.29
I0= 677.4 I1=1902.8
χ²ν= 1.34
274
S2367M413
l,b=236.75,-41.32
I0= 465.3 I1=1976.4
χ²ν= 1.28
275
S2371P188
l,b=237.10, 18.81
I0= 373.1 I1=2124.0
χ²ν= 1.29
276
S2372P255
l,b=237.17, 25.49
I0= 522.4 I1= 681.7
χ²ν= 1.33
277
S2373M564
l,b=237.32,-56.37
I0= 611.6 I1= 559.4
χ²ν= 1.27
278
S2378M377
l,b=237.79,-37.74
I0= 947.6 I1= 863.1
χ²ν= 1.20
279
S2378M455
l,b=237.81,-45.53
I0= 497.0 I1= 884.3
χ²ν= 1.24
280
S2392P686
l,b=239.22, 68.58
I0= 524.6 I1=2067.2
χ²ν= 1.28
281
S2396M168
l,b=239.55,-16.77
I0= 444.2 I1=3255.4
χ²ν= 1.14
282
S2399M734
l,b=239.87,-73.41
I0= 397.7 I1= 993.9
χ²ν= 1.27
283
S2408P344
l,b=240.76, 34.39
I0= 413.6 I1=1755.8
χ²ν= 1.35
284
S2421M288
l,b=242.15,-28.80
I0= 351.8 I1=2653.9
χ²ν= 1.35
285
S2425M653
l,b=242.49,-65.34
I0= 541.3 I1=2296.1
χ²ν= 2.59
286
S2432M399
l,b=243.17,-39.90
I0= 475.0 I1=1797.7
χ²ν= 1.27
287
S2437M448
l,b=243.73,-44.79
I0= 610.9 I1= 86.0
χ²ν= 2.12
288
X-RAY INTENSITY
0 500 1000 1500 2000
NEUTRAL HYDROGEN
0 2 4 6

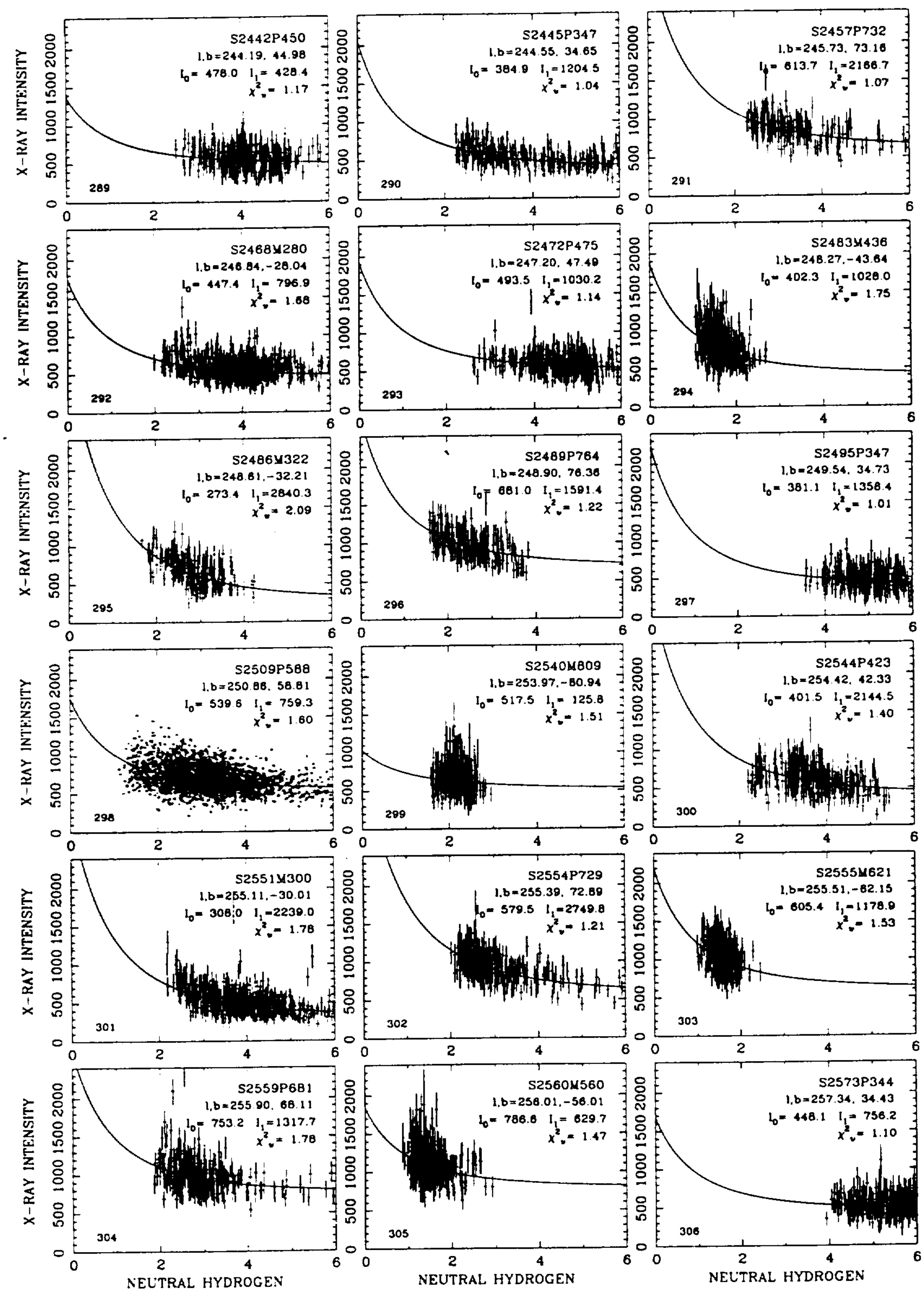

X-RAY INTENSITY
NEUTRAL HYDROGEN
S2442P450
l,b=244.19, 44.98
I_0= 478.0 I_1= 428.4
χ^2_ν= 1.17
289
S2445P347
l,b=244.55, 34.65
I_0= 384.9 I_1=1204.5
χ^2_ν= 1.04
290
S2457P732
l,b=245.73, 73.16
I_0= 613.7 I_1=2166.7
χ^2_ν= 1.07
291
S2468M280
l,b=246.84,-28.04
I_0= 447.4 I_1= 796.9
χ^2_ν= 1.66
292
S2472P475
l,b=247.20, 47.49
I_0= 493.5 I_1=1030.2
χ^2_ν= 1.14
293
S2483M436
l,b=248.27,-43.64
I_0= 402.3 I_1=1028.0
χ^2_ν= 1.75
294
S2486M322
l,b=248.61,-32.21
I_0= 273.4 I_1=2840.3
χ^2_ν= 2.09
295
S2489P764
l,b=248.90, 76.36
I_0= 661.0 I_1=1591.4
χ^2_ν= 1.22
296
S2495P347
l,b=249.54, 34.73
I_0= 381.1 I_1=1358.4
χ^2_ν= 1.01
297
S2509P588
l,b=250.86, 58.81
I_0= 539.6 I_1= 759.3
χ^2_ν= 1.60
298
S2540M809
l,b=253.97,-80.94
I_0= 517.5 I_1= 125.8
χ^2_ν= 1.51
299
S2544P423
l,b=254.42, 42.33
I_0= 401.5 I_1=2144.5
χ^2_ν= 1.40
300
S2551M300
l,b=255.11,-30.01
I_0= 308.0 I_1=2239.0
χ^2_ν= 1.78
301
S2554P729
l,b=255.39, 72.89
I_0= 579.5 I_1=2749.8
χ^2_ν= 1.21
302
S2555M621
l,b=255.51,-62.15
I_0= 605.4 I_1=1178.9
χ^2_ν= 1.53
303
S2559P681
l,b=255.90, 68.11
I_0= 753.2 I_1=1317.7
χ^2_ν= 1.78
304
S2560M560
l,b=256.01,-56.01
I_0= 786.6 I_1= 629.7
χ^2_ν= 1.47
305
S2573P344
l,b=257.34, 34.43
I_0= 448.1 I_1= 756.2
χ^2_ν= 1.10
306

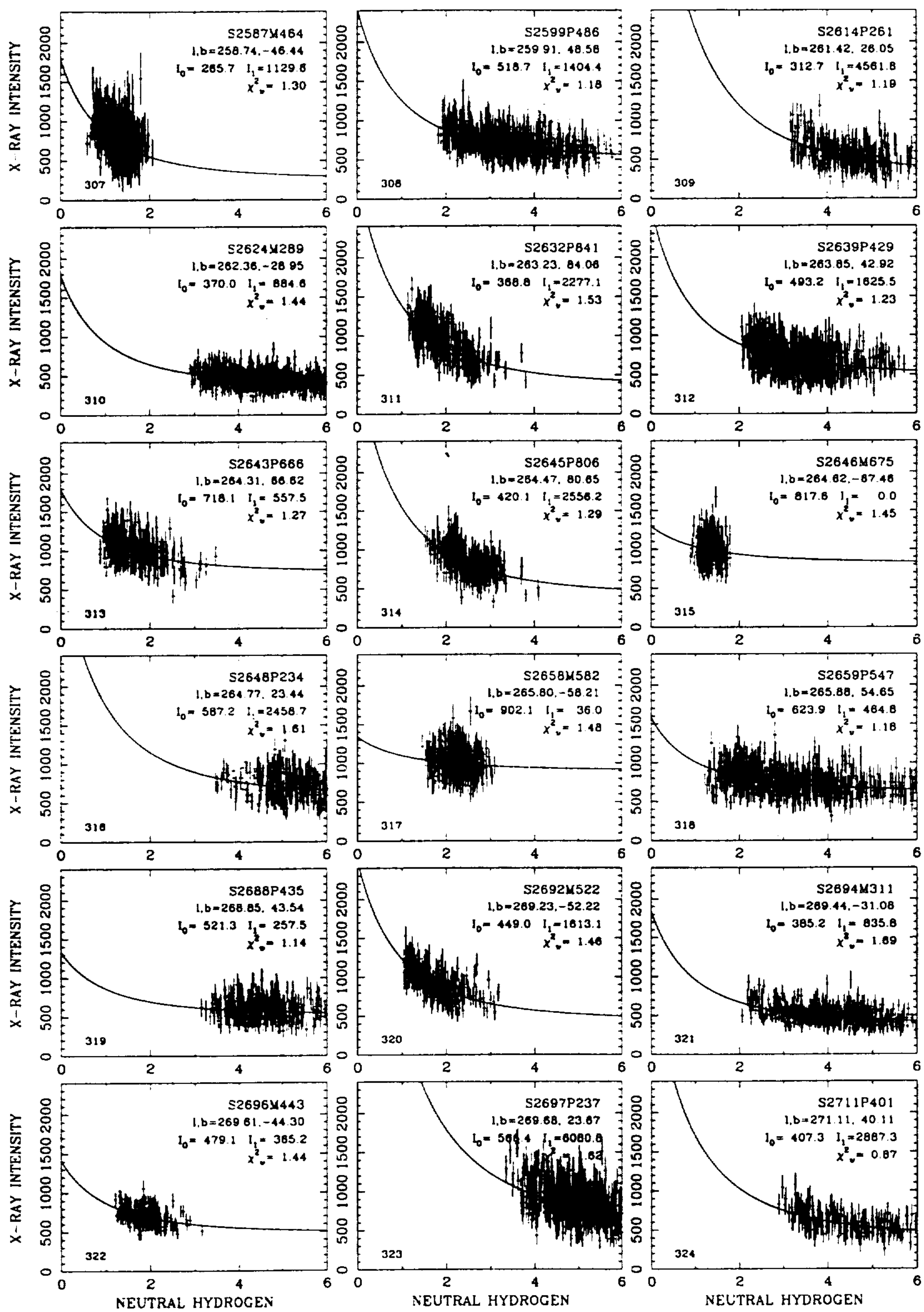
S2587M464
l,b=258.74,-46.44
I0= 265.7 I1=1129.6
χ²ν= 1.30
307
S2599P486
l,b=259.91, 48.58
I0= 518.7 I1=1404.4
χ²ν= 1.18
308
S2614P261
l,b=261.42, 26.05
I0= 312.7 I1=4561.8
χ²ν= 1.19
309
S2624M289
l,b=262.36,-28.95
I0= 370.0 I1= 884.6
χ²ν= 1.44
310
S2632P841
l,b=263.23, 84.08
I0= 368.8 I1=2277.1
χ²ν= 1.53
311
S2639P429
l,b=263.85, 42.92
I0= 493.2 I1=1625.5
χ²ν= 1.23
312
S2643P666
l,b=264.31, 66.62
I0= 718.1 I1= 557.5
χ²ν= 1.27
313
S2645P806
l,b=264.47, 80.65
I0= 420.1 I1=2556.2
χ²ν= 1.29
314
S2646M675
l,b=264.62,-67.46
I0= 817.6 I1= 0.0
χ²ν= 1.45
315
S2648P234
l,b=264.77, 23.44
I0= 587.2 I1=2458.7
χ²ν= 1.61
316
S2658M582
l,b=265.80,-58.21
I0= 902.1 I1= 36.0
χ²ν= 1.48
317
S2659P547
l,b=265.88, 54.65
I0= 623.9 I1= 464.8
χ²ν= 1.18
318
S2688P435
l,b=268.85, 43.54
I0= 521.3 I1= 257.5
χ²ν= 1.14
319
S2692M522
l,b=269.23,-52.22
I0= 449.0 I1=1613.1
χ²ν= 1.46
320
S2694M311
l,b=269.44,-31.08
I0= 385.2 I1= 835.8
χ²ν= 1.69
321
S2696M443
l,b=269.61,-44.30
I0= 479.1 I1= 365.2
χ²ν= 1.44
322
S2697P237
l,b=269.68, 23.67
I0= 566.4 I1=6080.8
χ²ν= 1.62
323
S2711P401
l,b=271.11, 40.11
I0= 407.3 I1=2887.3
χ²ν= 0.87
324
X-RAY INTENSITY
NEUTRAL HYDROGEN

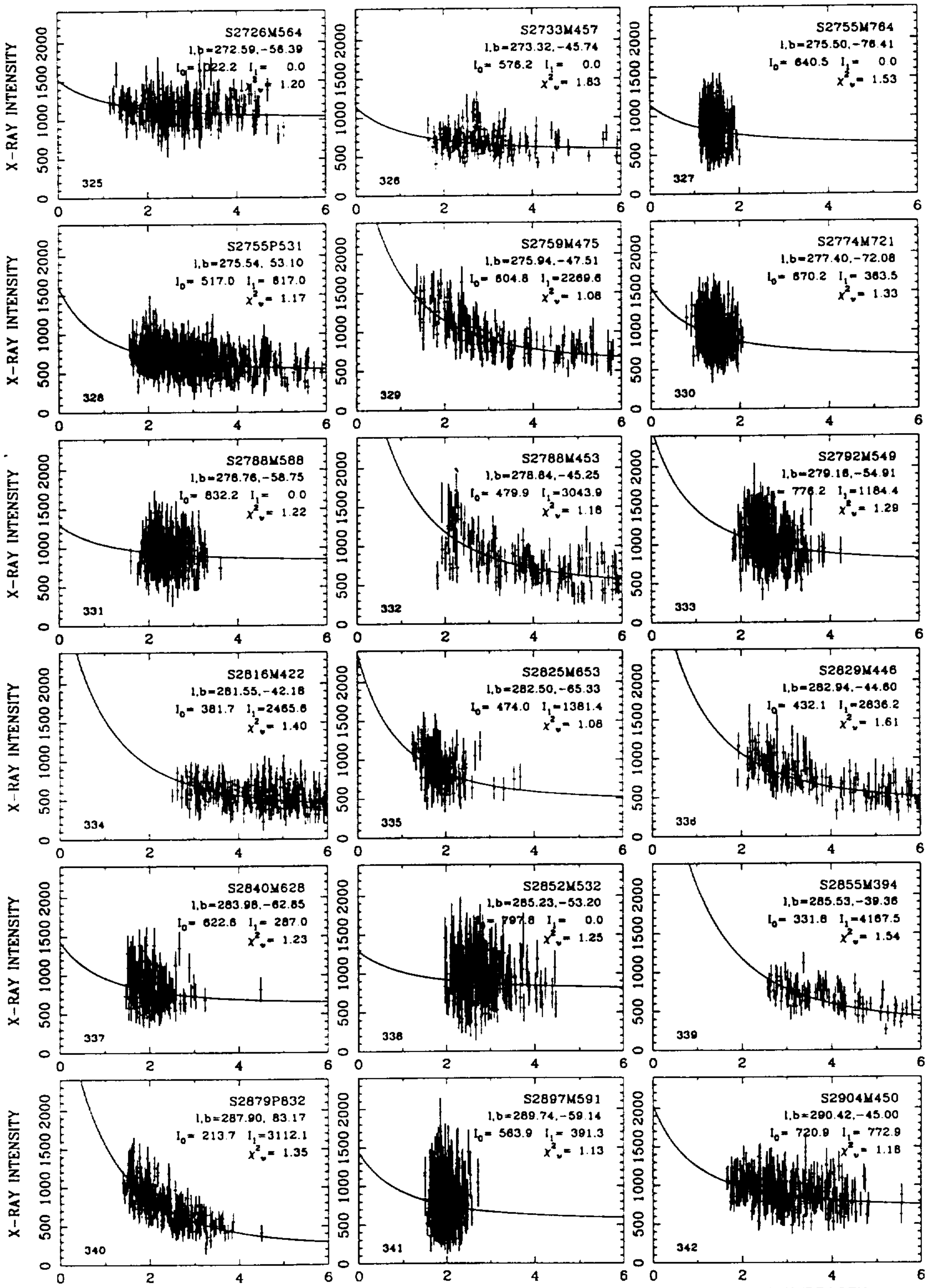
S2726M564
l,b=272.59,−56.39
I_0= 1022.2 I_1= 0.0
χ^2_ν= 1.20
325
S2733M457
l,b=273.32,−45.74
I_0= 576.2 I_1= 0.0
χ^2_ν= 1.83
326
S2755M764
l,b=275.50,−76.41
I_0= 640.5 I_1= 0.0
χ^2_ν= 1.53
327
S2755P531
l,b=275.54, 53.10
I_0= 517.0 I_1= 617.0
χ^2_ν= 1.17
328
S2759M475
l,b=275.94,−47.51
I_0= 604.8 I_1=2269.6
χ^2_ν= 1.08
329
S2774M721
l,b=277.40,−72.08
I_0= 670.2 I_1= 363.5
χ^2_ν= 1.33
330
S2788M588
l,b=278.76,−58.75
I_0= 832.2 I_1= 0.0
χ^2_ν= 1.22
331
S2788M453
l,b=278.84,−45.25
I_0= 479.9 I_1=3043.9
χ^2_ν= 1.16
332
S2792M549
l,b=279.16,−54.91
I_0= 776.2 I_1=1184.4
χ^2_ν= 1.29
333
S2816M422
l,b=281.55,−42.18
I_0= 381.7 I_1=2465.6
χ^2_ν= 1.40
334
S2825M653
l,b=282.50,−65.33
I_0= 474.0 I_1=1381.4
χ^2_ν= 1.08
335
S2829M446
l,b=282.94,−44.60
I_0= 432.1 I_1=2836.2
χ^2_ν= 1.61
336
S2840M628
l,b=283.98,−62.85
I_0= 622.6 I_1= 287.0
χ^2_ν= 1.23
337
S2852M532
l,b=285.23,−53.20
I_0= 797.8 I_1= 0.0
χ^2_ν= 1.25
338
S2855M394
l,b=285.53,−39.36
I_0= 331.8 I_1=4167.5
χ^2_ν= 1.54
339
S2879P832
l,b=287.90, 83.17
I_0= 213.7 I_1=3112.1
χ^2_ν= 1.35
340
S2897M591
l,b=289.74,−59.14
I_0= 563.9 I_1= 391.3
χ^2_ν= 1.13
341
S2904M450
l,b=290.42,−45.00
I_0= 720.9 I_1= 772.9
χ^2_ν= 1.18
342
X–RAY INTENSITY
NEUTRAL HYDROGEN

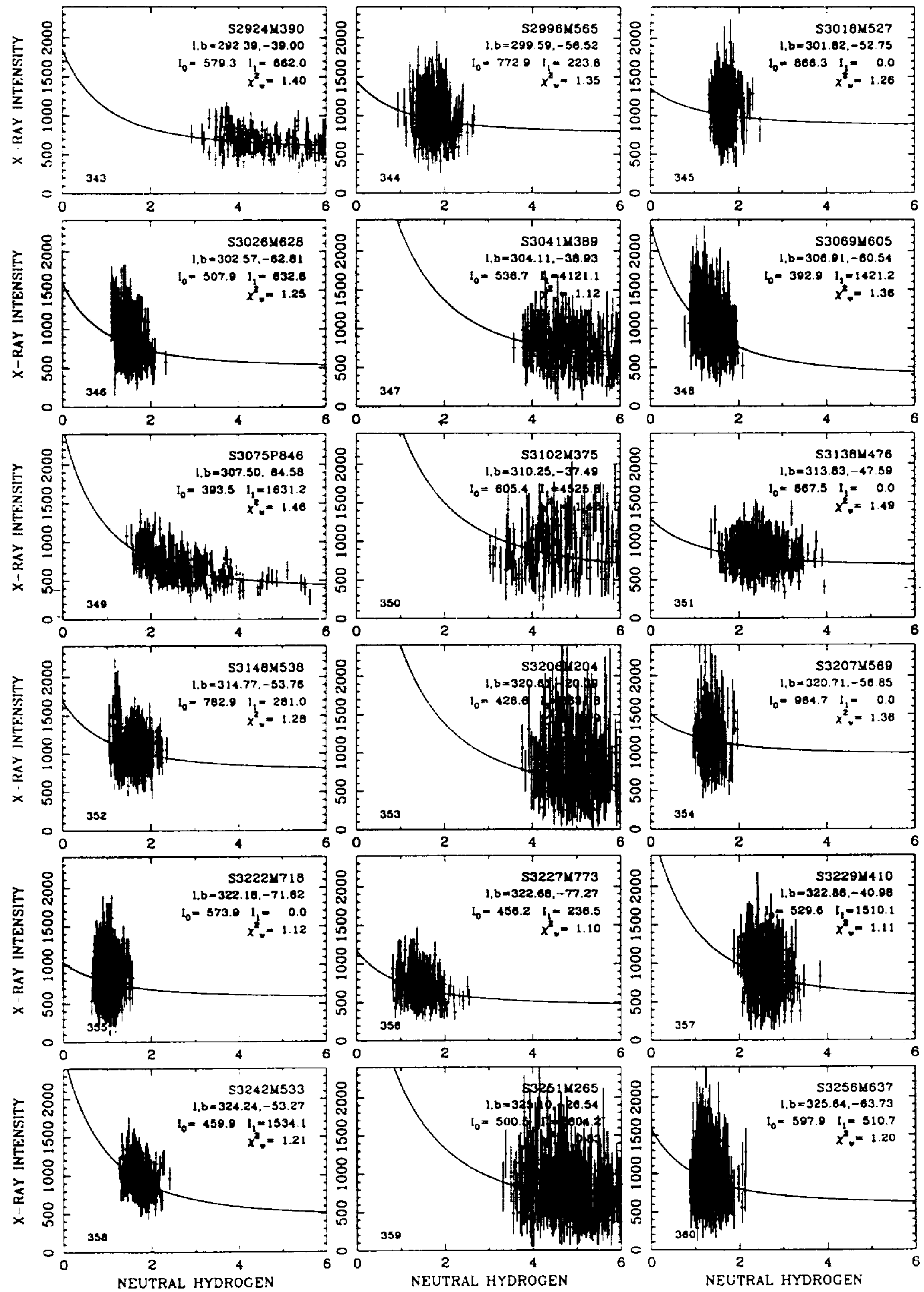
S2924M390
l,b=292.39,-39.00
I_0= 579.3 I_1= 662.0
χ^2_ν= 1.40
343
S2996M565
l,b=299.59,-56.52
I_0= 772.9 I_1= 223.8
χ^2_ν= 1.35
344
S3018M527
l,b=301.82,-52.75
I_0= 866.3 I_1= 0.0
χ^2_ν= 1.26
345
S3026M628
l,b=302.57,-62.81
I_0= 507.9 I_1= 632.8
χ^2_ν= 1.25
346
S3041M389
l,b=304.11,-38.93
I_0= 536.7
347
S3069M605
l,b=306.91,-60.54
I_0= 392.9 I_1=1421.2
χ^2_ν= 1.36
348
S3075P846
l,b=307.50, 84.58
I_0= 393.5 I_1=1631.2
χ^2_ν= 1.46
349
S3102M375
l,b=310.25,
I_0= 605.4
350
S3136M476
l,b=313.63,-47.59
I_0= 667.5 I_1= 0.0
χ^2_ν= 1.49
351
S3148M538
l,b=314.77,-53.76
I_0= 782.9 I_1= 281.0
χ^2_ν= 1.28
352
I_0= 426.6
353
S3207M569
l,b=320.71,-56.85
I_0= 964.7 I_1= 0.0
χ^2_ν= 1.36
354
S3222M718
l,b=322.16,-71.82
I_0= 573.9 I_1= 0.0
χ^2_ν= 1.12
355
S3227M773
l,b=322.66,-77.27
I_0= 456.2 I_1= 236.5
χ^2_ν= 1.10
356
S3229M410
l,b=322.86,-40.98
529.6 I_1=1510.1
χ^2_ν= 1.11
357
S3242M533
l,b=324.24,-53.27
I_0= 459.9 I_1=1534.1
χ^2_ν= 1.21
358
359
S3256M637
l,b=325.64,-63.73
I_0= 597.9 I_1= 510.7
χ^2_ν= 1.20
360
X-RAY INTENSITY
NEUTRAL HYDROGEN
0
500
1000
1500
2000
2
4
6

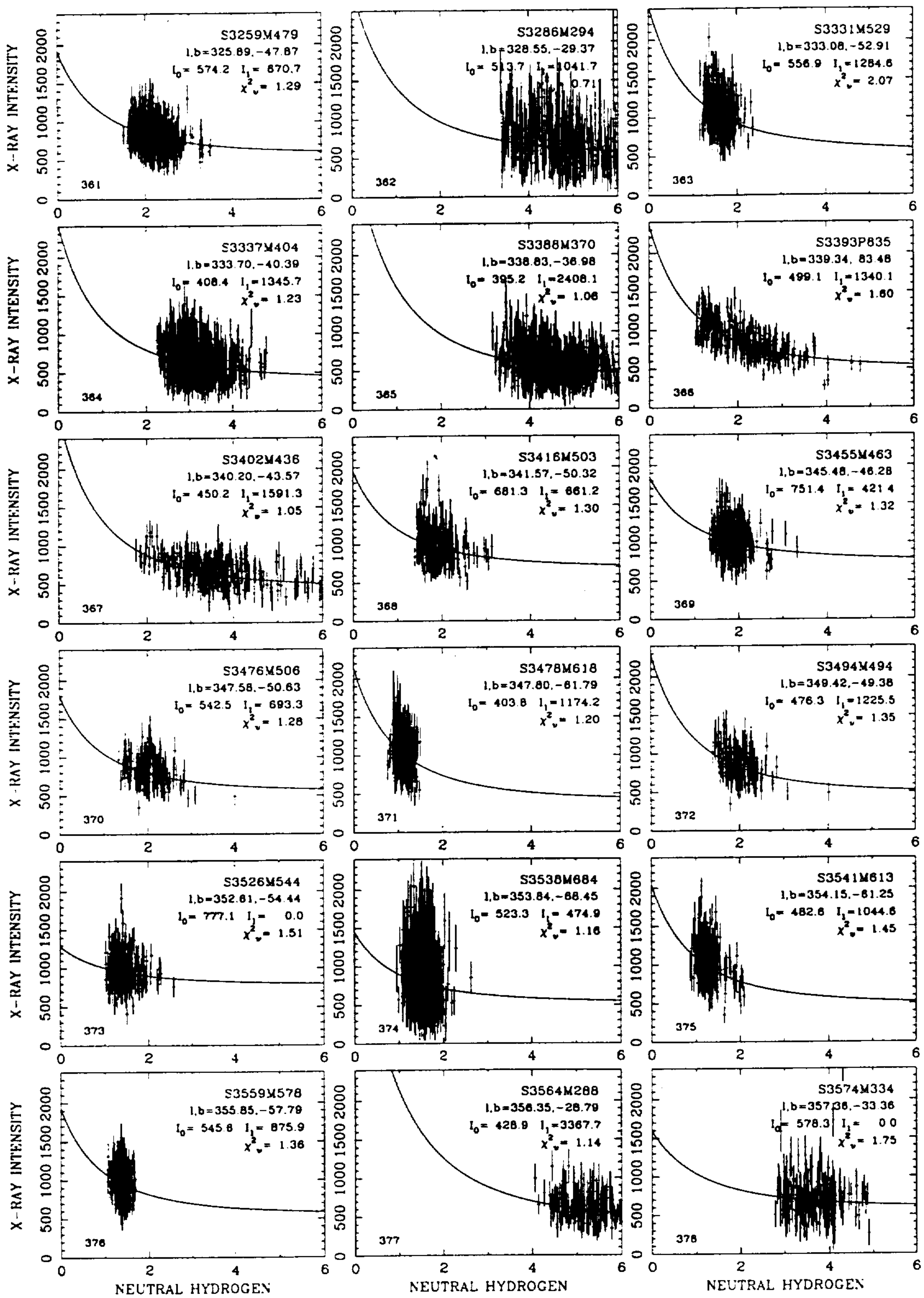
X-RAY INTENSITY
NEUTRAL HYDROGEN
S3259M479
l,b=325.89,-47.87
I_0= 574.2 I_1= 870.7
χ^2_ν= 1.29
361
S3286M294
l,b=328.55,-29.37
362
S3331M529
l,b=333.08,-52.91
I_0= 556.9 I_1=1284.6
χ^2_ν= 2.07
363
S3337M404
l,b=333.70,-40.39
I_0= 408.4 I_1=1345.7
χ^2_ν= 1.23
364
S3388M370
l,b=338.83,-36.98
I_0= 395.2 I_1=2408.1
χ^2_ν= 1.06
365
S3393P835
l,b=339.34, 83.48
I_0= 499.1 I_1=1340.1
χ^2_ν= 1.60
366
S3402M436
l,b=340.20,-43.57
I_0= 450.2 I_1=1591.3
χ^2_ν= 1.05
367
S3416M503
l,b=341.57,-50.32
I_0= 681.3 I_1= 661.2
χ^2_ν= 1.30
368
S3455M463
l,b=345.48,-46.28
I_0= 751.4 I_1= 421.4
χ^2_ν= 1.32
369
S3476M506
l,b=347.58,-50.63
I_0= 542.5 I_1= 693.3
χ^2_ν= 1.28
370
S3478M618
l,b=347.80,-61.79
I_0= 403.8 I_1=1174.2
χ^2_ν= 1.20
371
S3494M494
l,b=349.42,-49.38
I_0= 476.3 I_1=1225.5
χ^2_ν= 1.35
372
S3526M544
l,b=352.61,-54.44
I_0= 777.1 I_1= 0.0
χ^2_ν= 1.51
373
S3538M684
l,b=353.84,-68.45
I_0= 523.3 I_1= 474.9
χ^2_ν= 1.16
374
S3541M613
l,b=354.15,-61.25
I_0= 482.6 I_1=1044.6
χ^2_ν= 1.45
375
S3559M578
l,b=355.85,-57.79
I_0= 545.6 I_1= 875.9
χ^2_ν= 1.36
376
S3564M288
l,b=356.35,-28.79
I_0= 428.9 I_1=3367.7
χ^2_ν= 1.14
377
S3574M334
l,b=357.38,-33.36
I_0= 578.3 I_1= 0.0
χ^2_ν= 1.75
378

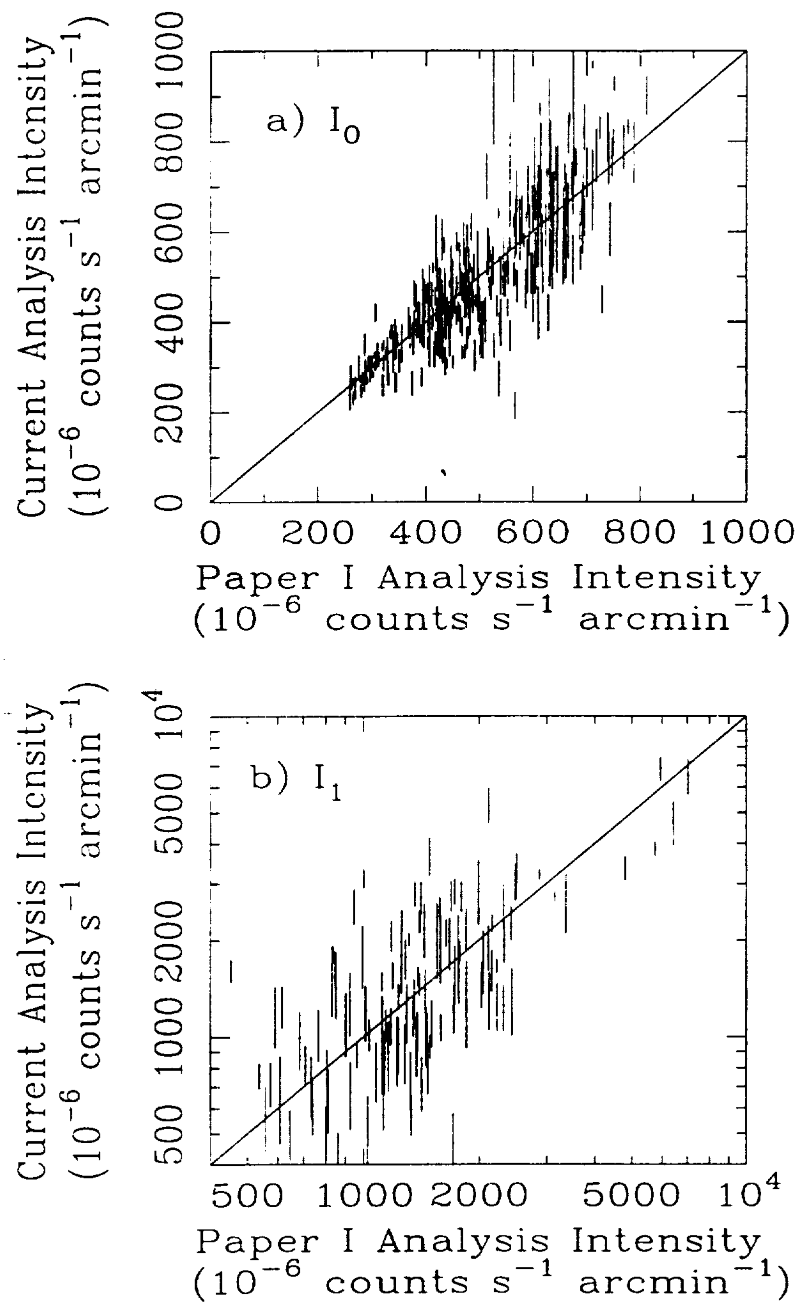
a) I_0
Current Analysis Intensity
(10^{-6} counts s^{-1} arcmin^{-1})
0
200
400
600
800
1000
Paper I Analysis Intensity
(10^{-6} counts s^{-1} arcmin^{-1})
b) I_1
500
1000
2000
5000
10^4

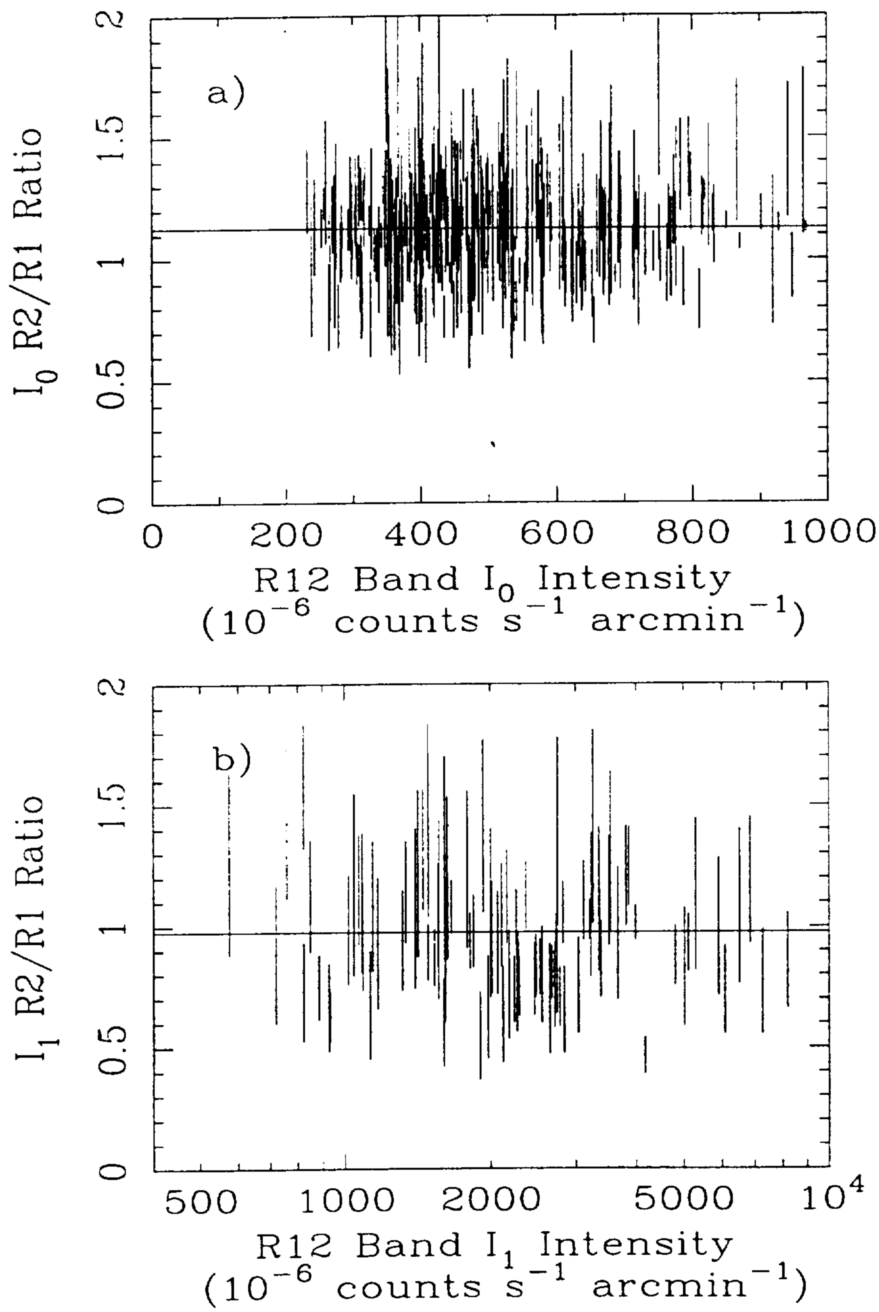
a)
I_0 R2/R1 Ratio
0
0.5
1
1.5
2
0
200
400
600
800
1000
R12 Band I_0 Intensity
(10^{-6} counts s^{-1} arcmin^{-1})
b)
I_1 R2/R1 Ratio
0
0.5
1
1.5
2
500
1000
2000
5000
10^4
R12 Band I_1 Intensity
(10^{-6} counts s^{-1} arcmin^{-1})

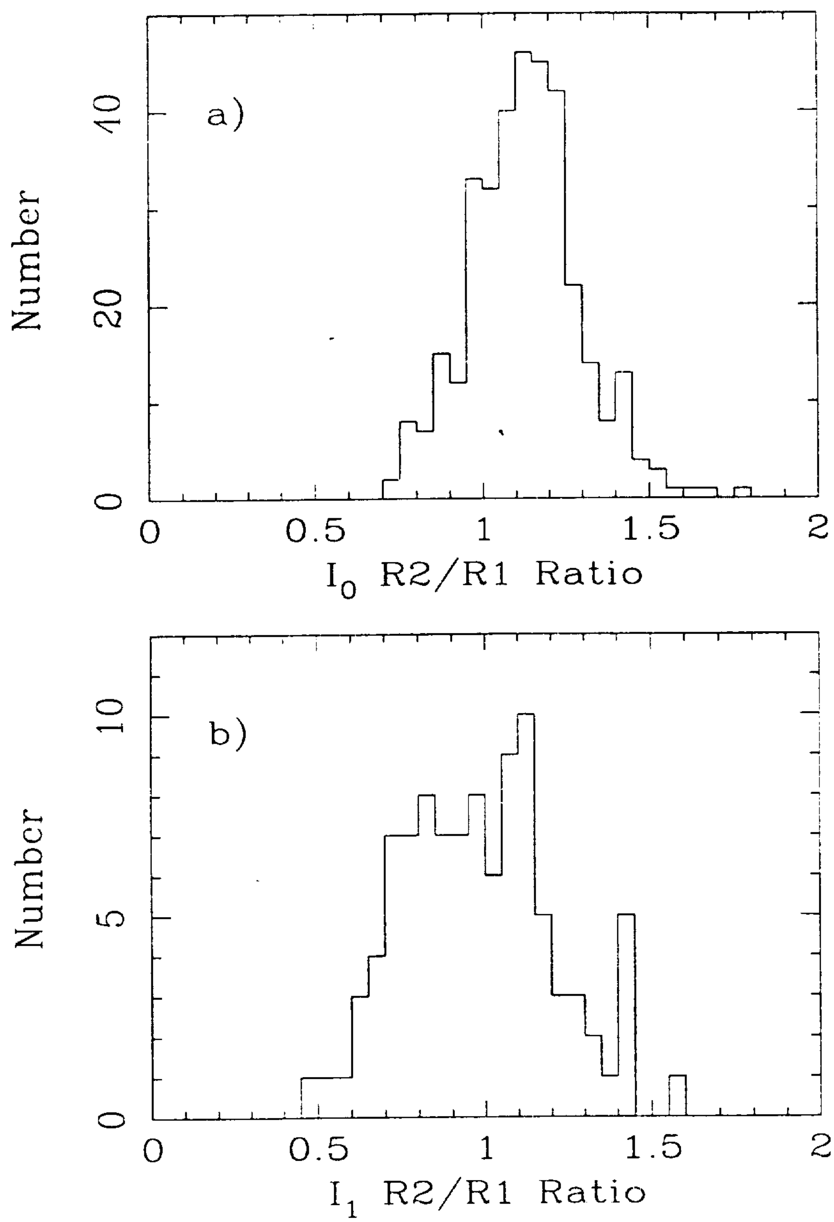

a)
Number
0
20
40
0
0.5
1
1.5
2
I0 R2/R1 Ratio
b)
Number
0
5
10
0
0.5
1
1.5
2
I1 R2/R1 Ratio

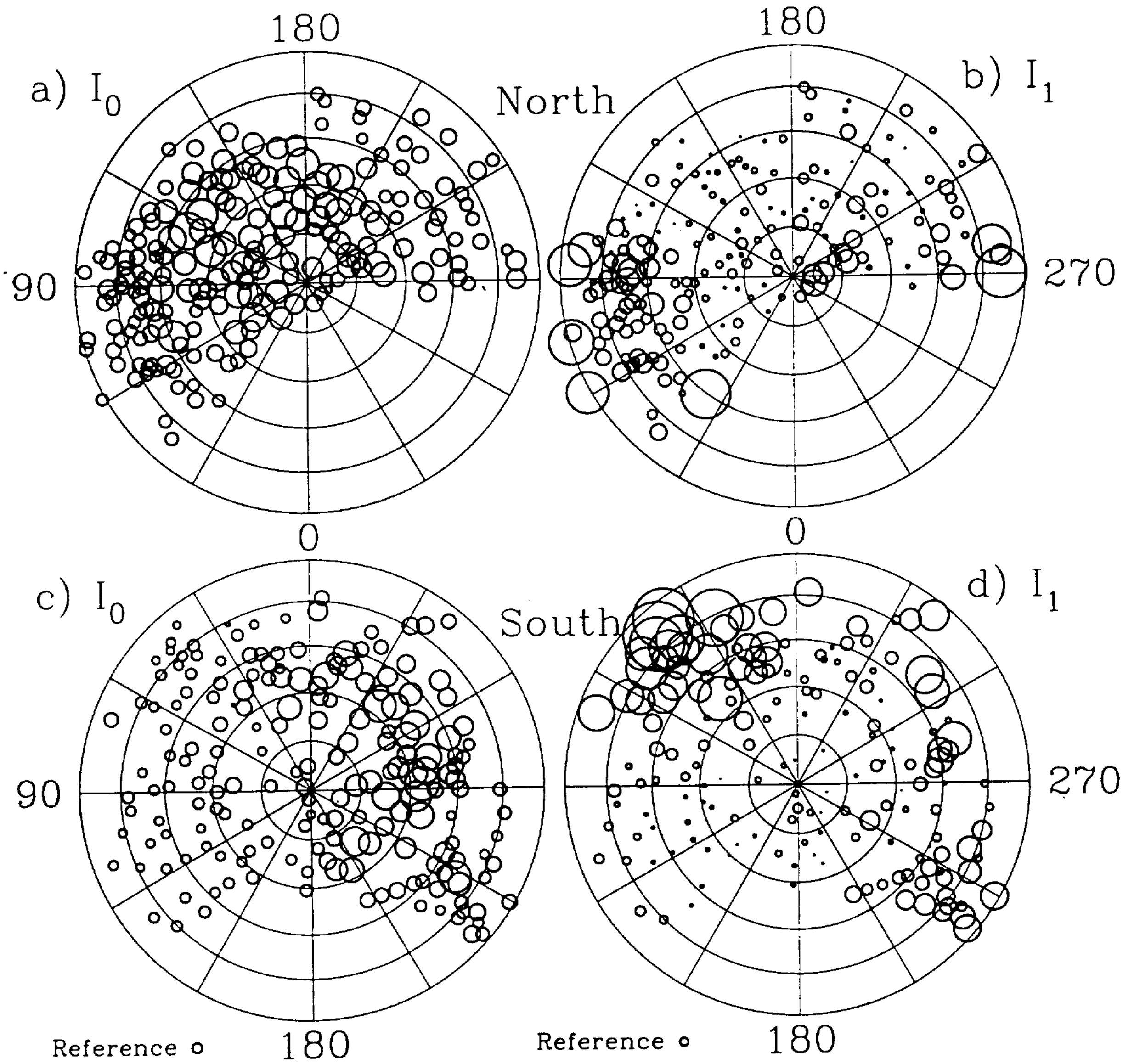
180
a) I_0
North
90
0
180
b) I_1
270
0
c) I_0
South
90
Reference o
180
0
d) I_1
270
Reference o
180

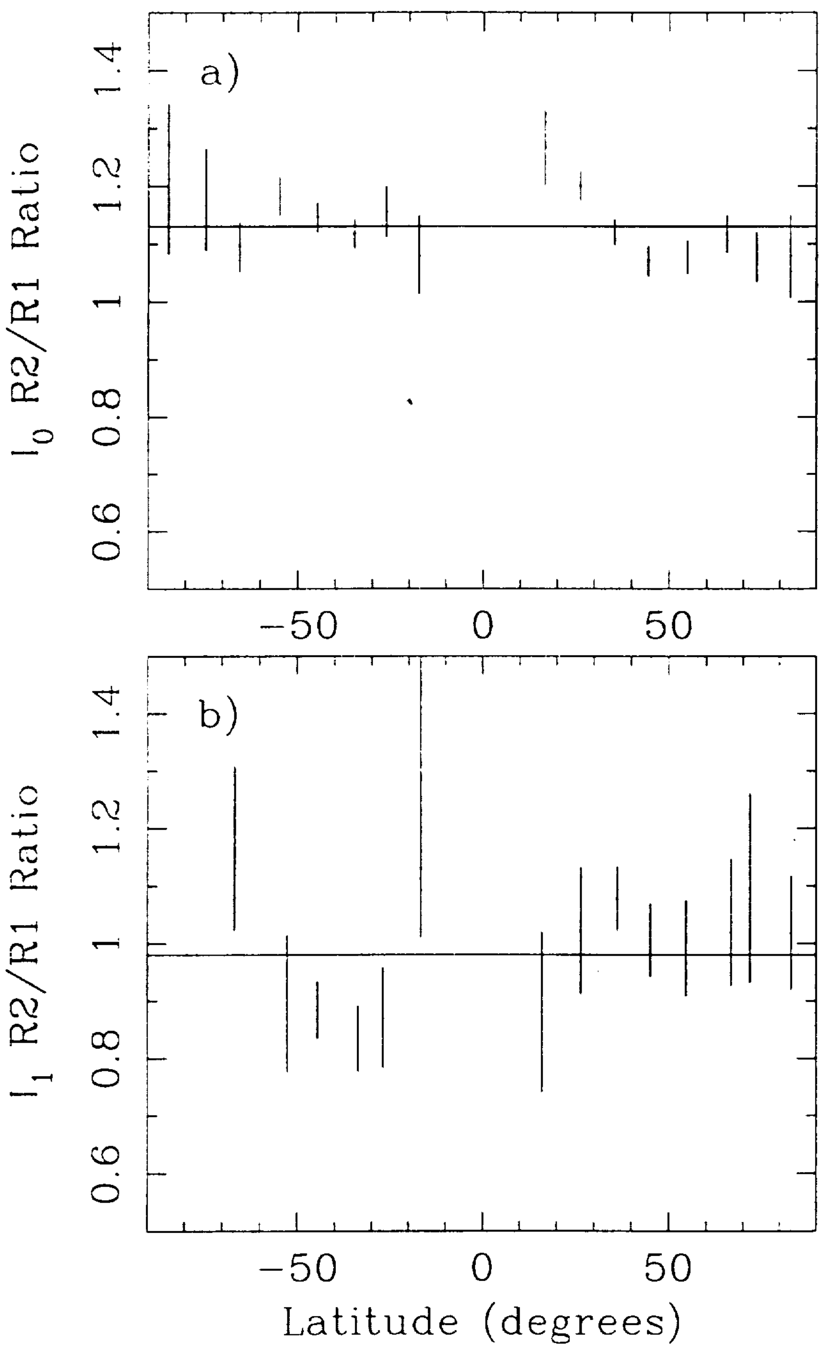
a)
b)
I_0 R2/R1 Ratio
I_1 R2/R1 Ratio
0.6
0.8
1
1.2
1.4
−50
0
50
Latitude (degrees)

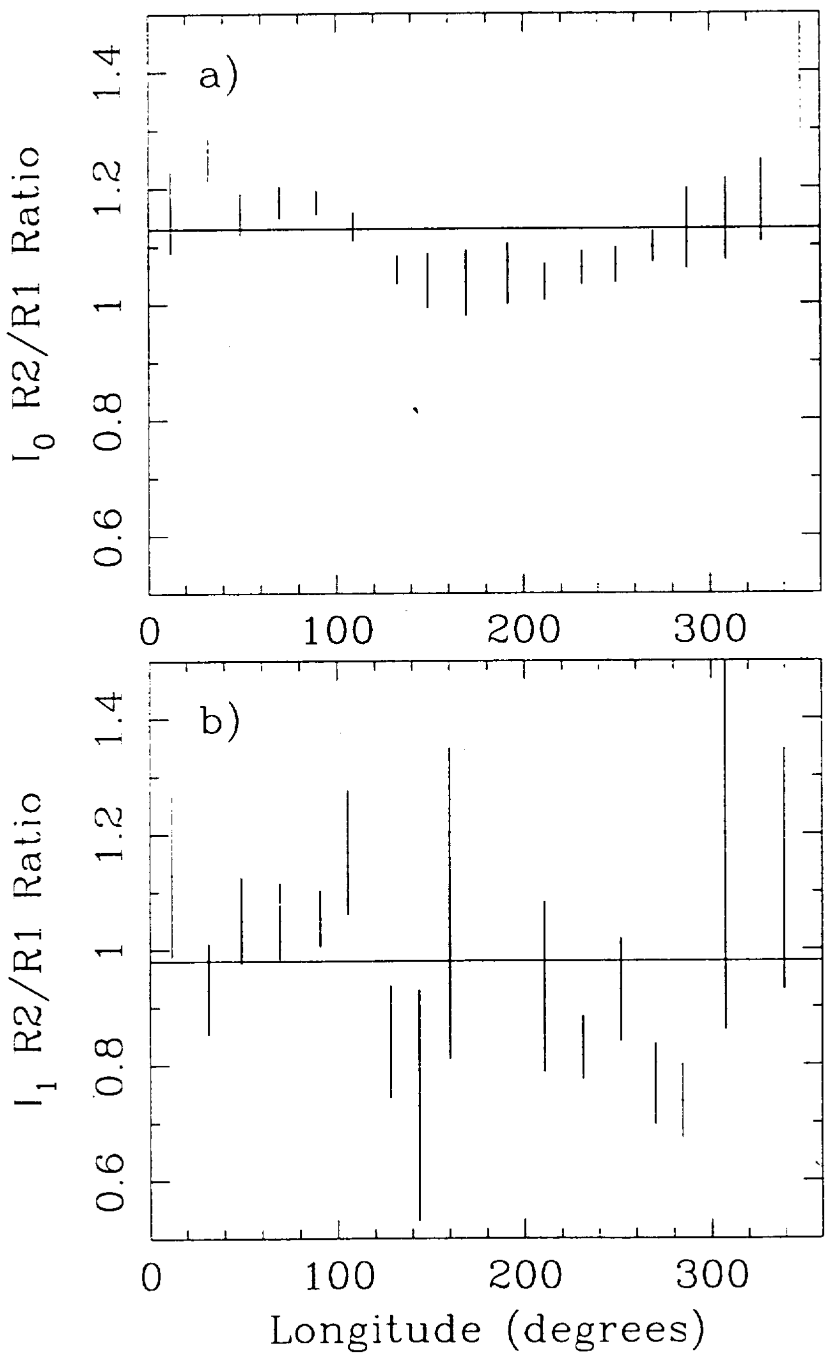

a)
b)
I_0 R2/R1 Ratio
I_1 R2/R1 Ratio
0.6
0.8
1
1.2
1.4
0
100
200
300
Longitude (degrees)

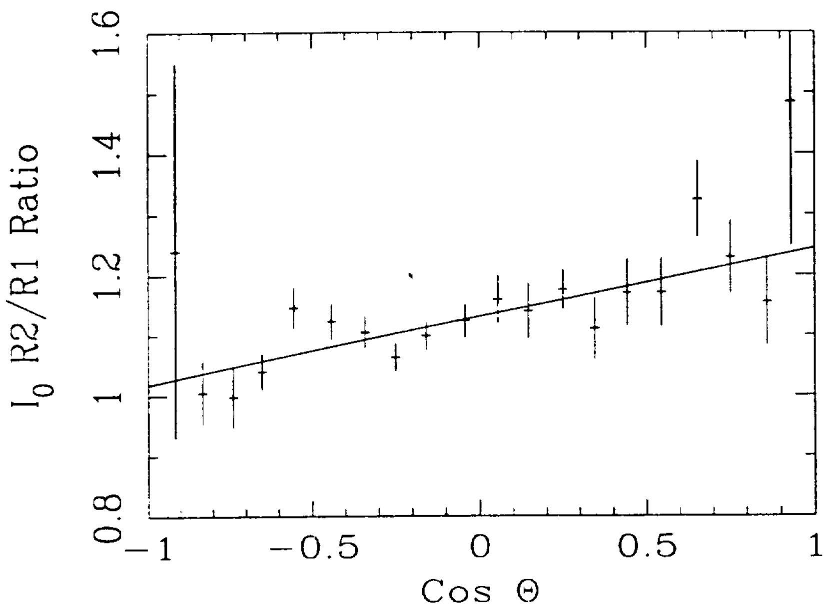

1.6
1.4
1.2
1
0.8
I_0 R2/R1 Ratio
−1
−0.5
0
0.5
1
Cos Θ

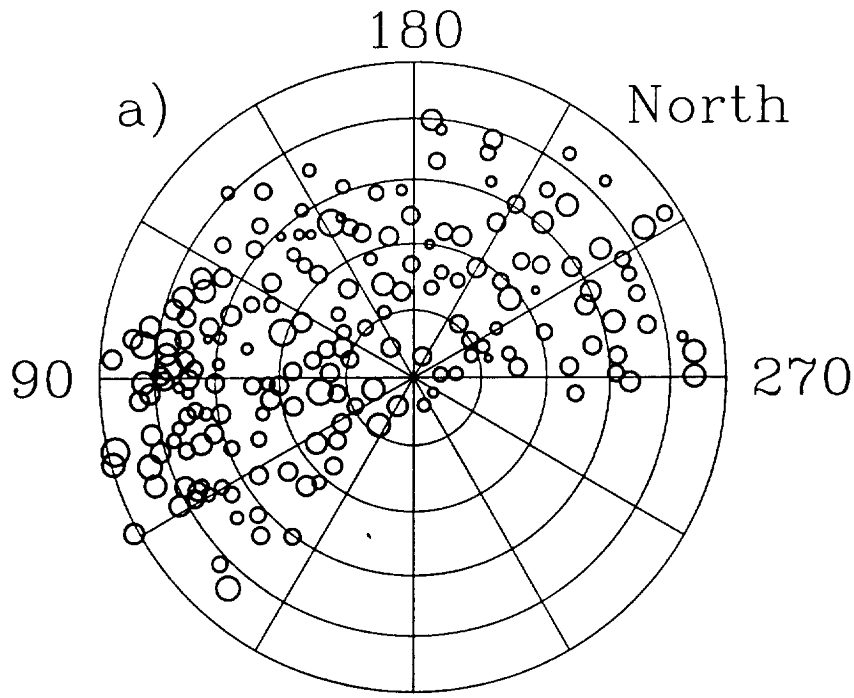
180
a)
North
90
270
0

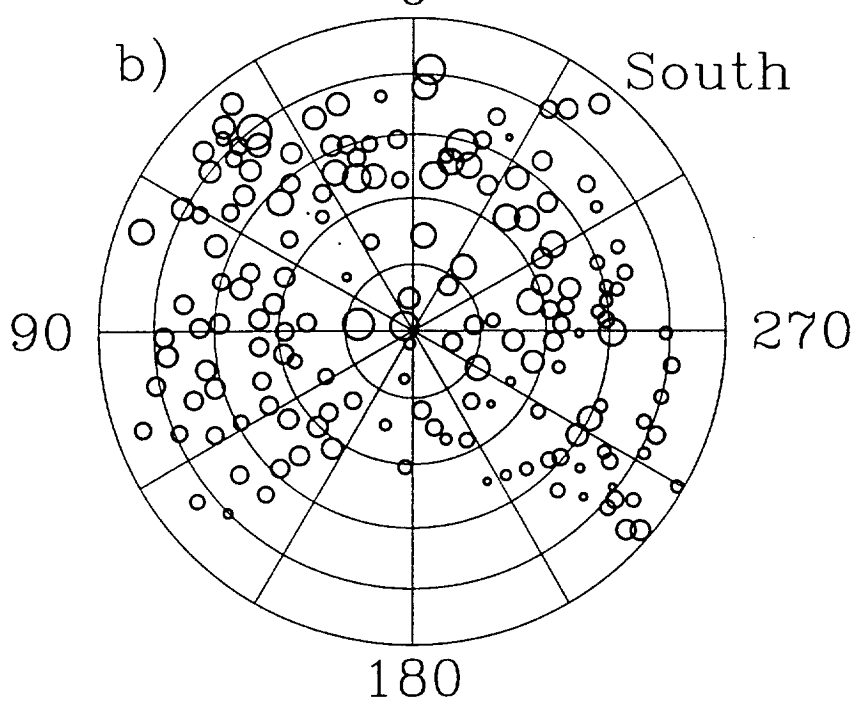
0
b)
South
90
270
180

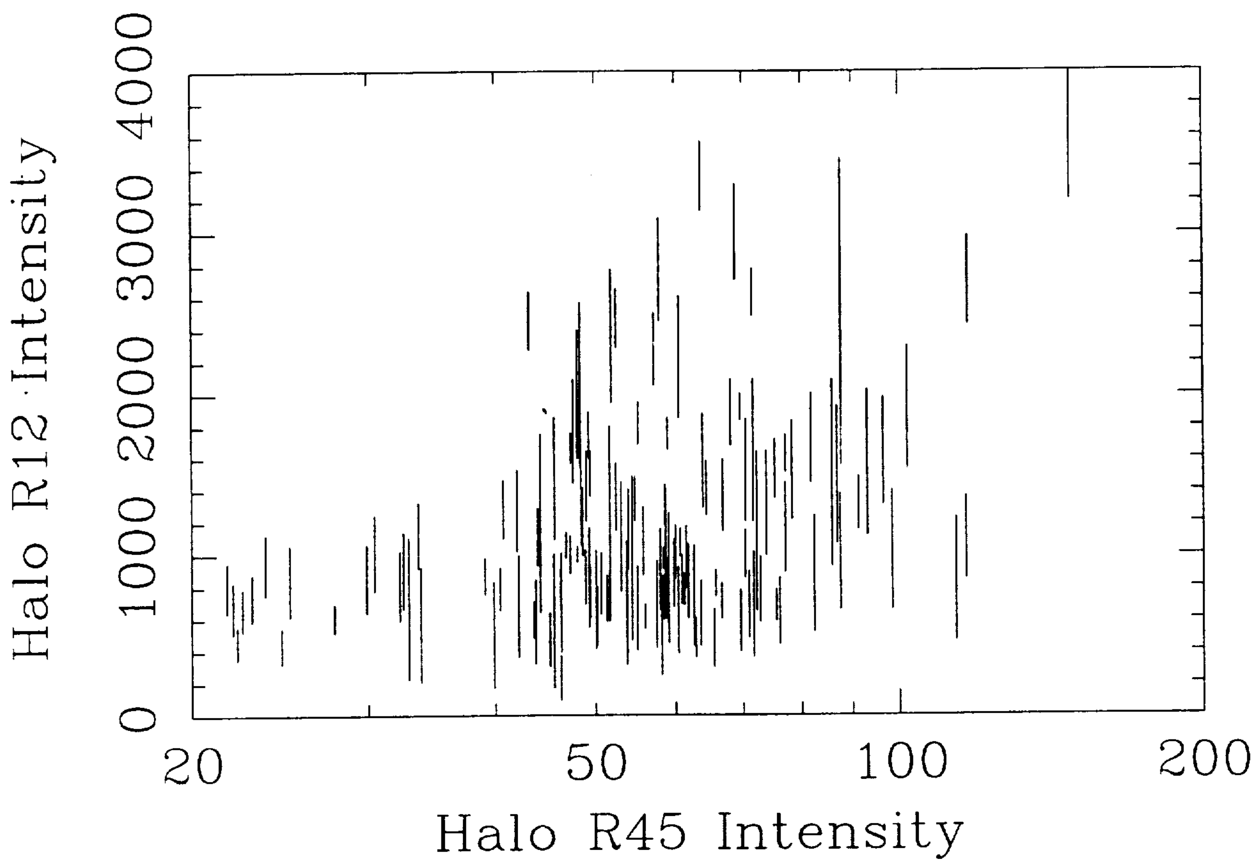
Halo R12 Intensity
0
1000
2000
3000
4000
20
50
100
200
Halo R45 Intensity

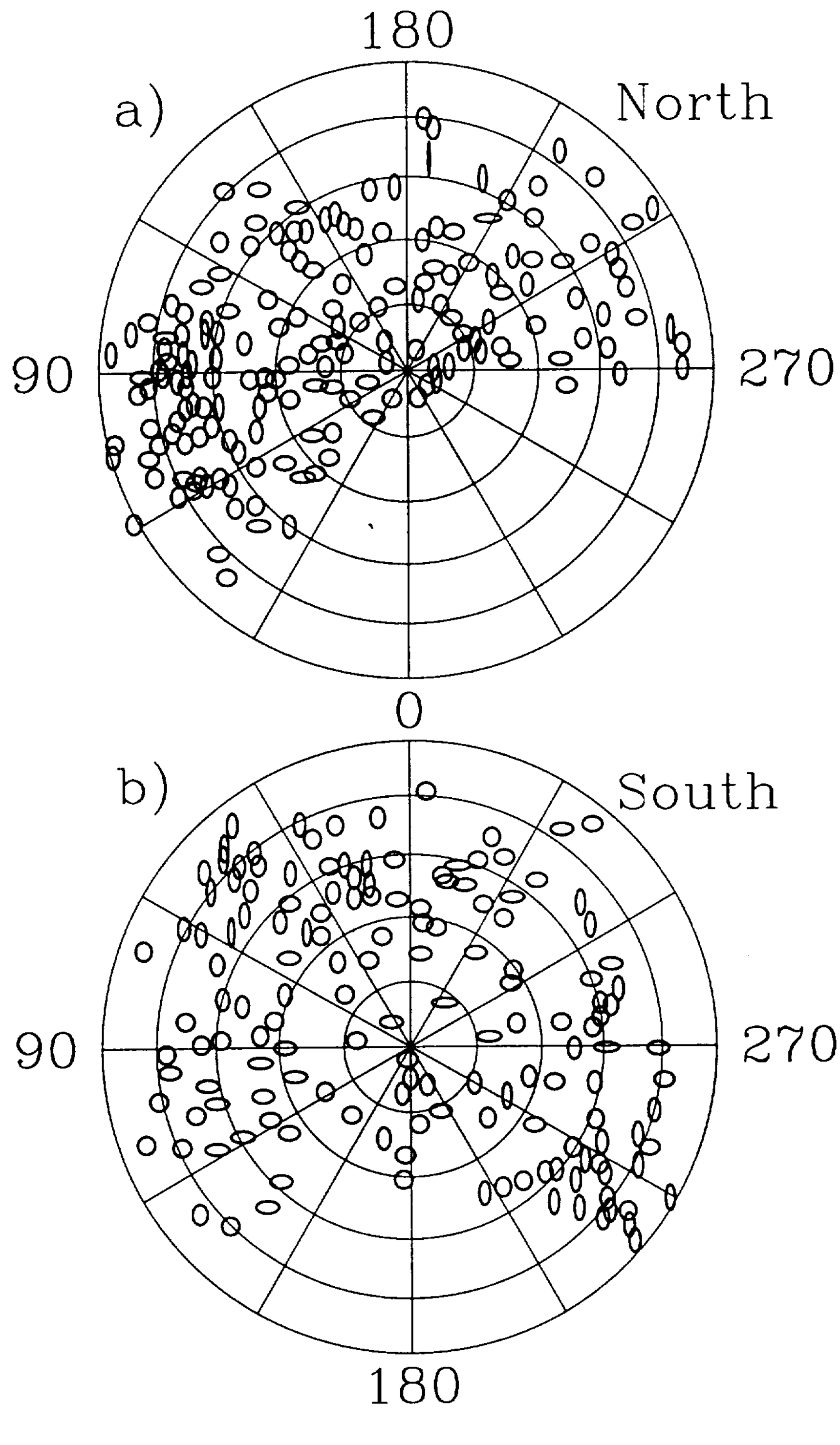
180
a)
North
90
270
0
b)
South
90
270
180